Doctoral Dissertation

Analyses of Protoporphyrin IX Photobleaching and its Photoproducts for Improving the Efficacies of Photodynamic Diagnosis and Therapy of Cancer

Ogbonna Sochi Judith

December 2023

Graduate School of Engineering,

Osaka University

Supervisor:

Assoc. Prof. HAZAMA Hisanao
(Medical Beam Physics Laboratory)

Assistant Supervisors:

Prof. MURATA Isao
(Quantum Reaction Engineering Laboratory)

Prof. SATO Fuminobu
(Quantum Beam and Biomaterials Engineering Laboratory)

Abstract

It is well known that cancer is one of the leading causes of death in the world. Early diagnosis and treatment are key to successful cancer treatment and reduced mortality. Various research on improving existing cancer diagnosis and treatment techniques and novel methods for treatment and diagnosis are increasing. One method that is becoming widespread owing to its high selectivity and minimal invasiveness is the photodynamic diagnosis (PDD) and photodynamic therapy (PDT). This technique exploits the reaction of photosensitzer and oxygen induced by light. Understanding the mechanism of the photodynamic processes and monitoring factors such as the concentration of the photosensitizer and the oxygen, the singlet oxygen yield, and the light fluence to the target area are important for efficient PDD and PDT. However, the direct monitoring of these factors during the diagnosis and treatment can be complex. As an alternative, studying the photosensitizer photobleaching is useful in implicitly monitoring these factors.

The analysis performed in this study aims to improve the diagnosis and treatment of PDD and PDT. It has been focused on the analyses of protoporphyrin IX (PpIX) photobleaching and the formation of its photoproducts, which would help improve the dosimetry estimation. PpIX photobleaching has been previously studied using fluorescence spectroscopy. However, the effect of the environment on the PpIX fluorescence quantum yield and the similar optical properties of PpIX with its photoproducts lead to discrepancies in the results of fluorescence-based analyses.

In the first part of this work, fundamental spectra analyses of PpIX and the relationship between concentration and intensities were analysed using fluorescence, absorption, and mass spectrometry (MS). PpIX photobleaching under PDD and PDT conditions was analysed and compared using MS and fluorescence spectroscopy. MS is an analytical technique that identifies compounds based on chemical composition. Thus, it is suitable for quantitative analysis of photobleaching. The photobleaching rates were investigated based on the wavelength of the irradiation light and the fluence rate. The photobleaching rates obtained with the two analysis methods were compared, and the photobleaching coefficients were derived. The results demonstrated the variation in the MS-based PpIX photobleaching coefficient from the fluorescence-based analysis. The difference may be attributed to the change in the fluorescence quantum yield of PpIX with its environment and the effect of fluorescence emission from the PpIX photoproducts, which affects the fluorescence-based analysis.

The second part of the study analyses the effects of 405 or 635 nm irradiation wavelengths and fluence rate on the formation of the PpIX photoproducts. Differences in the photoproducts formed with the PpIX irradiation wavelength were noted. The characterisation of the photoproducts was

attempted, and hypotheses were made for their formation mechanism. The results showed that PpIX photoproducts are primarily formed directly from PpIX by reacting with oxygen. The 635 nm irradiation of PpIX produced the hydroxyaldehyde photoproduct, photoprotoporphyrin, while the 405 nm irradiation of PpIX potentially yielded the formyl photoproduct, product II. The effect of the fluence rate on the amount of photoproducts formed was also observed. Since some studies have shown that some PpIX photoproducts may be used as photosensitizers, these observations would be beneficial.

In the last part of the dissertation, investigations were made to determine the potential use of PpIX photoproducts for the improved detection of deeply located tumours. The concept of fluorescence photoswitching was introduced. Fluorescence photoswitching aims to increase the fluorescence detection intensity and extend the fluorescence observation time during PDD of deeply located tumours by utilising fluorescence obtained by exciting the photosensitizer followed by the photoproducts. Fluorescence photoswitching using PpIX was investigated in solution, *ex vivo* using porcine mucosa, and *in vivo* performed in a tumour-bearing mouse. It was noted that depending on the irradiation fluence rate, fluorescence intensity similar to or even higher than the initial fluorescence emission from PpIX can be obtained with fluorescence photoswitching. Thus, there is a prospective use of fluorescence photoswitching for extending the fluorescence observation time for the PDD of deeply located tumours.

The differences between MS-based photobleaching and fluorescence-based photobleaching highlight the importance of recognising the potential significance of these discoveries in the PDD and PDT dosimetry and efficacy. Photobleaching rates and photoproduct formation rates vary with irradiation laser wavelength as well as the fluence rate. This information can be manipulated for improved treatment and tumour detection. Additionally, this work sets an antecedent for exploring the use of photoproducts for the dosimetry estimation as well as diagnosis and treatment.

Table of Contents

Abstract ----------i

Table of Contents ----------iii

List of Figures----------vii

List of Tables ----------xi

Chapter 1: Introduction ---------- 1

1.1. Photodynamic diagnosis and photodynamic therapy as a method for cancer diagnosis and treatment ----------1

1.2. Photosensitizers ---------- 2

1.3. Photobleaching and photoproducts of the photosensitizer as an implicit dosimetry 3

1.4 Aim of study ---------- 4

1.5. Outline of dissertation ---------- 4

Chapter 2: Basic analyses of the photosensitizer, protoporphyrin IX ---------- 8

2.1. Introduction ---------- 8

2.2. Materials and methods ---------- 9

2.2.1. Fluorescence analysis ---------- 9

2.2.2. Absorption analysis ---------- 9

2.2.3. Mass spectrometry analysis ---------- 9

2.3. Results and Discussion ----------11

2.3.1. Fluorescence analysis ----------11

2.3.2. Absorption analysis ----------13

2.3.3. Mass spectrometry analysis ----------14

2.4. Chapter conclusion----------16

Chapter 3: Analysis of protoporphyrin IX photobleaching ---------- 18

3.1. Introduction ----------18

3.2. Materials and methods ----------19

3.2.1. PpIX irradiation for photobleaching ----------19

3.2.2. Fluorescence analysis of photobleaching ----------20

3.2.3. MS analysis of photobleaching ----------20

3.3 Results ----------21
3.3.1. Fitting of the photobleaching curves ----------21
3.3.2. Fluorescence analysis of photobleaching ----------21
3.3.3. MS-based analyses of the PS photobleaching ----------24
3.4. Discussion ----------28
3.5. Chapter conclusion ----------30

Chapter 4: Analysis of protoporphyrin IX photoproducts ---------- 34
4.1. Introduction ----------34
4.2. Materials and methods ----------36
4.2.1. PpIX irradiation for photoproduct formation ----------36
4.2.2. Fluorescence analysis of photoproducts ----------36
4.2.3. MS analysis of the photoproducts ----------36
4.2.4. Absorption analysis of photoproducts ----------36
4.2.5. High-Performance Liquid Chromatography (HPLC) analysis of the photoproducts ----------36
4.3. Results ----------37
4.3.1. Photoproduct formation under red light irradiation of PpIX ----------37
4.3.2. Photoproduct formation under blue light irradiation of PpIX ----------46
4.4. Discussion ----------48
4.5 Chapter conclusion ----------53

Chapter 5: Photoproducts of PpIX for PDD of deeply located tumours ---------- 57
5.1. Introduction ----------57
5.5.1. Concept of fluorescence photoswitching ----------58
5.2. Materials and methods ----------59
5.2.1. Photoproducts detection with excitation wavelength ----------59
5.2.2. Solution analysis ----------59
5.2.3. Fluorescence imaging setup ----------60
5.2.4. Pellet preparation ----------61
5.2.5. *Ex vivo* analysis ----------61
5.2.6. *In vivo* analysis ----------61
5.3. Results ----------62

5.3.1. Photoproducts detection with excitation wavelength----------62
5.3.2. Fluorescence spectroscopic analysis----------63
5.3.3. Fluorescence imaging *ex vivo*----------65
5.3.4. Fluorescence imaging *in vivo* ----------67
5.4. Discussion----------70
5.5. Chapter conclusion----------73

Conclusion----------76
Acknowledgements ----------78
Research Achievements ----------79

List of Figures

Chapter 1

1.1. Jablonski diagram illustrating the mechanisms of PDD and PDT. ISC: Intersystem crossing.

Chapter 2

2.1. Schematic of electrospray ionisation (ESI) quadrupole time-of-flight mass spectrometer (Q-TOF Ultima API, micromass, UK).

2.2. Fluorescence spectra of 100 μM PpIX diluted with acetonitrile, methanol, acetone, DMF, or DMSO, excited at a wavelength of 405 nm.

2.3. Fluorescence spectra of different concentrations of PpIX dissolved in DMSO, excited at 405 nm. The concentration ranged between 0.001 and 10000 μM.

2.4. (a) Fluorescence spectra of different concentrations of PpIX dissolved in DMSO, excited at 405 nm. (b) A plot of fluorescence intensity at 633 nm against PpIX concentration. The concentration ranged between 0.8 and 12 μM.

2.5. (a) Absorption spectra of different concentrations of PpIX dissolved in DMSO (b) A plot of absorption intensity at 407 nm against PpIX concentration. The concentration ranged between 0.8 and 12 μM.

2.6. (a) Mass spectra of different concentrations of PpIX solution (b) A plot of mass signal intensity at $[M+H]^+$ against PpIX concentration. The concentration ranged between 0.8 and 12 μM.

Chapter 3

3.1. Sample irradiation setup.

3.2. Fluorescence spectra of 405 nm irradiated PpIX, with increasing energy density for the irradiation fluence rates of (a) 10, (b) 50, and (c) 100 mW/cm^2. The fluorescence spectra were obtained at 405 nm excitation. The data were obtained from 3 independent experiments and averaged.

3.3. Fluorescence spectra of 635 nm irradiated PpIX, with increasing energy density for the fluence rate of (a) 10, (b) 50, and (c) 100 mW/cm^2. The fluorescence spectra were excited at 405 nm. The data were obtained from 3 independent experiments and averaged.

3.4. Relationships between PpIX fluorescence intensity and PD dose obtained at wavelengths of 633 nm for the fluence rates of 10, 50, and 100 mW/cm^2 and irradiation laser wavelength of

(a) 405 nm, and (b) 635 nm. The error bars indicate the standard deviation from 3 independent experiments.

3.5. Mass spectra of PpIX with increasing irradiation energy density. Irradiation was done with a 405 nm laser having a fluence rate of (a) 10 and (c) 100 mW/cm^2. The data were obtained from 3 independent experiments and averaged.

3.6. Mass spectra of PpIX with increasing irradiation energy density. Irradiation was done with a 635 nm laser having a fluence rate of (a) 10 and (b) 100 mW/cm^2. The data were obtained from 3 independent experiments and averaged.

3.7. Relationships between PpIX concentration and PD dose obtained using MS. PpIX was irradiated at fluence rates of 10, 50, and 100 mW/cm^2 using a laser wavelength of (a) 405 nm and (b) 635 nm. The error bars indicate the standard deviation from 3 independent experiments.

Chapter 4

4.1. Basis spectra used in SVD fitting of acquired spectra. Spectra A–E have an area under the curve between 610 nm and 750 nm, equal to one. The amplitude of F is such that its addition to spectrum A will shift A by 1 nm.

4.2. Fluorescence spectra of PpIX before and after irradiation with a 635 nm laser and energy density of 100 J/cm^2 at the irradiation fluence rates of (a) 10 mW/cm^2 (F_{R10}) and (b) 100 mW/cm^2 (F_{R100}). The fluorescence spectra were obtained at 405 nm excitation.

4.3. Fluorescence intensity of 635 nm irradiated PpIX, monitored at 673 nm with increasing irradiation energy density. PpIX was irradiated at fluence rates of 10 and 100 mW/cm^2. The intensities at 673 nm were corrected to exclude the PpIX fluorescence intensities. The error bars indicate the standard deviation from at least 3 independent experiments.

4.4. Mass spectra of PpIX before and after 635 nm irradiation with an energy density of 100 J/cm^2 at the irradiation power densities of (a) 10 mW/cm^2 (M_{R10}) and (b) 100 mW/cm^2 (M_{R100}). The inset shows the mass spectra zoomed in around *m*/*z* 595.3, where the new peaks were observed.

4.5. Mass signal intensity with increasing irradiation energy density obtained (a) *m*/*z* 563.3 and (b) *m*/*z* 595.3 of PpIX irradiated with a 635 nm laser at fluence rates of 10 and 100 mW/cm^2. The error bars indicate the standard deviation from at least 3 independent experiments. The average intensity of the solvent for the *m*/*z* analysed is displayed in a dashed line.

4.6. (a) Absorption spectra of PpIX before and after irradiation with 635 nm laser. PpIX was irradiated for 100 J/cm^2 at fluence rates of 10 and 100 mW/cm^2. (b) Difference spectra of irradiated PpIX in (a). The spectrum of PpIX before irradiation was subtracted from the spectra after irradiation.

4.7. Total ion chromatogram (TIC) and extracted ion chromatogram (EIC) of PpIX (a) before and (b) 100 J/cm^2 irradiation at *m*/*z* 563.265 and *m*/*z* 595.255. PpIX was irradiated with a 635 nm light at 10 mW/cm^2. NL: Normalization Level.

4.8. Mass spectra at the chromatographic Peaks A, B, and C.

4.9. LC/MS/MS spectra of 635 nm irradiated PpIX at *m*/*z* 595.255 for the chromatographic peaks A–C. The collision energy was 60 eV.

4.10. Fluorescence spectra of PpIX before and after irradiation with a 405 nm laser for 1 and 2 J/cm^2 for the fluence rates of (a) 10 and (b) 100 mW/cm^2.

4.11. Mass spectra of PpIX before and after 405 nm irradiation with an energy density of 1 J/cm^2 at the irradiation power densities of (a) 10 mW/cm^2 (M_{B10}) and (b) 100 mW/cm^2 (M_{B100}).

4.12. (a)Absorption spectra of PpIX before and after irradiation with 405 nm laser. PpIX was irradiated for 2 J/cm^2 at fluence rates of 10 and 100 mW/cm^2. (b) Difference spectra of irradiated PpIX in (a). The spectrum of PpIX before irradiation was subtracted from the spectra after irradiation.

4.13. Structures of the hydroxyaldehyde photoproducts and their reaction scheme.

4.14. Structures of formyl-type photoproducts and their reaction scheme.

Chapter 5

5.1. Concept of fluorescence photoswitching.

5.2. Optical setup for fluorescence imaging.

5.3. Fluorescence spectra of 635 nm irradiated PpIX at a fluence rate of 10 mW/cm^2 for 20 J/cm^2. The fluorescence spectra were obtained for excitations at 405, 450, 514, and 532 nm.

5.4. Fluorescence spectra of PpIX (a) before, and (b) after irradiation with a 505 nm light at fluence rate of 20 mW/cm^2, and (c) after irradiation with a 505 nm light at fluence rate of 50 mW/cm^2. The fluorescence spectra were obtained at excitation wavelengths of 450 nm and 505 nm. The error bars represent standard deviations for 3 independent experiments.

5.5. Fluorescence intensity of 505 nm irradiated PpIX, monitored at peak intensities of 633 and 673 nm for irradiation fluence rates of (a) 20, and (b) 50 mW/cm^2. PpIX was excited at 505 nm (I_G) and 450 nm (I_B). The error bars represent standard deviations from 3 independent experiments. The point at which I_B and I_G crosses indicates the point of fluorescence photoswitching.

5.6. (a) Fluorescence images of the PpIX pellet within porcine mucosa with increasing irradiation. (b) A plot of fluorescence intensity of the PpIX pellet within the porcine mucosa vs irradiation energy density. (c) Fluorescence images of the pellet, outside the mucosa, before and after irradiation. The pellets were irradiated at 505 nm, while the fluorescence emissions were obtained at excitations of 455 and 505 nm.

5.7. A section view of the mucosa which was used in the *ex vivo* analysis. The depth at which the mucosa was placed was calculated by averaging the measured depths.

5.8. Fluorescence emission images of ALA-HCl-administered PC-3 tumour-bearing mouse with increasing irradiation. Irradiation was performed with a 505 nm LED. The fluorescence images were obtained at intervals for excitation wavelength of 505 nm (I_G) and 455 nm (I_B).

5.9. Images of the ALA-HCl administered lesion before and after irradiation with a 505 nm LED for 9.6 J/cm^2. The images were obtained with white light, 505 nm, and 455 nm excitation wavelengths. The skin of the mouse was sewn back in place before acquiring the images after irradiation.

5.10. A section view of the lesion used in the *in vivo* analysis. The lesion has been H&E stained for easier observation of the tumour size.

List of Tables

Chapter 2

2.1. Chemical information of protoporphyrin IX.

2.2. Measurement conditions of Q-TOF for PpIX analyses.

Chapter 3

3.1. Photobleaching coefficient of PpIX obtained with fluorescence-based and MS-based analyses. The values are measured at the PDD conditions using a laser with a wavelength of 405 nm and at the PDT conditions using a laser with a wavelength of 635 nm. Irradiation power densities of 10, 50, and 100 mW/cm^2 were investigated for both laser wavelengths.

Chapter 5

5.1. Summary of the results of the fluorescence photoswitching analysis. I_B and I_G indicate fluorescence intensity obtained at blue-light (450 or 455 nm) and green-light (505 nm) excitation, respectively.

Chapter 1
Introduction

1.1. Photodynamic diagnosis and photodynamic therapy as a method for cancer diagnosis and treatment

Cancer is one of the leading causes of death globally, with an estimated one in five deaths caused by cancer. Early diagnosis and complete removal of tumours play a significant role in successful cancer treatment and reduced mortality. Thus, research on improving existing cancer diagnosis and treatment techniques and novel methods for treatment and diagnosis are increasing in different parts of the world. One method that is promising and becoming widespread owing to high selectivity and minimal invasiveness is the photodynamic diagnosis (PDD) and photodynamic therapy (PDT) [1–8]. The technique utilises the photochemical reaction of a photosensitizer in the presence of oxygen. Administration of photosensitizer into the body leads to its selective accumulation in cancer cells. The photochemical reaction of the photosensitizer is activated with light having the absorption characteristic of the photosensitizer.

When a photosensitizer is irradiated, the following electronic transitions occur;

1 The ground state photosensitizer (S_0) absorbs energy and moves to a singlet excited state (S_1).
2 A fraction of S_1 photosensitizer moves back to S_0 via non-reactive relaxation (energy is transferred into vibration or rotation).
3 A fraction of S_1 photosensitizer moves back to S_0 by emitting photons (fluorescence).
4 A fraction of S_1 photosensitizer moves into a triplet excited state (T_1) (intersystem crossing).
5 A fraction of T_1 photosensitizer moves back to S_1 by emitting photons (phosphorescence).
6 Electron is transferred between a fraction of T_1 photosensitizer and an acceptor (including living tissue) to generate radicals.
7 A fraction of T_1 photosensitizer transfers energy to ground state oxygen, the photosensitizer moves back to S_0 and the ground state oxygen to a singlet excited state, producing reactive oxygen species, including singlet oxygen.

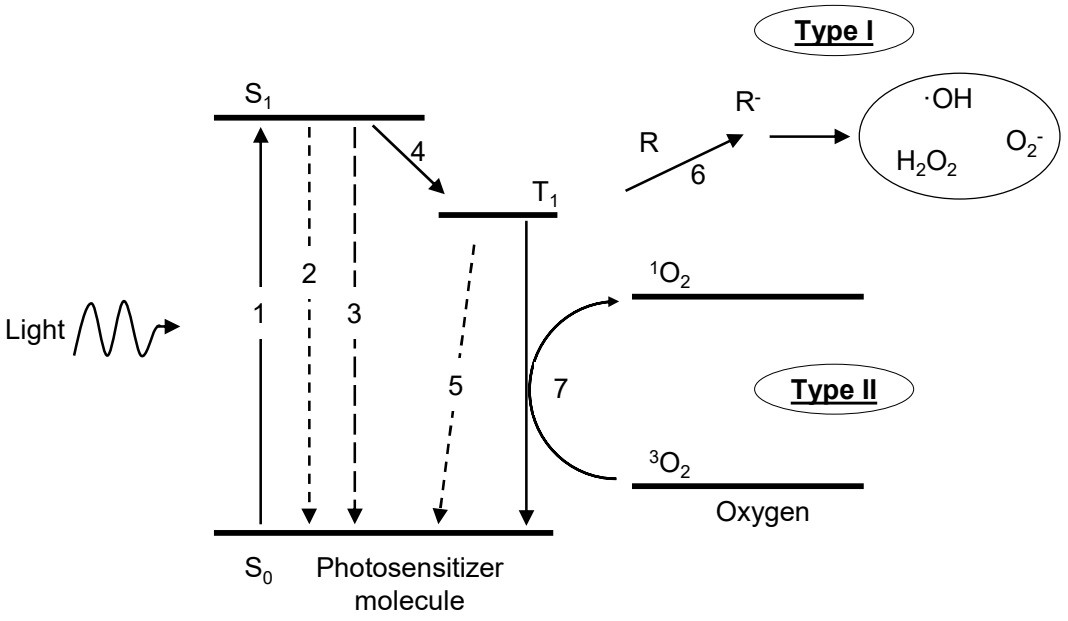

Figure 1.1: Jablonski diagram illustrating the mechanisms of PDD and PDT. ISC: Intersystem crossing.

The fluorescence emission (step 3) is used for fluorescence detection of tumours during PDD. PDT occurs at steps 6 and 7. The radicals generated in step 6 react with dissolved oxygen to generate oxygen-free radicals that damage targeted cells. This is called a Type I PDT process. The reactive oxygen species of step 7 kills target cells, leading to Type II PDT [9]. Type II process is considered the main cytotoxic factor during PDT [10]. PDD and PDT for certain types of lesions have received regulatory approval in some countries, such as Japan, the US, Canada, and parts of Europe like Germany, the Netherlands, and France [5,11,12].

1.2. Photosensitizers

Photosensitising agents are endogenous or exogenous compounds that transfer energy to neighbouring molecules when light of a specific wavelength is absorbed. They generate cytotoxic molecules such as singlet oxygen for targeted cell killing or emission of fluorescence for diagnosis upon excitation [3,4,13].

A good photosensitizer should have the following characteristics: i) little or no toxicity until activated with specific light, ii) high tumour selectivity, iii) easy elimination from the body, iv) relatively rapid clearance from normal tissues, and v) high triplet quantum yield, with efficient energy transfer to produce singlet oxygen [10,14,15]. Numerous types of photosensitizers can be employed in PDD and PDT. Chlorin e6 (Ce6) and its derivatives have been used in treating breast

cancer, bile duct carcinoma and hypopharyngeal cancer cells [16–18]. Application of porfimer sodium, talaporfin sodium, verteporfin and hematoporphyrin derivatives for lung, oesophagal, gastric, and uterine cervix cancer [12], and protoporphyrin IX (PpIX) in malignant glioma surgery as well as its fluorescence diagnosis and fluorescence diagnosis of bladder and prostate cancer [18,19] have been reported. PpIX induced from 5-aminolevulinic acid (ALA) is one of the photosensitizers widely used in PDD and PDT [18–22]. All discussions and analyses in this study have focused on PpIX-based PDD and PDT.

1.3. Photobleaching and photoproducts of the photosensitizer as an implicit dosimetry

Photosensitizer photobleaching

Monitoring and understanding the mechanism of the photodynamic processes are important for the diagnosis and treatment efficacy of PDD and PDT. During PDD and PDT, the concentration of the photosensitizer, the ground state oxygen, the singlet oxygen yield, and the light fluence to the target area need to be observed for dosimetry [23]. However, the direct monitoring of these factors during the diagnosis and treatment can be complex. Alternatively, photosensitizer photobleaching can be monitored as an implicit method for dosimetry analysis [2,24,25]. Photosensitizer photobleaching is the decrease in the concentration, absorption, or emission intensity of the photosensitizer with light irradiation [14,26]. The rate at which photobleaching occurs depends on most of the factors that need to be monitored. Thus, monitoring the photosensitizer photobleaching serves as a substitute.

Photoproducts

Photoproducts are formed concomitantly with photobleaching when photosensitizers are exposed to light. Photoproducts are compounds formed from the reaction of the photosensitizer with other molecules, such as radicals and oxygen, when irradiated [27,28]. Some of these photoproducts emit fluorescence when excited [20]. Photoproduct formation rates depend on internal factors similar to that of photobleaching [20,29]. Thus, studying the formation of the photosensitizer photoproducts could be a complementary approach for PDD and PDT dosimetry estimation.

Efficacy on PDD and PDT

The efficacy of PDD and PDT are affected by the photobleaching and the photoproducts of the

photosensitizer. A notable reduction in the concentration of PpIX induced by ALA has been seen during PDT [30,31]. The reduced concentration of the photosensitizer would result in the hindered production of cytotoxic species, thus progressively decreasing the effectiveness of PDT [32]. Additionally, reduced PpIX fluorescence emission intensity during PDD affects the diagnosis efficacy. Consequently, studies focusing on the analysis of the photosensitizer photobleaching and the formation of the photosensitizer photoproducts during the diagnosis and treatment process are important.

1.4. Aim of study

This study aims to improve the diagnosis and treatment of PDD and PDT. The analyses performed have been focused on the PpIX photobleaching and the formation of its photoproducts, which would be helpful in improving the dosimetry estimation. The occurrence of these phenomena under PDD and PDT conditions has been quantitatively analysed using fluorescence spectroscopy and mass spectrometry. The characterisation of the photoproduct and its utilisation as a photosensitizer for fluorescence diagnosis has been investigated.

1.5. Outline of dissertation

This study has been discussed in five chapters. In Chapter 2 of this write-up, the basic analysis of the target photosensitizer, PpIX and the relationship between concentration and intensities were analysed using fluorescence, absorption, and mass spectrometry (MS). Chapter 3 compares the PpIX photobleaching under PDD and PDT conditions using MS and fluorescence spectroscopy, and the photobleaching coefficients were derived. The formation of photoproducts from PpIX irradiations was investigated in Chapter 4. The effects of 405 or 635 nm irradiation wavelengths and fluence rate on the formation of the PpIX photoproducts were determined, and hypotheses were made for their formation mechanism. In Chapter 5, investigations aimed to improve the diagnostic efficacy of deeply located tumours were performed. The potential use of photoproducts for the fluorescence diagnosis of deeply located tumours was evaluated, which would lead to increased fluorescence observation time and intensity during the PDD. The final section discusses the overall conclusion of the study.

References

[1]. K. W. Teng and S. H. Lee, “Characterization of Protoporphyrin IX Species in Vitro Using Fluorescence Spectroscopy and Polar Plot Analysis,” *Journal of Physical Chemistry B*,

123(27), 5832–5840 (2019).

[2]. K. Huang, L. Chen, S. Lv, and J. Xiong, "Protoporphyrin IX photobleaching of subcellular distributed sites of leukemic HL60 cells based on ALA-PDT in vitro," *Journal of Biomedical Science and Engineering*, **05**(09), 548–555 (2012).

[3]. S. G. Bown and H. Stepp, "Photodynamic diagnosis and therapy - How bright is the future?," *Photonics and Lasers in Medicine*, **4**(1), 1–3 (2015).

[4]. C. Af Klinteberg, A. M. K. Enejder, I. Wang, S. Andersson-Engels, S. Svanberg, and K. Svanberg, "Kinetic fluorescence studies of 5-aminolaevulinic acid-induced protoporphyrin IX accumulation in basal cell carcinomas," *Journal of Photochemistry and Photobiology B: Biology*, **49**(2–3), 120–128 (1999).

[5]. T. Nakamura and T. Oinuma, "Usefulness of photodynamic diagnosis and therapy using talaporfin sodium for an advanced-aged patient with inoperable gastric cancer (a secondary publication)," *Laser Therapy*, **23**(3), 201–210 (2014).

[6]. K. Kishi, Y. Fujiwara, M. Yano, M. Motoori, K. Sugimura, M. Ohue, S. Noura, S. Marubashi, H. Takahashi, and M. Sakon, "Diagnostic laparoscopy with 5-aminolevulinic-acid-mediated photodynamic diagnosis enhances the detection of peritoneal micrometastases in advanced gastric cancer," *Oncology (Switzerland)*, **87**(5), 257–265 (2014).

[7]. T. Namikawa, T. Yatabe, K. Inoue, T. Shuin, and K. Hanazaki, "Clinical applications of 5-aminolevulinic acid-mediated fluorescence for gastric cancer," *World Journal of Gastroenterology*, **21**(29), 8817–8825 (2015).

[8]. N. W. Nompumelelo Simelane, C. A. Kruger, and H. Abrahamse, "Photodynamic diagnosis and photodynamic therapy of colorectal cancer: In vitro and in vivo," *RSC Advances*, **10**(68), 41560–41576 (2020).

[9]. C. H. Sibata, V. C. Colussi, N. L. Oleinick, and T. J. Kinsella, "Photodynamic therapy in oncology," *Expert opinion on pharmacotherapy*, **2**(6), 917–927 (2001).

[10]. H. Abrahamse and M. R. Hamblin, "New photosensitizers for photodynamic therapy," *The Biochemical Journal*, **473**(4), 347 (2016).

[11]. G. Gunaydin, M. E. Gedik, and S. Ayan, "Photodynamic Therapy for the Treatment and Diagnosis of Cancer–A Review of the Current Clinical Status," *Frontiers in Chemistry*, **9**, 686303 (2021).

[12]. T. Oinuma, T. Nakamura, and Y. Nishiwaki, "Report on the National Survey of Photodynamic Therapy (PDT) for Gastric Cancer in Japan (a secondary publication),"

Laser Therapy, **25**(2), 87 (2016).

[13]. J. O. Yoo and K. S. Ha, "New Insights into the Mechanisms for Photodynamic Therapy-Induced Cancer Cell Death," *International Review of Cell and Molecular Biology*, **295**, 139–174 (2012).

[14]. R. Bonnett and G. Martínez, "Photobleaching of sensitisers used in photodynamic therapy," *Tetrahedron*, **57**(47), 9513–9547 (2001).

[15]. R. R. Allison and K. Moghissi, "Photodynamic Therapy (PDT): PDT Mechanisms," *Clinical Endoscopy*, **46**(1), 24 (2013).

[16]. K. Kasuya, M. Shimazu, M. Suzuki, Y. Kuroiwa, J. Usuda, T. Itoi, A. Tsuchida, and T. Aoki, "Novel photodynamic therapy against biliary tract carcinoma using mono-L: -aspartyl chlorine e6: basic evaluation for its feasibility and efficacy," *Journal of hepato-biliary-pancreatic sciences*, **17**(3), 313–321 (2010).

[17]. A. Fernando and J. Gariépy, "Coupling Chlorin e6 to the surface of Nanoscale Gas Vesicles strongly enhance their intracellular delivery and photodynamic killing of cancer cells," *Scientific Reports*, **10**(1), (2020).

[18]. A. Escudero, C. Carrillo-Carrión, M. C. Castillejos, E. Romero-Ben, C. Rosales-Barrios, and N. Khiar, "Photodynamic therapy: photosensitizers and nanostructures," *Materials Chemistry Frontiers*, **5**(10), 3788–3812 (2021).

[19]. T. Nakayama, S. Otsuka, T. Kobayashi, H. Okajima, K. Matsumoto, Y. Hagiya, K. Inoue, T. Shuin, M. Nakajima, T. Tanaka, and S. I. Ogura, "Dormant cancer cells accumulate high protoporphyrin IX levels and are sensitive to 5-aminolevulinic acid-based photodynamic therapy," *Scientific reports*, **6**, (2016).

[20]. S. Bagdonas, L. W. Ma, V. Iani, R. Rotomskis, P. Juzenas, and J. Moan, "Phototransformations of 5-Aminolevulinic Acid–induced Protoporphyrin IX in vitro: A Spectroscopic Study," *Photochemistry and Photobiology*, **72**(2), 186–192 (2000).

[21]. I. Buzalewicz, I. Hołowacz, A. Ulatowska-Jarża, and H. Podbielska, "Towards dosimetry for photodynamic diagnosis with the low-level dose of photosensitizer," *Journal of Photochemistry and Photobiology B: Biology*, **173**, 333–343 (2017).

[22]. T. Hirano, Y. Hagiya, H. Fukuhara, K. Inoue, T. Shuin, K. Matsumoto, K. Inoue, T. Tanaka, I. Okura, and S. I. Ogura, "Improvement of aminolevulinic acid (ALA)-mediated photodynamic diagnosis using n-propyl gallate," *Photodiagnosis and Photodynamic Therapy*, **10**(1), 28–32 (2013).

[23]. I. Georgakoudi and T. H. Foster, "Singlet Oxygen-Versus Nonsinglet Oxygen-Mediated

Mechanisms of Sensitizer Photobleaching and Their Effects on Photodynamic Dosimetry," *Photochemistry and Photobiology*, **67**(6), 612–625 (1998).

[24]. J. S. Dysart and M. S. Patterson, "Photobleaching kinetics, photoproduct formation, and dose estimation during ALA induced PpIX PDT of MLL cells under well oxygenated and hypoxic conditions," *Photochemical and Photobiological Sciences*, **5**(1), 73–81 (2006).

[25]. K. Efendiev, P. Alekseeva, A. Shiryaev, A. Voitova, K. Linkov, T. Pisareva, I. Reshetov, and V. Loschenov, "Near-infrared phototheranostics of tumors with protoporphyrin IX and chlorin e6 photosensitizers," *Photodiagnosis and Photodynamic Therapy*, **42**, 103566 (2023).

[26]. B. C. Wilson, M. S. Patterson, and L. Lilge, "Implicit and explicit dosimetry in photodynamic therapy: A new paradigm," *Lasers in Medical Science*, **12**(3), 182–199 (1997).

[27]. L. Ma, S. Bagdonas, and J. Moan, "The photosensitizing effect of the photoproduct of protoporphyrin IX," *Journal of Photochemistry and Photobiology B: Biology*, **60**(2–3), 108–113 (2001).

[28]. L. Brancaleon and H. Moseley, "Effects of photoproducts on the binding properties of protoporphyrin IX to proteins," *Biophysical Chemistry*, **96**(1), 77–87 (2002).

[29]. J. Moan, G. Streckyte, S. Bagdonas, Ø. Bech, and K. Berg, "Photobleaching of protoporphyrin IX in cells incubated with 5-aminolevulinic acid," *International Journal of Cancer*, **70**, 90–97 (1997).

[30]. J. C. Finlay, D. L. Conover, E. L. Hull, and T. H. Foster, "Porphyrin Bleaching and PDT-induced Spectral Changes are Irradiance Dependent in ALA-sensitized Normal Rat Skin In Vivo," *Photochemistry and Photobiology*, **73**(1), 54–63 (2001).

[31]. D. J. Robinson, H. S. De Bruijn, N. Van Der Veen, M. R. Stringer, S. B. Brown, and W. M. Star, "Fluorescence Photobleaching of ALA-induced Protoporphyrin IX during Photodynamic Therapy of Normal Hairless Mouse Skin: The Effect of Light Dose and Irradiance and the Resulting Biological Effect," *Photochemistry and Photobiology*, **67**(1), 140–149 (1998).

[32]. D. J. Robinson, M. R. Stringer, and W. R. Crum, "Rate-equation analysis of Protoporphyrin IX photo-oxidation," *Photochemotherapy: Photodynamic Therapy and Other Modalities*, **2625**, 413–418 (1996).

Chapter 2
Basic analyses of the photosensitizer, protoporphyrin IX

2.1. Introduction

Protoporphyrin IX (PpIX) is a natural intermediate in the heme synthesis pathway and a photosensitizer generated from 5-aminolevulinic acid (ALA). ALA is a natural amino acid found in many animals and plants and is metabolised in the body to produce PpIX [1,2]. PpIX falls under the porphyrin-type photosensitizer, which is stable, has a high singlet oxygen quantum yield, and a wide absorption band [3]. Table 2.1 shows the chemical structure and the chemical information of PpIX.

Table 2.1 Chemical information of protoporphyrin IX.

Chemical Formula	$C_{34}H_{34}N_4O_4$
Chemical Structure	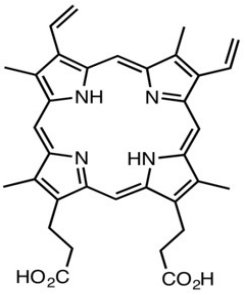
Monoisotopic Mass [u]	562.258
Molecular Mass [g/mol]	562.658

In this chapter, fluorescence, absorption and mass spectrometry analysis of PpIX in solution were performed as a basis for the analysis that would be performed in other chapters. The relationships between intensity and PpIX concentration were investigated.

2.2. Materials and methods

The PpIX used for the analyses was acquired from Sigma-Aldrich (P8293, USA). All analyses were performed in a dark room to avoid the photoreaction of PpIX.

2.2.1. Fluorescence analysis

Solvent suitability

The suitable solvent for PpIX was investigated by diluting PpIX in acetonitrile, methanol, acetone, dimethylformamide (DMF), or dimethylsulfoxide (DMSO). PpIX was diluted to 100 µM using each of the solvents. Each diluted PpIX was placed in the wells of a clear-bottomed black 96-well plate (353219, Falcon, USA). The fluorescence emissions from the PpIX were measured using a fluorescence microplate reader (Spectra Max Gemini EM, Molecular Devices, USA), with the emission intensities detected from the bottom of the well plate. A xenon flash lamp was used to excite the samples at 405 nm, and the fluorescence emissions were recorded between 550 and 750 nm.

Relationship between concentration and fluorescence intensity

PpIX was dissolved in DMSO to a concentration ranging from 0.001 µM to 10 mM. The PpIX solutions were placed in the 96-well plate and analysed using the fluorescence microplate reader excited at 405 nm. The fluorescence emissions were recorded between 550 and 750 nm. A similar analysis was conducted for PpIX concentration between 0.8 and 12 µM.

2.2.2. Absorption analysis

PpIX was dissolved to a concentration ranging between 0.8 and 12 µM with DMSO. Each concentration of PpIX was placed in a glass cuvette with an optical path length of 1 mm and analysed using a UV-visible spectrophotometer (Hitachi, U-3500). The absorption intensities were recorded between 400 and 800 nm.

2.2.3. Mass spectrometry analysis

PpIX was dissolved in DMSO to a concentration between 0.8 and 12 µM. The PpIX solutions were further diluted to 1/100th of the initial concentration with a solution of liquid chromatography-mass spectrometry grade methanol (34966, Honeywell, Germany) and water (39253, Honeywell) (v/v 1:1) with 1 % acetic acid (00212-85, Nacalai Tesque, Japan). An electrospray ionisation (ESI)

quadrupole time-of-flight mass spectrometer (Q-TOF Ultima API, micromass, UK) was used in the positive ion mode to measure the mass spectra of each concentration. The schematic of the Q-TOF mass spectrometer is shown in Fig.2.1. For the acquisition, the sample injection flow rate was 5 μL/min, and the mass spectra were measured every 0.34 s with an interval of 0.1 s. The signals obtained were integrated for 3 minutes. Other measurement conditions used are summarised in Table 2.2.

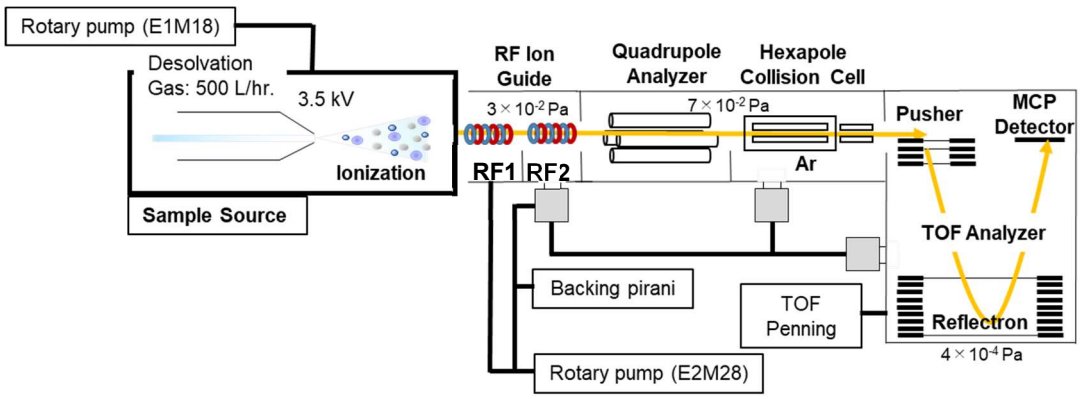

Figure 2.1: Schematic of electrospray ionisation (ESI) quadrupole time-of-flight mass spectrometer (Q-TOF Ultima API, micromass, UK).

Table 2.2 Measurement conditions of Q-TOF for PpIX analyses.

Capillary [kV]	3.5
Radiofrequency (RF) Lens 1 [V]	100
Source Temp [°C]	80
Desolvation Temp [°C]	150
Acceleration voltage for Time of Flight [kV]	9.1
Voltage applied to the Micro Channel Plate (MCP) [V]	2200

2.3. Results and Discussion

2.3.1. Fluorescence analysis

The fluorescence emission spectra of 100 µM PpIX dissolved in acetonitrile, methanol, acetone, DMF, or DMSO, under excitation in the Soret band, are shown in Fig. 2.2. The fluorescence spectrum shape of PpIX diluted with acetonitrile, acetone, DMF, and DMSO (Fig. 2.2) conforms with that reported in other studies [2,4–6]. The fluorescence spectrum of PpIX has a maximum peak at around 633 nm and a shoulder at 710 nm. Amongst the solvents investigated, PpIX diluted with DMSO had the highest fluorescence intensity. Thus, all further analyses of PpIX were performed with dilution in DMSO.

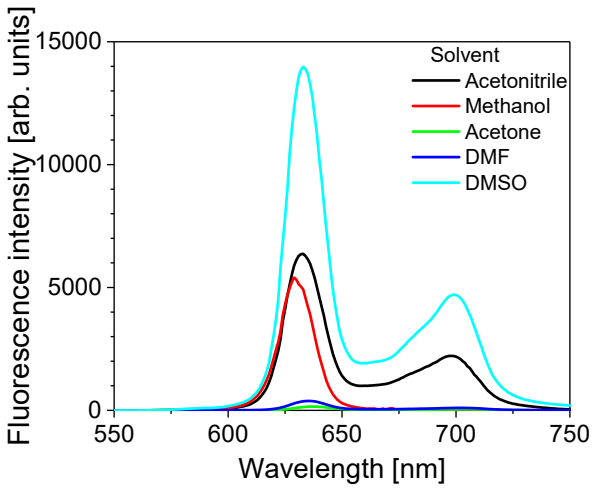

Figure 2.2: Fluorescence spectra of 100 µM PpIX diluted with acetonitrile, methanol, acetone, DMF, or DMSO, excited at a wavelength of 405 nm.

Figure 2.3 shows the fluorescence spectra of PpIX diluted in DMSO at various concentrations between 0.001 µM and 10 mM. For concentrations up to 100 µM, an increase in concentration led to a rise in the fluorescence intensity. A similar fluorescence intensity as 100 µM was noted for 1 mM, and an increase in the concentration to 10 mM resulted in reduced fluorescence intensity. The ceased increase in the fluorescence intensity of PpIX above the concentration of 100 µM may be caused by the aggregation of PpIX. Factors such as concentration, pH, and solvents used can lead to PpIX aggregation [7–9]. With aggregation, reduced fluorescence and singlet oxygen quantum yield can occur [10,11].

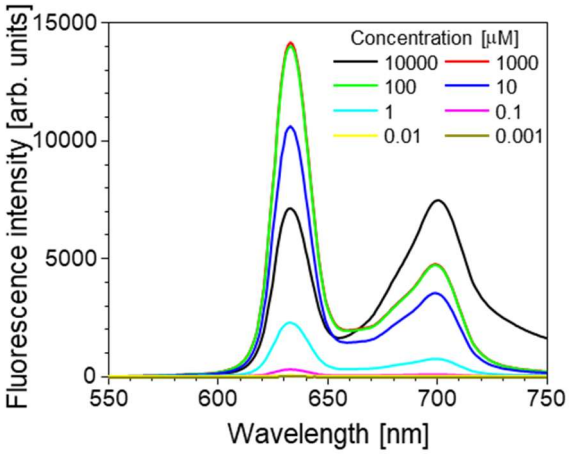

Figure 2.3: Fluorescence spectra of different concentrations of PpIX dissolved in DMSO, excited at 405 nm. The concentration ranged between 0.001 and 10000 μM.

At lower concentrations between 0.8 and 12 μM, a continuous rise in the fluorescence intensity with concentration was observed (Fig 2.4 (a)). The signal intensities at the 633 nm peak for each concentration were plotted in Fig. 2.4 (b). The obtained plot shows a nonlinear relationship between intensity and concentration. The nonlinearity could also be attributed to the effect of aggregation, as a similar effect has been reported [8]. Since the increase in the fluorescence intensity is not proportional to PpIX concentration, it is hard to obtain a relationship between the two. Hence, the fluorescence-based analysis performed in the rest of this work has been studied using its fluorescence intensity.

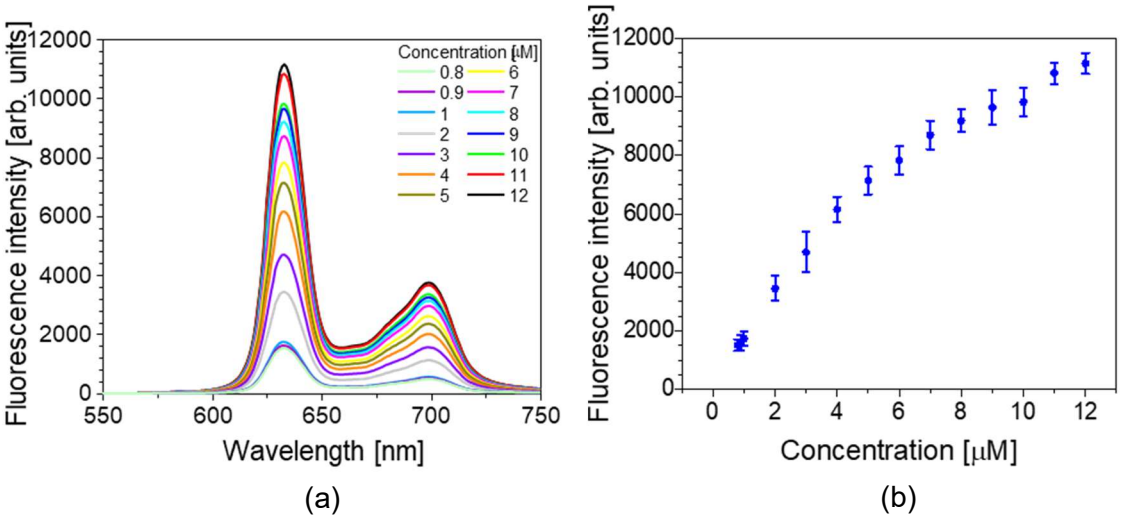

Figure 2.4: (a) Fluorescence spectra of different concentrations of PpIX dissolved in DMSO, excited at 405 nm. (b) A plot of fluorescence intensity at 633 nm against PpIX concentration. The concentration ranged between 0.8 and 12 μM.

2.3.2. *Absorption analysis*

Absorption spectra of PpIX with increasing concentration are shown in Fig. 2.5(a). The absorption spectra show a strong Soret absorption band at 407 nm and four peaks in the Q band at 505, 541, 575, and 630 nm. The peaks observed fall within the range seen in other studies [12,13]. The intensity of all peaks increased with increasing concentrations for the range of concentrations investigated. The intensity at 407 nm was plotted for each concentration, and the rise in the intensity was observed to be linear with increasing concentration (Fig. 2.5(b)). Using the Beer-Lambert equation ($A = \varepsilon lc$; A = absorbance, ε = molar extinction coefficient, l = optical path length, and c = concentration), ε was obtained for all concentrations. The molar extinction coefficient is a constant value for a particular compound. However, in the range of concentrations investigated, its value had a margin of error of $\pm\ 51\times10^3\ M^{-1}cm^{-1}$. Thus, there may be a slight effect of aggregation on the absorption result.

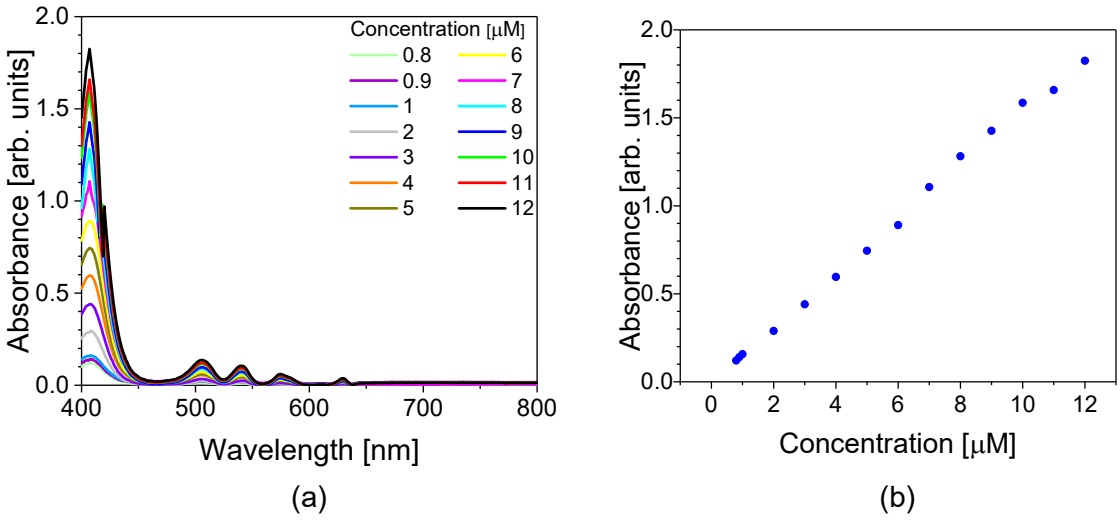

Figure 2.5: (a) Absorption spectra of different concentrations of PpIX dissolved in DMSO (b) A plot of absorption intensity at 407 nm against PpIX concentration. The concentration ranged between 0.8 and 12 μM.

2.3.3. *Mass spectrometry analysis*

The protonated ion peak, $[M+H]^+$, of PpIX at *m*/*z* 563.3 and its isotope peaks were seen in the mass spectra of various concentrations of PpX (Fig. 2.6(a)). The peak signal intensity of the monoisotopic ion of the protonated PpIX was plotted against concentration (Fig. 2.6(b)). The MS signal intensity rose linearly with concentration. A relationship between the signal intensity and concentration was obtained by fitting the plot linearly as,

$$\boldsymbol{I_{MS} = a + bC}, \qquad \boldsymbol{(2.1)}$$

where I_{MS} [arb. units] is the MS signal intensity of protonated PpIX at PpIX concentration C [μM], and a and b are constants. Each sample was measured twice to consider the variation in the signal intensity due to sample ionisation. The data used were obtained from at least 3 independent experiments and averaged.

Accordingly, a relationship,

$$\boldsymbol{I_{MS} = 13.2 + 101.2C}, \qquad \boldsymbol{(2.2)}$$

with $R^2 = 0.994$, was acquired by fitting Fig. 2.6(b).

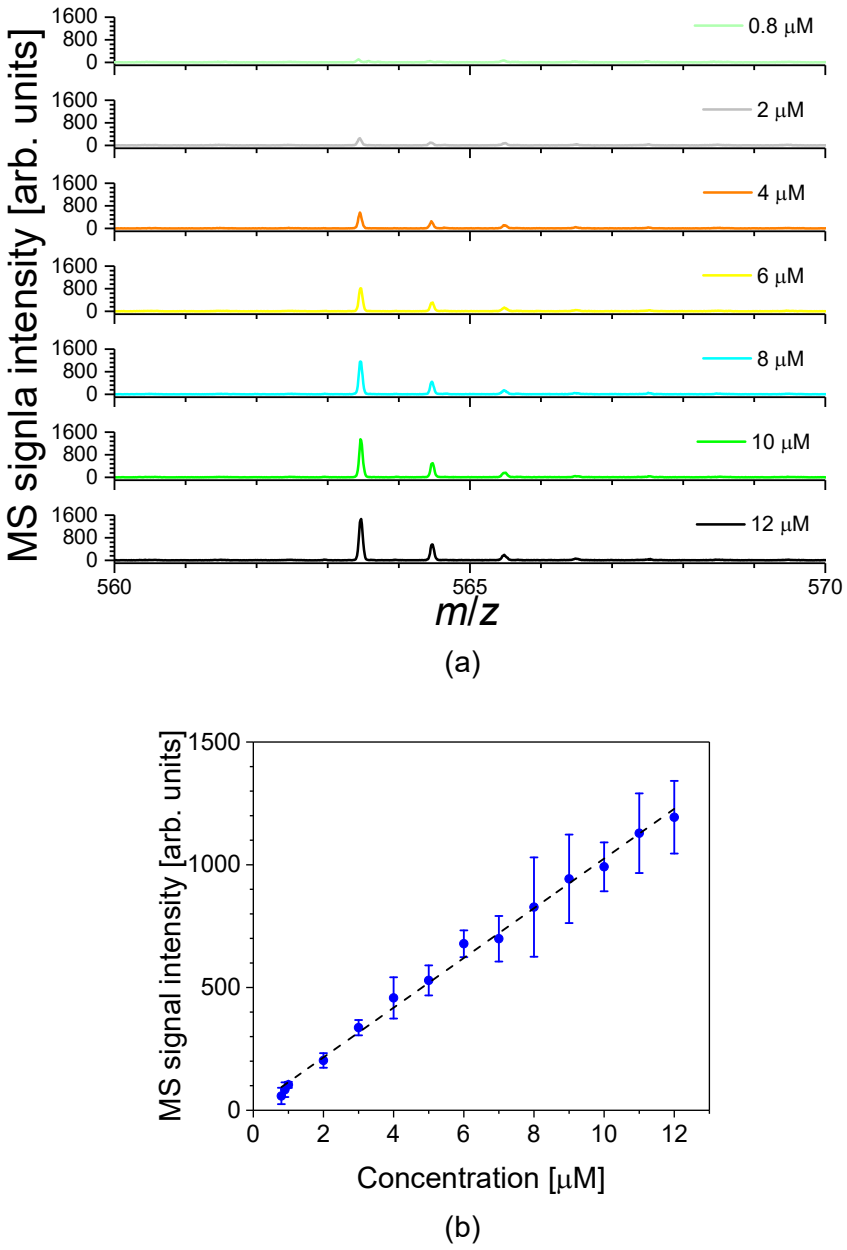

Figure 2.6: (a) Mass spectra of different concentrations of PpIX solution (b) A plot of mass signal intensity at $[M+H]^+$ against PpIX concentration. The concentration ranged between 0.8 and 12 μM.

2.4. Chapter conclusion

Spectral analysis of PpIX has been performed using fluorescence spectroscopy, absorption spectroscopy, and mass spectrometry. The changes in the intensities with concentrations were investigated, and observations were made that the fluorescence and the absorption-based analysis of PpIX may be affected by aggregation with increasing concentration. Thus, a relationship could not be derived in these analysis methods. On the other hand, a relationship between signal intensity and concentration was obtained in the MS analysis. The obtained relationship was used in determining the PpIX concentration during the photobleaching analysis.

References

[1]. Q. Peng, K. Berg, J. Moan, M. Kongshaug, and J. M. Nesland, "5-Aminolevulinic acid-based photodynamic therapy: Principles and experimental research," *Photochemistry and Photobiology*, **65**(2), 235–251 (1997).

[2]. S. Bagdonas, L. W. Ma, V. Iani, R. Rotomskis, P. Juzenas, and J. Moan, "Phototransformations of 5-Aminolevulinic Acid–induced Protoporphyrin IX in vitro: A Spectroscopic Study," *Photochemistry and Photobiology*, **72**(2), 186–192 (2000).

[3]. R. Bonnett and G. Martínez, "Photobleaching of sensitisers used in photodynamic therapy," *Tetrahedron*, **57**(47), 9513–9547 (2001).

[4]. K. Koenig and H. Schneckenburger, "Laser-induced autofluorescence for medical diagnosis," *Journal of Fluorescence*, **4**(1), 17–40 (1994).

[5]. L. Ma, S. Bagdonas, and J. Moan, "The photosensitizing effect of the photoproduct of protoporphyrin IX," *Journal of Photochemistry and Photobiology B: Biology*, **60**(2–3), 108–113 (2001).

[6]. J. S. Dysart and M. S. Patterson, "Photobleaching kinetics, photoproduct formation, and dose estimation during ALA induced PpIX PDT of MLL cells under well oxygenated and hypoxic conditions," *Photochemical and Photobiological Sciences*, **5**(1), 73–81 (2006).

[7]. K. W. Teng and S. H. Lee, "Characterization of Protoporphyrin IX Species in Vitro Using Fluorescence Spectroscopy and Polar Plot Analysis," *Journal of Physical Chemistry B*, **123**(27), 5832–5840 (2019).

[8]. R. Margalit, N. Shaklai, S. C.-B. Journal, and undefined 1983, "Fluorimetric studies on the dimerization equilibrium of protoporphyrin IX and its haemato derivative," *Biochemical Journal,* **209**, 547–552 (1983).

[9]. L. Monsù Scolaro, M. Castriciano, A. Romeo, S. Patanè, E. Cefalì, and M. Allegrini,

"Aggregation behavior of protoporphyrin IX in aqueous solutions: Clear evidence of vesicle formation," *Journal of Physical Chemistry B*, **106**(10), 2453–2459 (2002).

[10]. B. Myrzakhmetov, P. Arnoux, S. Mordon, S. Acherar, I. Tsoy, and C. Frochot, "Photophysical Properties of Protoporphyrin IX, Pyropheophorbide-a, and Photofrin® in Different Conditions," *Pharmaceuticals 2021, Vol. 14, Page 138*, **14**(2), 138 (2021).

[11]. L. Bezdetnaya, N. Zeghari, I. Belitchenko, M. Barberi-Heyob, J. L. Merlln, A. Potapenko, and F. Guillemin, "Spectroscopic and Biological Testing of Photobleaching of Porphyrins in Solutions," *Photochemistry and Photobiology*, **64**(2), 382–386 (1996).

[12]. D. W. Roberts, J. D. Olson, L. T. Evans, K. K. Kolste, S. C. Kanick, X. Fan, J. J. Bravo, B. C. Wilson, F. Leblond, M. Marois, and K. D. Paulsen, "Red-light excitation of protoporphyrin IX fluorescence for subsurface tumor detection," *Journal of Neurosurgery*, **128**(6), 1690–1697 (2018).

[13]. N. A. Markwardt, N. Haj-Hosseini, B. Hollnburger, H. Stepp, P. Zelenkov, and A. Rühm, "405 nm versus 633 nm for protoporphyrin IX excitation in fluorescence-guided stereotactic biopsy of brain tumors," *Journal of biophotonics*, **9**(9), 901–912 (2016).

Chapter 3
Analysis of protoporphyrin IX photobleaching

3.1. Introduction

Photosensitizer photobleaching is the decrease in the concentration of the photosensitizer (thus, the absorption and emission intensity of the photosensitizer) with light irradiation [1,2]. Photobleaching occurs due to the photo transformation of the photosensitizer when it reacts with reactive intermediates such as singlet oxygen [3]. Monitoring of the photosensitizer photobleaching serves as an implicit method of estimating the concentration of the photosensitizer, the ground state oxygen, the singlet oxygen yield, and the light fluence to the target area during PDD and PDT [4–6]. In addition, photobleaching of the photosensitizer affects the diagnostics and treatment efficacy of PDD and PDT. The reduced concentration of the photosensitizer would result in the hindered production of cytotoxic species, thus progressively reducing the effectiveness of PDT [7], and the reduced PpIX fluorescence emission intensity during PDD affects the diagnosis efficacy. Based on the above, studies focusing on the analysis of photosensitizer photobleaching during the diagnosis and treatment process are important.

Numerous analyses of the PpIX photobleaching have been performed [3–5,8–10]. These analyses have used fluorescence spectroscopy and other optical property measurement methods as their primary analysis method. Unfortunately, the dependence of the PpIX fluorescence quantum yield on its region of localisation *in vitro* and *in vivo* [3,5,10,11], the pH of the photosensitizer's surrounding [11,12], and the fluorescence emitted from photoproducts of the photosensitizers [13] lead to variations in the fluorescence-based analyses of the photobleaching.

In this chapter, we have investigated and compared the PpIX photobleaching analysed using fluorescence spectroscopy and mass spectrometry (MS). Analysis with mass spectrometry is hypothesised to offer higher accuracy than the fluorescence analysis method in that mass spectrometry identifies compounds based on their chemical composition. The factors affecting the fluorescence and other optical methods do not affect the MS analysis method. The photobleaching analyses were performed for PpIX in solution. A fixed concentration of PpIX solution was subjected to various irradiation conditions by changing the fluence rate and the irradiation energy density for laser wavelengths of 405 and 635 nm. The rate of reduction in the concentration or intensity of

PpIX for each irradiation condition was investigated using both mass spectrometry and fluorescence spectroscopy. The photobleaching with the irradiation power density and the photobleaching coefficients were compared and discussed for both methods. It is believed that studying the photobleaching in solution would be fundamental to understanding its mechanism in other conditions.

3.2. Materials and methods

3.2.1. PpIX irradiation for photobleaching

200 µL of PpIX diluted in DMSO to 10 µM was dropped per well into eleven wells of a clear-bottomed black 96-well plate (353219, Falcon, USA). The bottom of each well was irradiated using the conditions described below. The well plate temperature was maintained at 37 °C using a micro-warm plate (KM-1, As One, Japan) during the irradiation.

Photobleaching under PDD condition

The PpIX solutions were subjected to a 405 nm blue-violet laser for energy densities between 0 and 10 J/cm^2. The laser light was generated from a laser diode (VLM 500, Sumitomo Electric Industries, Japan), delivered through a multimode fibre (M29L01, Thorlabs).

Photobleaching under PDT condition

The PpIX solutions were subjected to irradiation energy density ranging from 0 to 100 J/cm^2. Each sample was irradiated using a red laser having a wavelength of 635 nm generated from a laser diode (HL6388MG, Thorlabs, USA) mounted on a temperature-controlled laser diode mount (TCLDM9, Thorlabs) and controlled with a laser diode controller (LDC205C, Thorlabs) and temperature controller (TED200C, Thorlabs). The current and temperature of the laser diode were set at 22.0 °C and 340 mA, respectively. The laser light was delivered through an optical fibre (M22L02, Thorlabs).

Three fluence rates, 10, 50, and 100 mW/cm^2, were investigated for both irradiation conditions. The laser power was measured using a power sensor (PD-300 UV, Ophir Optronics, Israel) with a filter attached to a display (Nova II, Ophir Optronics). The irradiation power densities were set at the bottom of the well plate using a variable neutral density filter (NDHN-50, Sigmakoki, Japan). The light was passed through an iris diaphragm (IH-50R-N, Sigmakoki, Japan) to maintain the light beam diameter before being cast to the bottom of the well. The laser irradiation time was controlled

by changing the position of the well plate using a two-axis motorised linear stage (SGSP26-150(XY), Sigmakoki, Japan) and a two-axis stage controller (SHOT-702, Sigmakoki). The schematic for the sample laser irradiation setup is shown in Fig. 3.1.

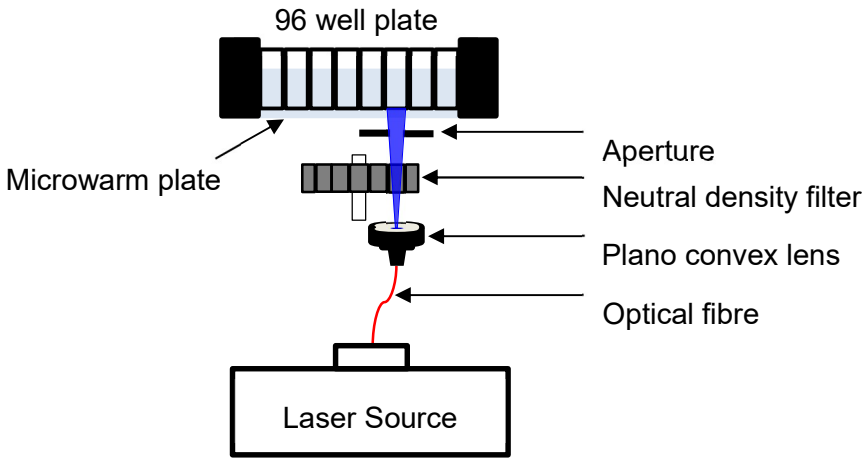

Figure 3.1: Sample irradiation setup.

3.2.2. *Fluorescence analysis of photobleaching*

The samples were maintained in the well plate, and the fluorescence emissions from the PpIX were measured using a fluorescence microplate reader (Spectra Max Gemini EM, Molecular Devices, USA), with the sample excitation at 405 nm, and the fluorescence emissions recorded between 550 and 750 nm. The temperature of the well plate was maintained at 37 °C during the fluorescence measurement.

3.2.3. *MS analysis of photobleaching*

The irradiated PpIX solutions were further diluted to one-hundredth of their concentration with liquid chromatography-mass spectrometry grade methanol (34966, Honeywell, Germany) and water (39253, Honeywell) mixed at a 1:1 volume ratio and 1% acetic acid (00212-85, Nacalai Tesque, Japan). The mass spectrometer with conditions described in Sec. 2.2.3 was used to obtain the mass spectrum of the irradiated PpIX. The obtained mass signal intensities of PpIX were converted to concentration using Eqn 2.2.

3.3. Results

3.3.1. Fitting of the photobleaching curves

The photobleaching of PpIX in solution follows a first-order photobleaching kinetics [14]. Thus, all the photobleaching curves were fitted using a single exponential with a relationship;

$$C \text{ or } I_F = Ae^{-\frac{D}{\beta}}, \tag{3.1}$$

where C [μM] and I_F [arb. units] are the concentration and the fluorescence intensity of PpIX, respectively, after laser irradiation with an energy density D [J/cm^2]. β [J/cm^2] is the photobleaching coefficient, and A is a constant. Work by Iinuma et al. reports the use of such a single exponential relationship for fitting the PpIX photobleaching [8].

3.3.2. Fluorescence analysis of photobleaching

Since our primary aim was to observe the spectral changes of PpIX with irradiation, no form of spectral decomposition was used in our analysis.

PpIX fluorescence spectra under PDD irradiation condition

The fluorescence spectra of PpIX irradiated with a 405 nm laser for the various fluence rates investigated are shown in Fig. 3.2. With irradiation, a decrease in the intensity at 633 and 710 nm was noted. The primary peak of PpIX at 633 nm was observed for the photobleaching of PpIX. With the increase in the irradiation energy density, there was a continuous reduction in the fluorescence intensity at 633 nm. PpIX irradiation also led to an intensity rise at 654 nm. For all fluence rates, the 654 nm intensity rises continually up until energy density between 4 and 6 J/cm^2, after which the intensity decreases. The intensity at 654 nm observed was higher for the irradiation fluence rate of 50 and 100 mW/cm^2 compared to that for the fluence rate of 10 mW/cm^2.

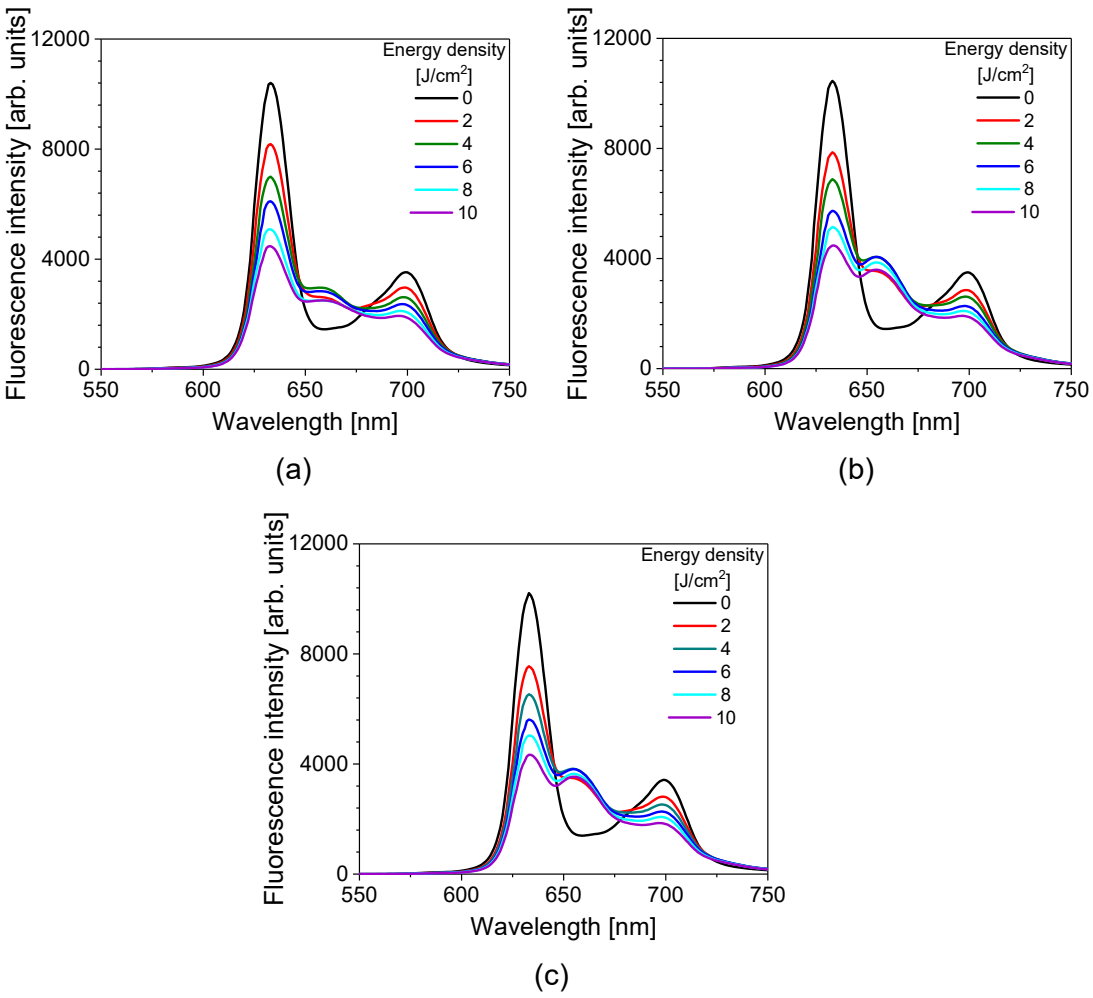

Figure 3.2: Fluorescence spectra of 405 nm irradiated PpIX, with increasing energy density for the irradiation fluence rates of (a) 10, (b) 50, and (c) 100 mW/cm^2. The fluorescence spectra were obtained at 405 nm excitation. The data were obtained from 3 independent experiments and averaged.

PpIX fluorescence spectra under PDT irradiation condition

The fluorescence spectra of PpIX irradiated at 635 nm with increasing energy density are shown in Fig. 3.3. Similar to PpIX irradiation with 405 nm, irradiation with 635 nm reduced PpIX intensities at 633 and 710 nm. However, different from the 405 nm irradiation of PpIX, a gradual increase in the fluorescence intensity is seen at 673 nm. This intensity continued to rise up to the maximum energy density investigated (100 J/cm^2). Higher fluorescence intensity at 673 nm was emitted with PpIX irradiation at a lower fluence rate (compare Figs. 3.3 (a), (b), and (c)).

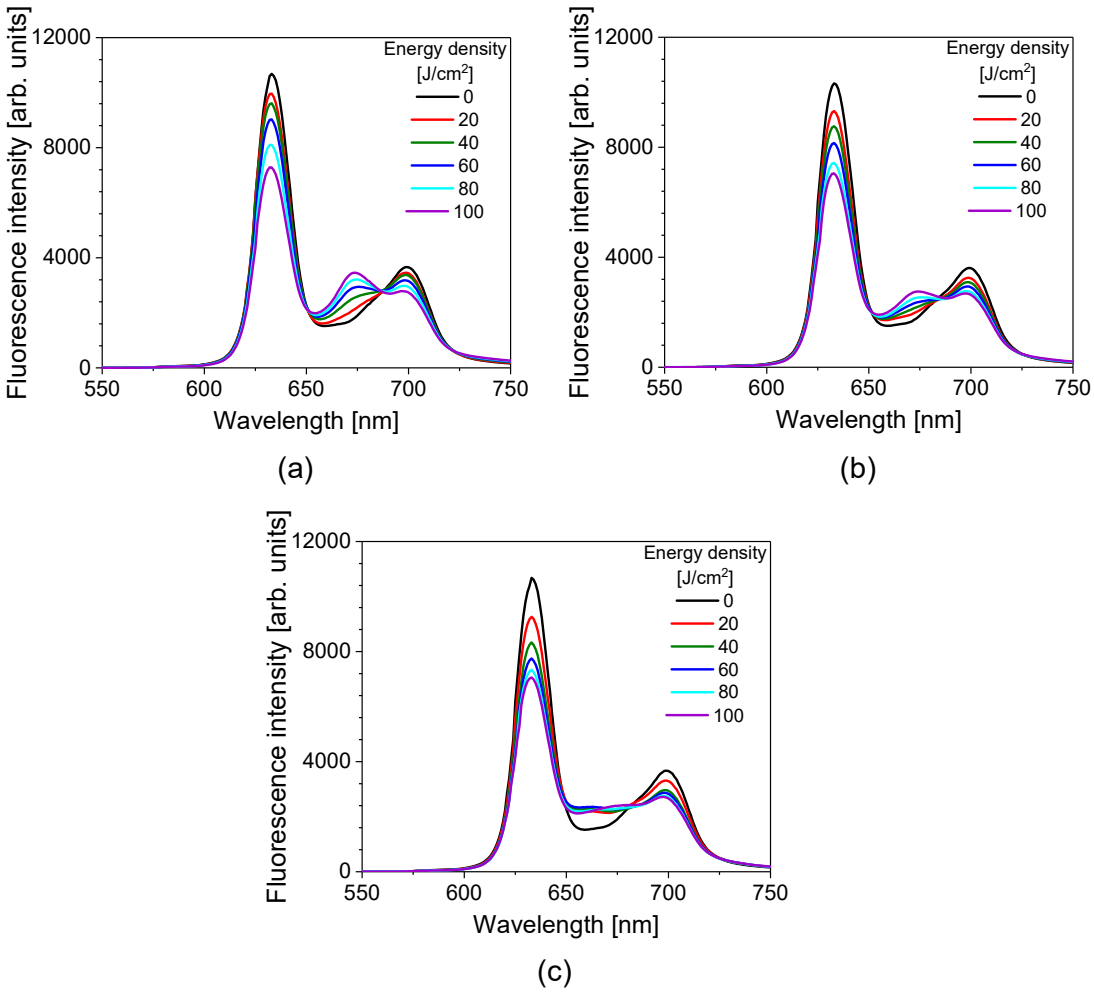

Figure 3.3: Fluorescence spectra of 635 nm irradiated PpIX, with increasing energy density for the fluence rate of (a) 10, (b) 50, and (c) 100 mW/cm^2. The fluorescence spectra were excited at 405 nm. The data were obtained from 3 independent experiments and averaged.

Photobleaching analysis

The intensities at the 633 nm peak of the irradiated PpIX were normalised with the intensity at 633 nm before irradiation, and the changes in the intensities with increased irradiation energy density were plotted (Fig. 3.4). Faster photobleaching was observed for PpIX irradiation with 405 nm (Fig. 3.4 (a)) than with 635 nm (Fig. 3.4(b)). When the photobleaching with variation in the irradiation fluence rate for the same laser wavelength was compared, there was no comparable deviation among the three fluence rates for the 405 nm laser (Fig. 3.4 (a)). For photobleaching investigated with a 635 nm laser, a slight deviation among the fluence rates was observed (Fig. 3.4 (b)). However,

the differences had no statistical significance on the photobleaching rate, $F(2, 30) = 1.04$, $p > 0.05$. The plots were fitted using the relationship described in Sec. 3.3.1.

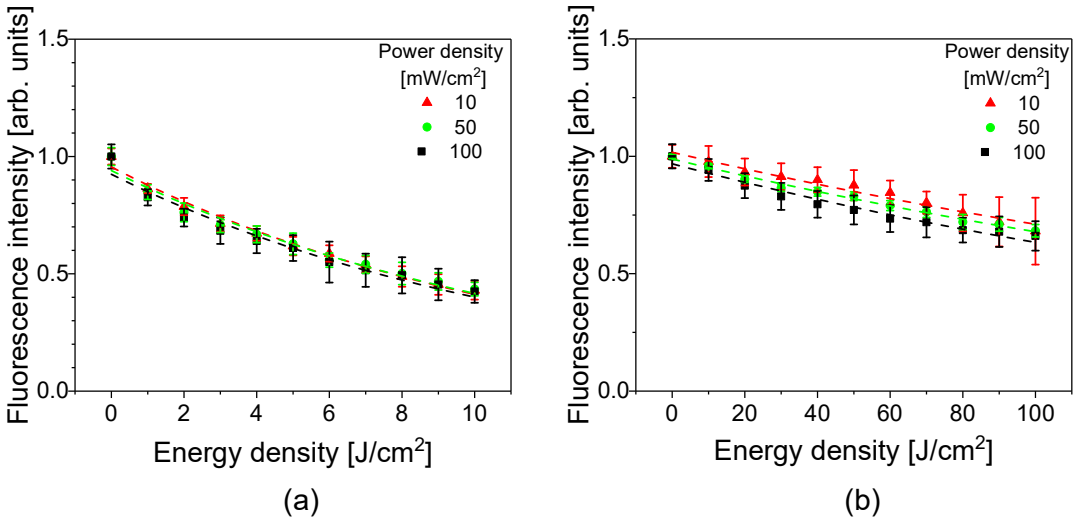

Figure 3.4: Relationships between PpIX fluorescence intensity and PD dose obtained at wavelengths of 633 nm for the fluence rates of 10, 50, and 100 mW/cm^2 and irradiation laser wavelength of (a) 405 nm, and (b) 635 nm. The error bars indicate the standard deviation from 3 independent experiments.

3.3.3. MS-based analyses of the PS photobleaching

The changes in the mass spectra of PpIX with the increase in irradiation performed using 405 nm and 635 nm laser are shown in Figs 3.5 and 3.6, respectively. The photobleaching of PpIX is indicated by the decrease in the mass signal intensity of $[H+M]^+$ peak of PpIX. The rate at which this intensity reduced varied with the fluence rate. The difference between the PpIX irradiated with the two fluence rates was more notable in the blue-light irradiated PpIX (Fig. 3.5).

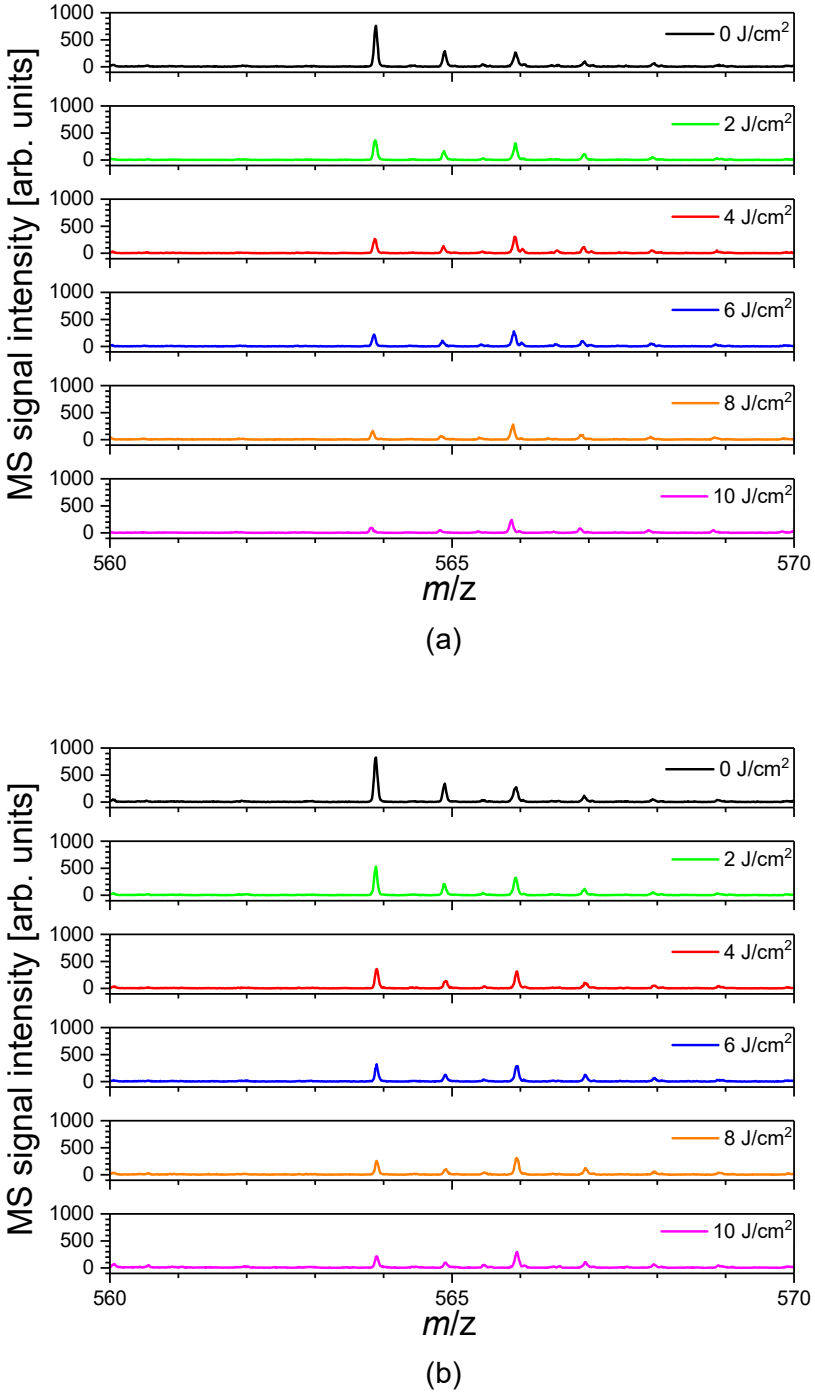

Figure 3.5: Mass spectra of PpIX with increasing irradiation energy density. Irradiation was done with a 405 nm laser having a fluence rate of (a) 10 and (c) 100 mW/cm^2. The data were obtained from 3 independent experiments and averaged.

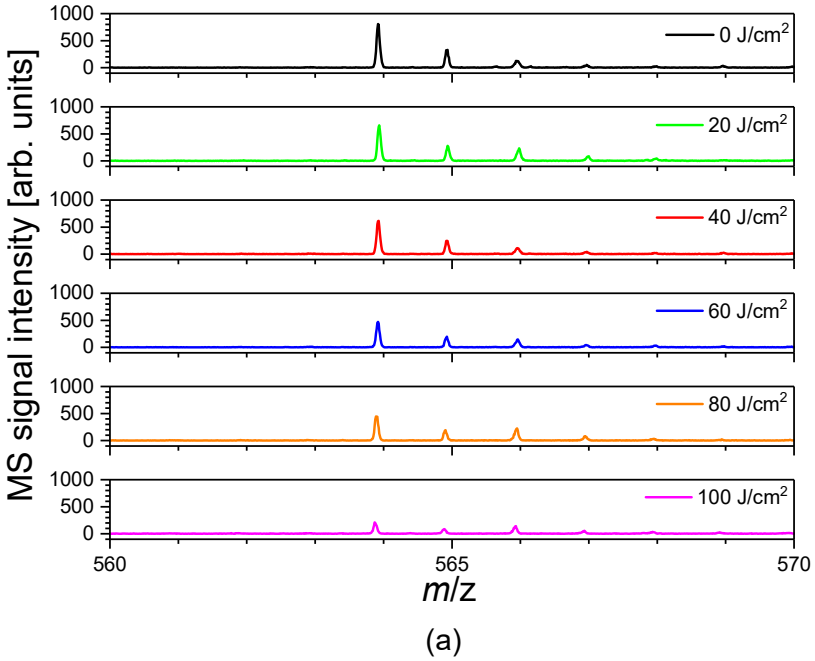

(a)

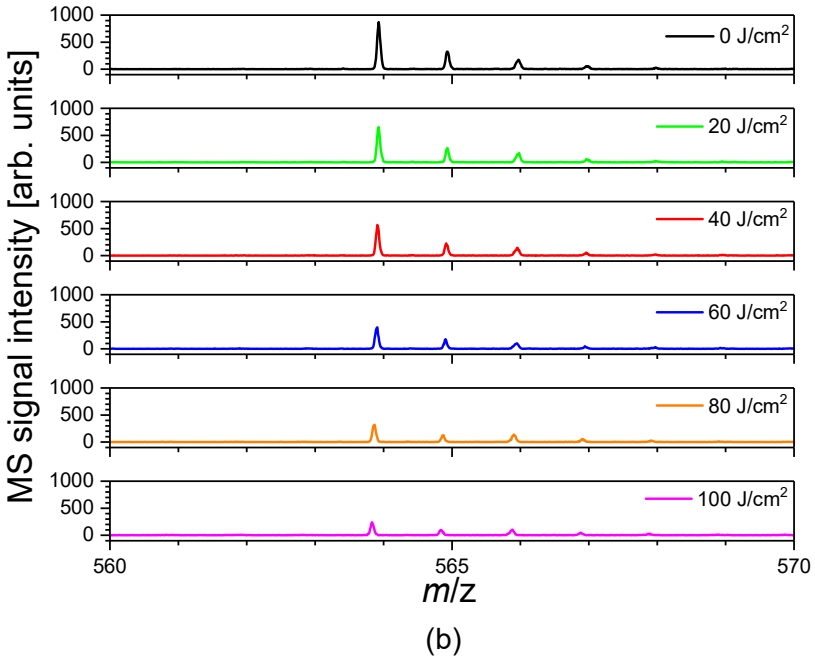

(b)

Figure 3.6: Mass spectra of PpIX with increasing irradiation energy density. Irradiation was done with a 635 nm laser having a fluence rate of (a) 10 and (b) 100 mW/cm^2. The data were obtained from 3 independent experiments and averaged.

Photobleaching analysis

Figure 3.7 shows the plot of PpIX concentration changes with increasing light irradiation. The MS intensities of the protonated monoisotopic peak, $[M+H]^+$ of PpIX, were converted to concentration using the relationship obtained in Sec 2.3.3. In line with the result of the fluorescence analysis, the PpIX photobleaching rate was faster in PpIX irradiated with a 405 nm (Fig. 3.7(a)) than with a 635 nm laser (Fig. 3.7(b)) for the three fluence rates investigated. 405 nm irradiation of PpIX (Fig. 3.7(a)) shows the fastest PpIX photobleaching for the lowest fluence rate (10 mW/cm^2). The PpIX photobleaching observed in the higher fluence rates (50 and 100 mW/cm^2) were comparable. On the other hand, slower photobleaching rates were noted for the fluence rates of 10 and 50 mW/cm^2 in comparison with the 100 mW/cm^2 in the photobleaching analysis using red light (Fig. 3.7(b)).

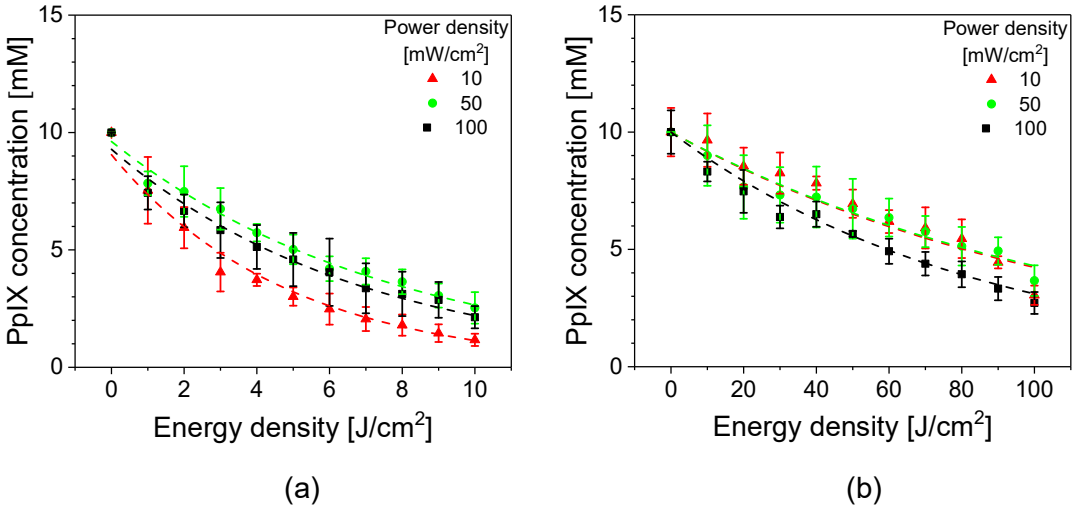

Figure 3.7: Relationships between PpIX concentration and PD dose obtained using MS. PpIX was irradiated at fluence rates of 10, 50, and 100 mW/cm^2 using a laser wavelength of (a) 405 nm and (b) 635 nm. The error bars indicate the standard deviation from 3 independent experiments.

The PpIX photobleaching relationships obtained under PDD and PDT conditions for both fluorescence and MS analyses are shown in Table 3.1.

Table 3.1 Photobleaching coefficient of PpIX obtained with fluorescence-based and MS-based analyses. The values are measured at the PDD conditions using a laser with a wavelength of 405 nm and at the PDT conditions using a laser with a wavelength of 635 nm. Irradiation power densities of 10, 50, and 100 mW/cm^2 were investigated for both laser wavelengths.

Laser wavelength [nm]	Power density [mW/cm^2]	β [J/cm^2]	
		Fluorescence	MS
405	10	11.91 ± 0.47	4.25 ± 0.11
	50	12.28 ± 0.66	7.32 ± 0.25
	100	11.96 ± 0.80	6.24 ± 0.33
635	10	278.96 ± 17.11	116.34 ± 7.28
	50	266.01 ± 8.82	118.29 ± 4.49
	100	235.90 ± 14.20	85.5 ± 1.98

3.4. Discussion

Effect of wavelength on photobleaching

In both fluorescence (Fig. 3.4) and MS analyses (Fig. 3.7), the photobleaching rate of PpIX observed under PDD conditions was faster than that in the PDT conditions. Although the irradiation under the PDT condition was 10 times longer than that of the PDD condition, the fluorescence intensity and concentration of PpIX after final irradiation were higher than that of PDD conditions. Since the 405 nm wavelength used in the irradiation under PDD conditions is the highest absorption band of PpIX while 635 nm is the lowest (Fig. 2.4) [15], considerable differences in the two photobleaching rates observed is expected.

Effect of fluence rate on photobleaching

The result of photobleaching obtained using fluorescence analysis (Fig. 3.4) showed no notable differences in the photobleaching rate with the three fluence rates investigated. Other

photobleaching analyses based on fluorescence have shown a similar result in rat tumour models and mouse skin [8,16]. The variations observed in the red light irradiated PpIX (Fig 3.4 (b)) were statistically negligible and were within the margin of error observed by Sørensen et al. [16]. Some have seen discrepancies in their results and observed variations in the photobleaching rate with irradiation fluence rate [9,17,18]. The reasons for the observed differences are not certain. A possible explanation may be the availability of oxygen. The results that indicated changes in the photobleaching rate with the fluence rate reported reduced oxygen to the target area with an increased fluence rate. The reduced oxygen availability may affect the photobleaching rate. On the other hand, in the studies where no notable variation in the photobleaching rate with the fluence rate was seen, no reduction in the oxygen was observed during the analysis. Considering that our analysis was performed with PpIX in solution, we presume that there was no limitation of oxygen supply to PpIX. Furthermore, the fluence rate effect is less prominent at medium and high fluence rates [9,19]. Thus, based on the fluence rates used in the PpIX irradiation, no notable differences in the photobleaching rates with fluence rates may be detected.

The photobleaching obtained using MS differed from fluorescence (Figs. 3.7 and 3.4). The photobleaching analysed using MS (Fig. 3.7) showed a dependence of photobleaching rate with fluence rate. A more visible variation in PpIX concentration reduction rate is seen for the fluence of 10 mW/cm^2 of blue-violet laser irradiation (Fig. 3.7(a)) and the fluence of 100 mW/cm^2 of red laser irradiation (Fig. 3.7 (b)). As no other analysis of the photobleaching performed with MS has been reported, no comparison can be made as a reference.

In the photobleaching analysed with fluorescence, there is a possible interference of the fluorescence emitted from the photoproducts on the PpIX intensity at 633 nm. The peak at 654 nm observed in the blue-light irradiated PpIX (Fig. 3.2) can be presumed to be photoproduct II (Pp II), and the peak at 673 nm in the red-light irradiated PpIX (Fig. 3.3) as photoprotoporphyrin, Ppp, as they have emission peaks reported by Dysart et al. [5]. The fluorescence emission intensity of Pp II with increased irradiation energy density for the fluence rate of 10 mW/cm^2 differed from 50 and 100 mW/cm^2 for 405 nm laser irradiation, and the fluence rate of 100 mW/cm^2 from 10 and 50 mW/cm^2 for 635 nm laser irradiation. The fluence rates where there was notable photoproduct formation were those with a more visible variation in the PpIX concentration reduction.

Faster photobleaching is seen in the MS than in the fluorescence analysis. The fluorescence intensity of PpIX may aggregate depending on the pH and the concentration. Aggregation of PpIX decreases the fluorescence emission from a photosensitizer [20]. Again, with increasing pH, the fluorescence quantum yield of PpIX reduces [21]. Finally, there is an overlap of the emission band

of the photoproducts with that of PpIX. These factors may affect the actual concentration of PpIX obtained during the fluorescence analysis of photobleaching. On the other hand, these factors do not affect the results of the MS analysis.

The photobleaching coefficient, β

The photobleaching curves were all fitted using the best fit for a single exponential described in Sec. 3.3.1. The fit was made in such a way that back-solving the relationship at 0 J/cm^2 would give PpIX concentration of 10 μM, or fluorescence intensity between 0.92 and 1 [arbs. units]. The β values obtained using fluorescence were greater than those of MS. Fluorescence-based photobleaching coefficients obtained from a mathematical model of ALA-induced PpIX *in vivo* under PDT conditions ranged between 1.8 and 33 J/cm^2 [9,22–25]. Our fluorescence-based investigation of β under PDT conditions (Fig. 3.4(b)) is not within the range in the previous literature. In *in vivo* analysis, factors such as the time between administration of the photosensitizer to the commencement of treatment, the concentration of photosensitizer accumulated on the target lesion, and the type of tumour that is being treated can affect the photosensitizer photobleaching [25]. Most of these factors were absent in our investigation. Thus, this may have resulted in the differences in our β value from those of the literature.

3.5. Chapter conclusion

Analysis performed in this chapter showed a considerable difference between the PpIX photobleaching rates obtained from the fluorescence and MS analyses. Variations in the photobleaching rates can occur due to numerous factors. However, given that the analysis conditions for both fluorescence and MS analyses were the same, it is thought that a direct comparison of the photobleaching rates obtained from the two analysis methods should pose no issue. The photobleaching in the fluorescence analysis was independent of the fluence rate, while variations in the photobleaching with the fluence rate were seen in the MS analysis. The difference may be attributed to the effect of fluorescence emission from the PpIX photoproducts, which affects the fluorescence-based analysis. It is speculated that the photobleaching rates would differ *in vivo* as factors such as oxygen availability and controlling the initial concentration of the photosensitizer come into play. Consequently, such analysis would be necessary to better understand the photobleaching process. Nonetheless, it is important to recognise the potential importance of the result of this study, as photobleaching is used in the dosimetry estimation of PDT and PDD.

References

[1]. B. C. Wilson, M. S. Patterson, and L. Lilge, "Implicit and explicit dosimetry in photodynamic therapy: A new paradigm," *Lasers in Medical Science*, **12**(3), 182–199 (1997).

[2]. R. Bonnett and G. Martínez, "Photobleaching of sensitisers used in photodynamic therapy," *Tetrahedron*, **57**(47), 9513–9547 (2001).

[3]. S. Bagdonas, L. W. Ma, V. Iani, R. Rotomskis, P. Juzenas, and J. Moan, "Phototransformations of 5-Aminolevulinic Acid–induced Protoporphyrin IX in vitro: A Spectroscopic Study," *Photochemistry and Photobiology*, **72**(2), 186–192 (2000).

[4]. K. Huang, L. Chen, S. Lv, and J. Xiong, "Protoporphyrin IX photobleaching of subcellular distributed sites of leukemic HL60 cells based on ALA-PDT in vitro," *Journal of Biomedical Science and Engineering*, **05**(09), 548–555 (2012).

[5]. J. S. Dysart and M. S. Patterson, "Photobleaching kinetics, photoproduct formation, and dose estimation during ALA induced PpIX PDT of MLL cells under well oxygenated and hypoxic conditions," *Photochemical and Photobiological Sciences*, **5**(1), 73–81 (2006).

[6]. K. Efendiev, P. Alekseeva, A. Shiryaev, A. Voitova, K. Linkov, T. Pisareva, I. Reshetov, and V. Loschenov, "Near-infrared phototheranostics of tumors with protoporphyrin IX and chlorin e6 photosensitizers," *Photodiagnosis and Photodynamic Therapy*, **42**, 103566 (2023).

[7]. D. J. Robinson, M. R. Stringer, and W. R. Crum, "Rate-equation analysis of Protoporphyrin IX photo-oxidation," *Photochemotherapy: Photodynamic Therapy and Other Modalities*, **2625**, 413–418 (1996).

[8]. S. Iinuma, K. Schomacker, G. Wagnières, M. Rajadhyaksha, M. Bamberg, T. Momma, and T. Hasan, "In vivo fluence rate and fractionation effects on tumor response and photobleaching: Photodynamic therapy with two photosensitizers in an orthotopic rat tumor model," *Cancer research*, **59**, 6164–6170 (2000).

[9]. D. J. Robinson, H. S. De Bruijn, N. Van Der Veen, M. R. Stringer, S. B. Brown, and W. M. Star, "Fluorescence Photobleaching of ALA-induced Protoporphyrin IX during Photodynamic Therapy of Normal Hairless Mouse Skin: The Effect of Light Dose and Irradiance and the Resulting Biological Effect," *Photochemistry and Photobiology*, **67**(1), 140–149 (1998).

[10]. J. Moan, G. Streckyte, S. Bagdonas, Ø. Bech, and K. Berg, "Photobleaching of protoporphyrin IX in cells incubated with 5-aminolevulinic acid," *International Journal of Cancer*, **70**, 90–97 (1997).

[11]. W. S. L. Strauss, R. Sailer, M. H. Gschwend, H. Emmert, R. Steiner, and H. Schneckenburger, "Selective Examination of Plasma Membrane-Associated Photosensitizers Using Total Internal Reflection Fluorescence Spectroscopy: Correlation between Photobleaching and Photodynamic Efficacy of Protoporphyrin IX," *Photochemistry and Photobiology*, **67**(3), 363–369 (1998).

[12]. K. W. Teng and S. H. Lee, "Characterization of Protoporphyrin IX Species in Vitro Using Fluorescence Spectroscopy and Polar Plot Analysis," *Journal of Physical Chemistry B*, **123**(27), 5832–5840 (2019).

[13]. K. König, H. Schneckenburger, A. Rück, and R. Steiner, "In vivo photoproduct formation during PDT with ALA-induced endogenous porphyrins," *Journal of Photochemistry and Photobiology, B: Biology*, **18**(2–3), 287–290 (1993).

[14]. L. Song, E. J. Hennink, I. T. Young, and H. J. Tanke, "Photobleaching kinetics of fluorescein in quantitative fluorescence microscopy," *Biophysical Journal*, **68**(6), 2588–2600 (1995).

[15]. V. Nadeau, M. O'Dwyer, K. Hamdan, I. Tait, and M. Padgett, "In vivo measurement of 5-aminolaevulinic acid-induced protoporphyrin IX photobleaching: A comparison of red and blue light of various intensities," *Photodermatology Photoimmunology and Photomedicine*, **20**(4), 170–174 (2004).

[16]. R. Sørensen, V. Iani, and J. Moan, "Kinetics of Photobleaching of Protoporphyrin IX in the Skin of Nude Mice Exposed to Different Fluence Rates of Red Light," *Photochemistry and Photobiology*, **68**(6), 835–840 (1998).

[17]. J. C. Finlay, D. L. Conover, E. L. Hull, and T. H. Foster, "Porphyrin Bleaching and PDT-induced Spectral Changes are Irradiance Dependent in ALA-sensitized Normal Rat Skin In Vivo," *Photochemistry and Photobiology*, **73**(1), 54–63 (2001).

[18]. C. D. Sudworth, M. R. Stringer, J. E. Cruse-Sawyer, and S. B. Brown, "Fluorescence microspectroscopy technique for the study of intracellular protoporphyrin IX dynamics," *Applied Spectroscopy*, **57**(6), 682–688 (2003).

[19]. K. Langmack, R. Mehta, P. Twyman, and P. Norris, "Topical photodynamic therapy at low fluence rates – theory and practice," *Journal of Photochemistry and Photobiology B: Biology*, **60**(1), 37–43 (2001).

[20]. L. Bezdetnaya, N. Zeghari, I. Belitchenko, M. Barberi-Heyob, J. L. Merlln, A. Potapenko, and F. Guillemin, "Spectroscopic and Biological Testing of Photobleaching of Porphyrins in Solutions," *Photochemistry and Photobiology*, **64**(2), 382–386 (1996).

[21]. A. Datta, A. Dube, B. Jain, A. Tiwari, and P. K. Gupta, "The Effect of pH and Surfactant on

the Aggregation Behavior of Chlorin p6: A Fluorescence Spectroscopic Study¶," *Photochemistry and Photobiology*, **75**(5), 488–494 (2007).

[22]. M. B. Ericson, C. Sandberg, B. Stenquist, F. Gudmundson, M. Karlsson, A. M. Ros, A. Rosén, O. Larkö, A. M. Wennberg, and I. Rosdahl, "Photodynamic therapy of actinic keratosis at varying fluence rates: Assessment of photobleaching, pain and primary clinical outcome," *British Journal of Dermatology*, **151**(6), 1204–1212 (2004).

[23]. T. J. Farrell, R. P. Hawkes, M. S. Patterson, and B. C. Wilson, "Modeling of photosensitizer fluorescence emission and photobleaching for photodynamic therapy dosimetry," *Applied Optics*, **37**(31), 7168 (1998).

[24]. A. J. L. Jongen and H. J. C. M. Sterenborg, "Mathematical description of photobleaching in vivo describing the influence of tissue optics on measured fluorescence signals," *Physics in Medicine and Biology*, **42**(9), 1701–1716 (1997).

[25]. R. M. Valentine, C. T. A. Brown, H. Moseley, S. Ibbotson, and K. Wood, "Monte Carlo modeling of in vivo protoporphyrin IX fluorescence and singlet oxygen production during photodynamic therapy for patients presenting with superficial basal cell carcinomas," *Journal of Biomedical Optics*, **16**(4), 048002 (2011).

Chapter 4
Analysis of protoporphyrin IX photoproducts

4.1. Introduction

When photosensitizers are exposed to light, they react with molecules, such as radicals and oxygen, to form photoproducts [1,2]. Various studies report the formation of photoproducts with light irradiation of PpIX in solution, in cells, and *in vivo* [2–10]. Most of these photoproduct analyses have been done based on fluorescence, investigated by observing the changes in the fluorescence spectra of PpIX after certain light irradiation. Three main photoproducts of PpIX have been identified based on their fluorescence emission wavelength: photoprotoporphyrin (Ppp) with a peak intensity centred around 674 nm, product II (Pp II) at 655 nm, and product III (Pp III) at around 618 nm [7]. The basis fluorescence spectra of these photoproducts fitted using singular value decomposition are shown in Fig. 4.1.

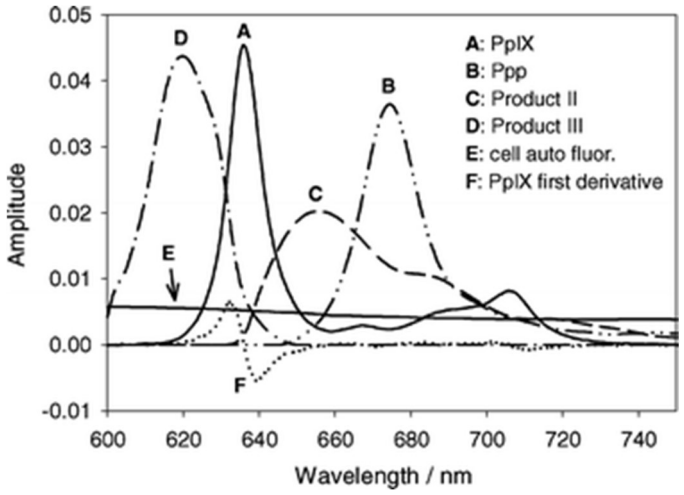

Figure 4.1: Basis spectra used in SVD fitting of acquired spectra. Spectra A–E have an area under the curve between 610 nm and 750 nm, equal to one. The amplitude of F is such that its addition to spectrum A will shift A by 1 nm [7].

The drawback of the fluorescence method is the overlap of the fluorescence peak of the photoproducts with that of PpIX and the effect of the environment on the fluorescence emission intensity [8,11], making the photoproduct quantification difficult. Additionally, the chemical structure of the photoproducts cannot be determined with the fluorescence analysis. The chemical structure of one of the photoproducts, Ppp, has been identified by Inhoffen et al., and its formation explained by the reduction of the double bond of PpIX by the cycloaddition of singlet oxygen to either of the two vinyl groups [12]. However, Dysart et al. observed fluorescence emission at 674 nm, which is the emission wavelength of Ppp, when PpIX was irradiated under hypoxia [7]. The study hypothesised that other mechanisms for the formation of Ppp exist [7]. The same study reports Ppp fluorescence photobleaching in the presence of oxygen to generate Pp II [7]. Pp III is generated from uroporphyrin and coproporphyrin produced as intermediates in steps of the heme synthesis.

Photoproducts for dosimetry estimation, fluorescence diagnosis, and therapy

Photoproduct formation rates depend on internal and external factors similar to that of photobleaching [3,8]. Hence, monitoring the formation of the photosensitizer photoproducts could be a complementary approach for the PDD and PDT dosimetry estimation. By combining the monitoring of PpIX photobleaching and the photoproduct formation, an improved dosimetry estimation of both the light dose and the photosensitizer concentration may be achieved. Furthermore, these photoproducts are fluorophores and emit fluorescence when excited [8]. Some of the PpIX photoproducts have also been reported to be a photosensitizers [1,13,14], with their singlet oxygen quantum yields almost similar to that of PpIX [15,16]. Thus, the photoproducts may be used for PDD and PDT. Although studies have shown the potential of PpIX photoproducts for PDD and PDT, the rate of their formation under various treatment and diagnosis conditions has not been studied in detail. Most studies on the PpIX photoproducts have focused on the determination of their fluorescence emission and absorption bands and their formation mechanisms [2,8–10,17,18].

In this chapter, we aimed to study the formation of PpIX photoproducts by irradiating PpIX in organic solvent and analysing the photoproducts based on fluorescence, absorption, mass spectra, and high-performance liquid chorograms. The photoproducts formed from PpIX irradiated with 635 nm (red) and 405 nm (blue) light, were investigated at high and low fluence rates and increasing fluence. These irradiation conditions are within the ranges of lights used for PDT and PDD. Thus, the effect of wavelength, irradiation fluence rates, and fluence on the formation of PpIX

photoproducts was studied.

4.2. Materials and methods

4.2.1. PpIX irradiation for photoproduct formation

PpIX dissolved in DMSO to a concentration of 10 µM was irradiated using the irradiation protocol described in Sec. 3.2.1 at 635 nm or 405 nm. Photoproduct formation from PpIX solution irradiated at fluence rates of 10 and 100 mW/cm^2 was investigated for each light source. The irradiation energy densities for the 635 nm irradiation were investigated in steps of 10 J/cm^2 between 0 and 100 J/cm^2. For irradiation with 405 nm, PpIX was irradiated at irradiation energy densities of 0, 1, and 2 J/cm^2.

4.2.2. Fluorescence analysis of photoproducts

The fluorescence measurements were performed as described in Sec. 3.2.2.

4.2.3. MS analysis of the photoproducts

The irradiated PpIX solutions were further diluted as described in Sec. 2.2.3. The mass spectrometer described in Sec. 2.2.3 was used in the positive ion mode. The sample was injected at a flow rate of 30 µL/min, the mass spectra were measured every 0.34 s with a 0.1 s interval, and the signal intensity of the mass spectrum integrated for 3 min was analysed. Each 3 min measurement for each sample was performed 3 times.

4.2.4. Absorption analysis of photoproducts

The absorption spectra of PpIX irradiated with 635 nm light for 100 J/cm^2 and with 405 nm light for 2 J/cm^2 for the irradiation fluence rates of 10 and 100 mW/cm^2 were investigated. The absorption spectra were obtained using the method described in Sec. 2.2.2.

4.2.5. High-Performance Liquid Chromatography (HPLC) analysis of the photoproducts

The unirradiated PpIX (0 J/cm^2) and irradiated PpIX (irradiated with a 635 nm light at 10 mW/cm^2 for 100 J/cm^2) were chromatographically separated using HPLC (Vanquish Flex, Thermo Scientific). The HPLC was performed with an LC column (L-column2 ODS, 3 µm, 2.1 × 50 mm, Metal-free column) maintained at 40 °C with a gradient elution of mobile phases A (distilled water + 0.1 % formic acid) and B (acetonitrile + 0.1 % formic acid) and a flow rate of 0.3 mL/min. The mobile

phase ratio A:B (v/v) was started at 50:50, changed to 5:95 (2–4 min), and back to 50:50 (4–6 min). The output of the HPLC was coupled to an Orbitrap MS (Orbitrap Exploris 240, Thermo Scientific), and the separated samples were analysed in positive and negative ion modes. Tandem mass spectrometry analysis was performed at a collision energies of 40, 60, 80, and 120 eV.

4.3. Results

4.3.1. Photoproduct formation under red light irradiation of PpIX

Fluorescence analysis

Figure 4.2 shows the changes in the fluorescence spectra of PpIX under red light irradiation for power densities of 10 and 100 mW/cm^2 (hereafter referred to as F_{R10} and F_{R100}, respectively[1]). The spectra were obtained after irradiation with 0 and 100 J/cm^2 energy densities. The emergence of a new fluorescence peak at around 673 nm is attributed to the formation of a photoproduct. The fluorescence intensity of the photoproduct was more dominant in the irradiation with the low fluence rate (Fig. 4.2(a)).

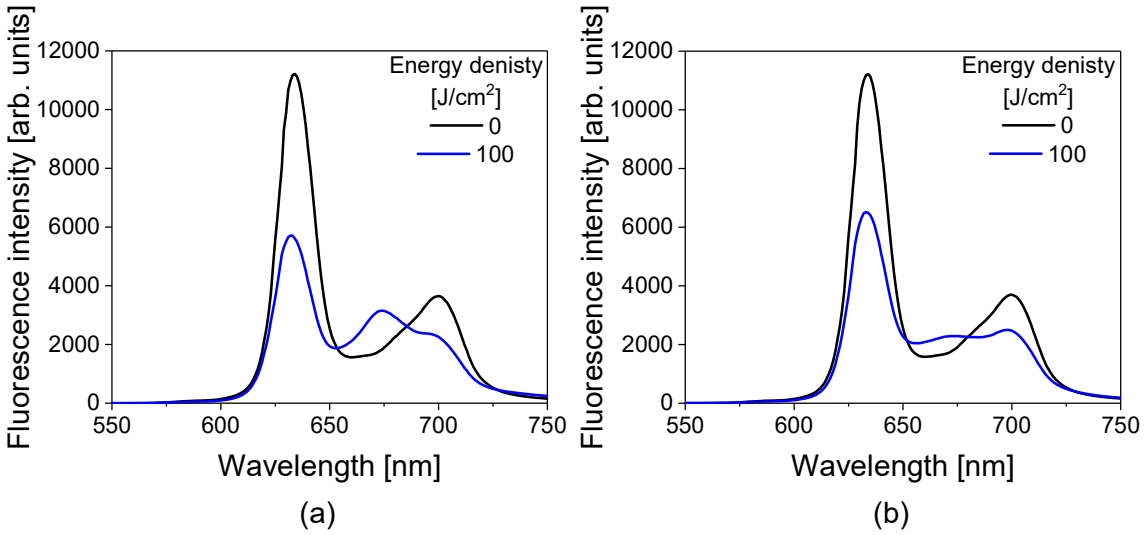

Figure 4.2: Fluorescence spectra of PpIX before and after irradiation with a 635 nm laser and energy density of 100 J/cm^2 at the irradiation fluence rates of (a) 10 mW/cm^2 (F_{R10}) and (b) 100 mW/cm^2 (F_{R100}). The fluorescence spectra were obtained at 405 nm excitation.

[1] F_{R10} and F_{R100}: Fluorescence of PpIX after irradiation with a 635 nm laser at fluence rates of 10 and 100 mW/cm^2, respectively.

The formation of the new band of photoproduct at 673 nm with increased irradiation was monitored for the two fluence rates (Fig. 4.3). The intensity at 673 nm was corrected to exclude the fluorescence intensity of PpIX that is present at that wavelength by applying the method utilised by Bagdonas et al. [8]. The ratio of the initial fluorescence intensity of PpIX at 673 and 633 nm multiplied by the fluorescence intensity at 633 nm after a given irradiation was subtracted from the fluorescence intensity at 673 nm at that given irradiation. The plot of Fig. 4.3 shows evident differences in the rate of photoproduct formations between the two irradiation fluence rates. The photoproduct formation plateaus at around irradiation energy density of 40 J/cm^2 for F_{R100}. On the other hand, for F_{R10}, no obvious fluorescence intensity decay of the photoproduct is seen within the energy densities investigated. The intensity ratio of photoproduct (673 nm) after 100 J/cm^2 irradiation between the two irradiation fluence rates (F_{R10}/ F_{R100}) was 1.8. A 1.77 times increase in the photoproduct intensity (673 nm) occurred in *F*R10 after 100 J/cm^2 irradiation (Fig. 4.2(a)), PpIX intensity (633 nm) reduced to 51 % of its initial intensity, and the intensity of the photoproduct was 0.41±0.01 times PpIX.

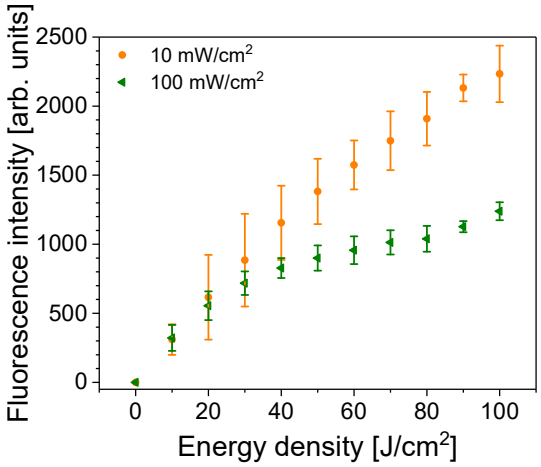

Figure 4.3: Fluorescence intensity of 635 nm irradiated PpIX, monitored at 673 nm with increasing irradiation energy density. PpIX was irradiated at fluence rates of 10 and 100 mW/cm^2. The intensities at 673 nm were corrected to exclude the PpIX fluorescence intensities. The error bars indicate the standard deviation from at least 3 independent experiments.

MS analysis

The mass spectra of PpIX irradiated with a 635 nm laser with power densities of 10 and 100 mW/cm^2 (hereafter referred to as M_{R10} and M_{R100}, respectively[2]) are shown in Fig. 4.4. For lower fluence rate (Fig. 4.4(a)), a peak at around *m*/*z* 595.3 and its isotope components appears after irradiation. These peaks were absent in the spectra of unirradiated PpIX. The insets of Fig. 4.4 show a closer view of the *m*/*z* where the new peaks were observed. The detected new peaks were assumed to be attributed to that of a photoproduct, and the changes in the signal intensity of the new peak at *m*/*z* 595.3 with irradiation were plotted (Fig. 4.5). Similar to the result of fluorescence analysis, the rise in the intensity of the photoproduct (*m*/*z* 595.3) with irradiation was more dominant in M_{R10} than in M_{R100}. For the PpIX irradiation with 100 mW/cm^2, the intensity at *m*/*z* 595.3 remained almost similar to that of the background signal with increased irradiation energy density. The intensity ratio at *m*/*z* 595.3 between the two fluence rates after 100 J/cm^2 was 2.8. In M_{R10}, the photoproduct intensity (*m*/*z* 595.3) rose to 3.58 times its initial intensity, while PpIX photobleached to 35 % after 100 J/cm^2 irradiation. The intensity of the photoproduct to PpIX after 100 J/cm^2 was 0.40±0.01 times PpIX.

[2] M_{R10} and M_{R100}: Mass spectra of PpIX after irradiation with a 635 nm laser at fluence rates of 10 and 100 mW/cm^2, respectively.

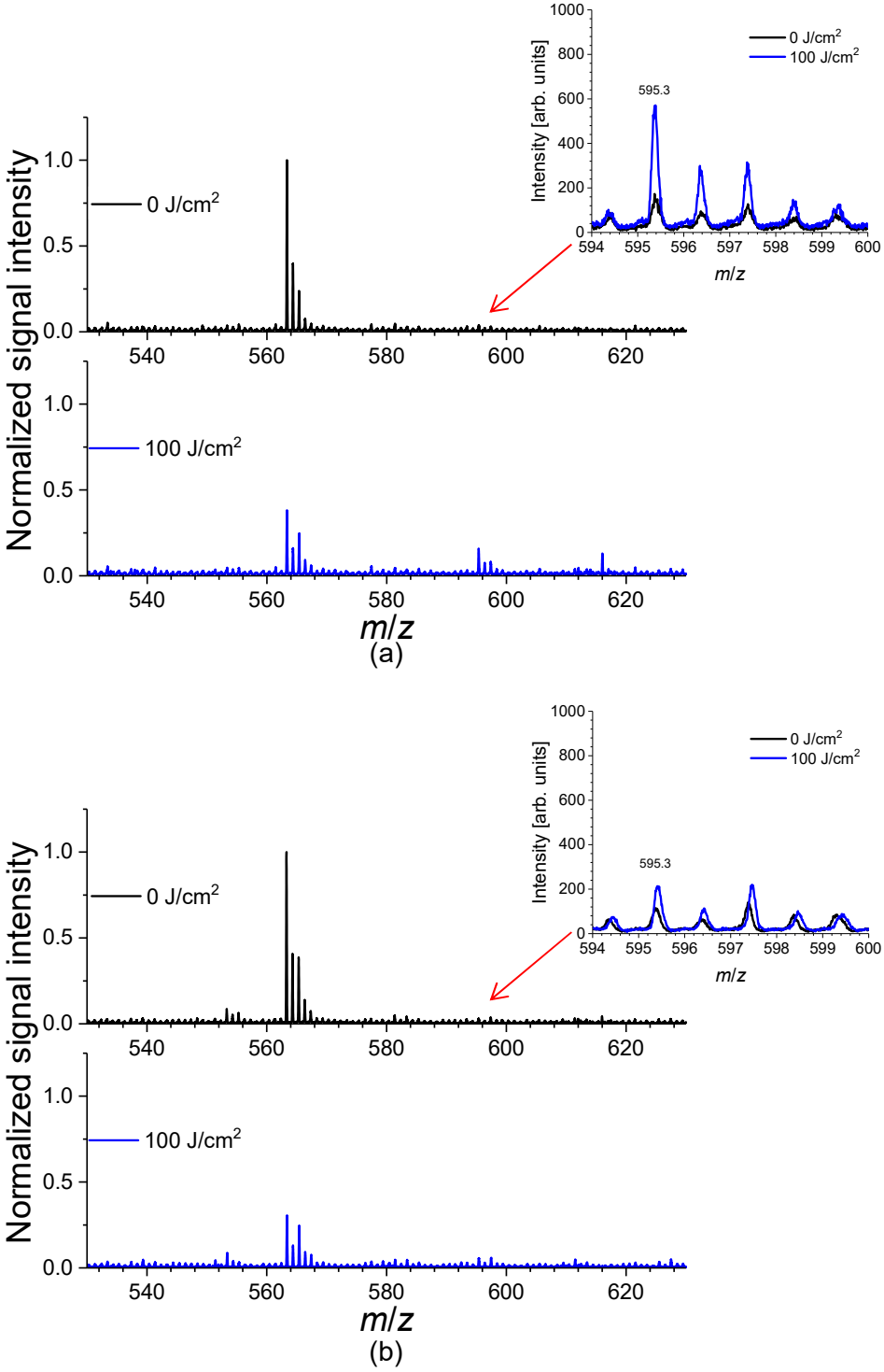

Figure 4.4: Mass spectra of PpIX before and after 635 nm irradiation with an energy density of 100 J/cm^2 at the irradiation power densities of (a) 10 mW/cm^2 (M_{R10}) and (b) 100 mW/cm^2 (M_{R100}). The inset shows the mass spectra zoomed in around *m*/*z* 595.3, where the new peaks were observed.

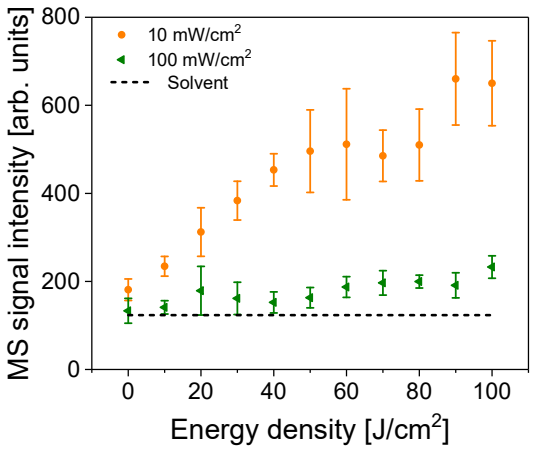

Figure 4.5: Mass signal intensity with increasing irradiation energy density obtained (a) *m*/*z* 563.3 and (b) *m*/*z* 595.3 of PpIX irradiated with a 635 nm laser at fluence rates of 10 and 100 mW/cm^2. The error bars indicate the standard deviation from at least 3 independent experiments. The average intensity of the solvent for the *m*/*z* analysed is displayed in a dashed line.

Absorption analysis

The absorption spectra of PpIX before and after irradiation with a red light at fluence rates of 10 and 100 mW/cm^2 are given in Fig. 4.6. PpIX irradiation resulted in the reduction in the intensities of PpIX peaks in both Soret and the Q bands. The irradiated spectra also exhibited an absorption band around 670 nm. The intensity of this band was higher for PpIX irradiation at a low fluence rate. The difference spectra in Fig 4.6(b) were generated by subtracting the spectra of PpIX before irradiation from the irradiated spectrum for each fluence rate. The difference spectra indicated 4 peak increases at 450 and 668 nm, caused by the formation of the photoproducts. These intensities were notably higher for PpIX irradiated at 10 mW/cm^2.

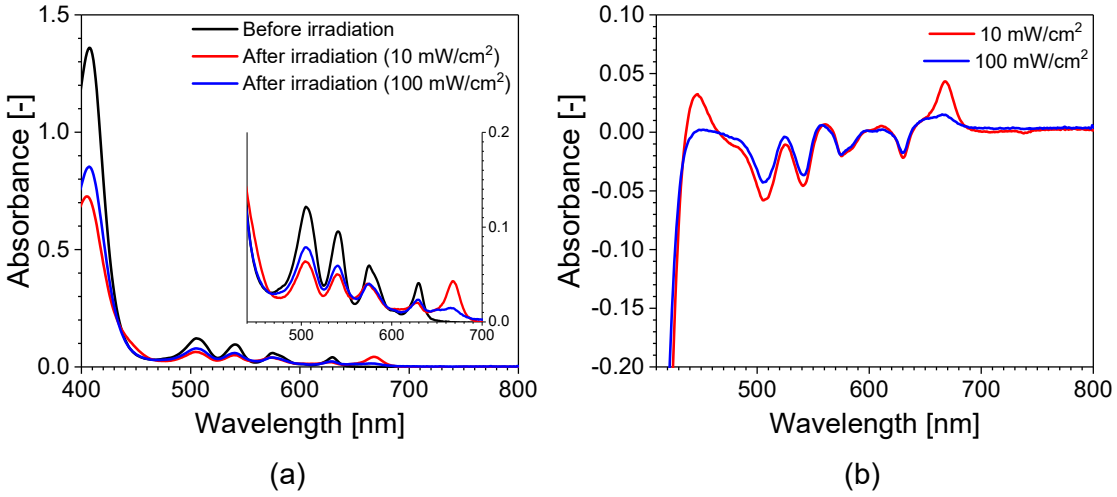

Fig. 4.6 (a) Absorption spectra of PpIX before and after irradiation with 635 nm laser. PpIX was irradiated for 100 J/cm^2 at fluence rates of 10 and 100 mW/cm^2. (b) Difference spectra of irradiated PpIX in (a). The spectrum of PpIX before irradiation was subtracted from the spectra after irradiation.

HPLC analysis

The extracted ion chromatograms of PpIX before and after irradiation with a 635 nm light are presented in Fig. 4.7. For the positive ion mode analysis, the *m*/*z* 563.3 and *m*/*z* 595.3 were extracted as the $[M+H]^+$ of PpIX and Ppp, respectively. The *m*/*z* 561.3 and *m*/*z* 593.3, indicating $[M-H]^-$ of PpIX and Ppp, respectively, were extracted for the negative ion mode analysis.

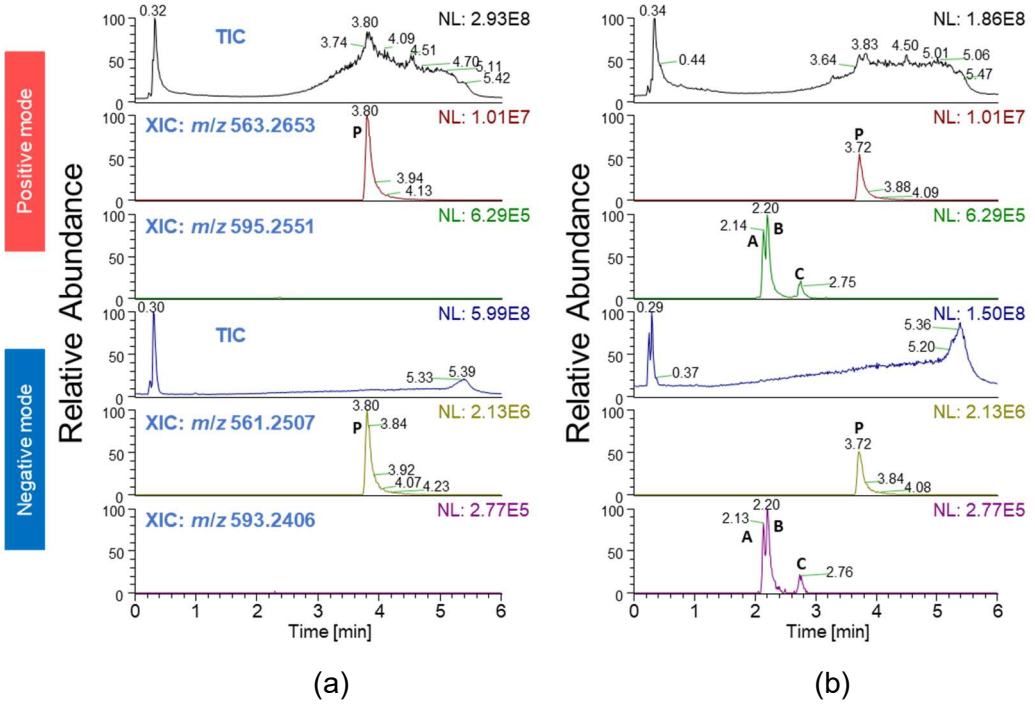

Figure 4.7: Total ion chromatogram (TIC) and extracted ion chromatogram (EIC) of PpIX (a) before and (b) 100 J/cm^2 irradiation at *m*/*z* 563.265 and *m*/*z* 595.255. PpIX was irradiated with a 635 nm light at 10 mW/cm^2. NL: Normalization Level.

The chromatogram at *m*/*z* 563.3 and 561.3 (Peak P) decreased in intensity after irradiation. No peak is visible in the extracted ion chromatogram at *m*/*z* 595.3 nor 593.3 in the unirradiated PpIX (Fig. 4.7(a)). Irradiation of PpIX resulted in three chromatographic peaks (Peaks A, B, and C). The chromatographic peaks indicate three possible isomers of the newly formed molecule. The mass spectra of the observed chromatographic peaks A, B, and C are shown in Fig. 4.8. The isotopic components of these peaks can be observed in the mass spectra obtained in both positive ion mode (Fig. 4.8 (a)) and negative ion mode (Fig. 4.8 (b)). The tandem mass spectra at *m*/*z* 595.3 for the three new peaks (Fig. 4.9) indicate that most fragmentation peaks of Peaks A, B, and C occurred at similar *m*/*z*, further indicating that these three compounds have similar molecular structures.

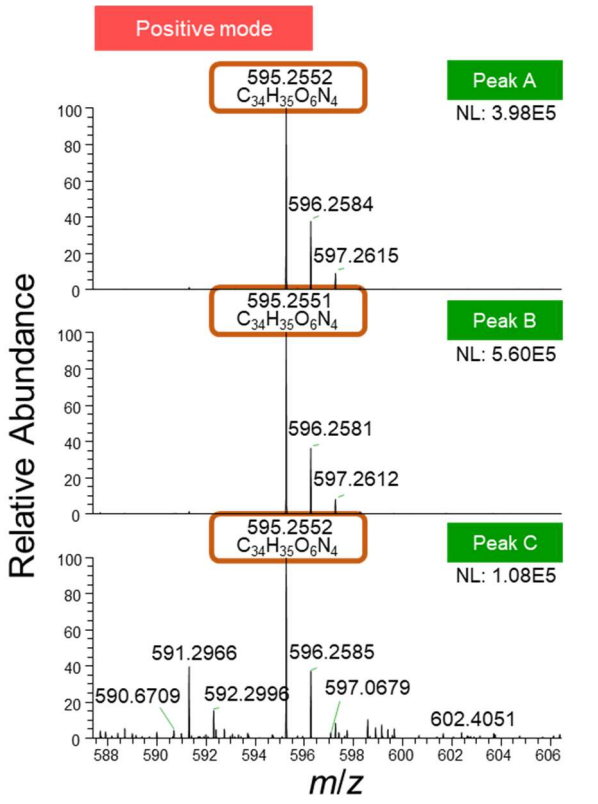

(a)

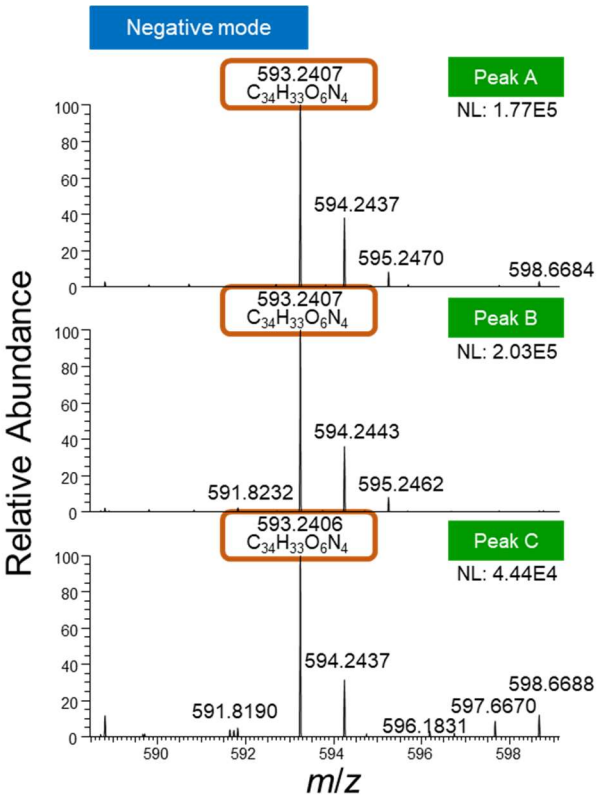

(b)

Figure 4.8: Mass spectra at the chromatographic Peaks A, B, and C.

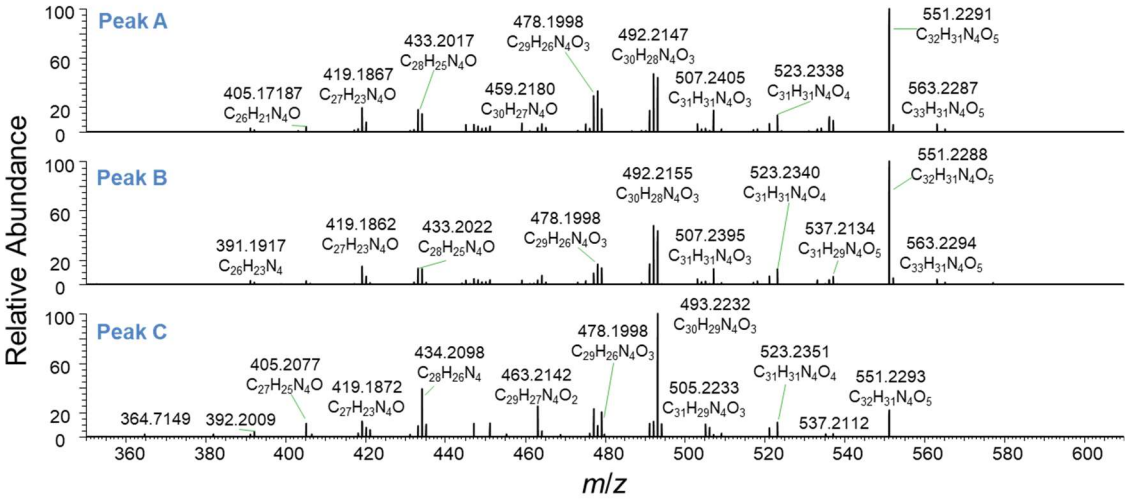

Figure 4.9: LC/MS/MS spectra of 635 nm irradiated PpIX at *m*/*z* 595.255 for the chromatographic peaks A–C. The collision energy was 60 eV.

4.3.2. *Photoproduct formation under blue light irradiation of PpIX*

Fluorescence analysis

PpIX exposure to blue light also resulted in a new peak, with the peak occurring at 654 nm (Fig. 4.10). The peak intensity at 654 nm was more abundant after irradiation at a high fluence rate. This is more evident in irradiation performed with a higher fluence (Chapter 3 Sec. 3.3.2). The intensity increased by 1.3 and 1.7 times for irradiation at 10 and 100 mW/cm^2 fluence rates, respectively, after irradiation energy density of 2 J/cm^2. The photobleaching rate was similar between the two fluence rates. Irradiation performed at 10 mW/cm^2 had 74.4 % of PpIX left after 2 J/cm^2 of irradiation, while the irradiation at 100 mW/cm^2 had 73.1% PpIX left after similar irradiation fluence.

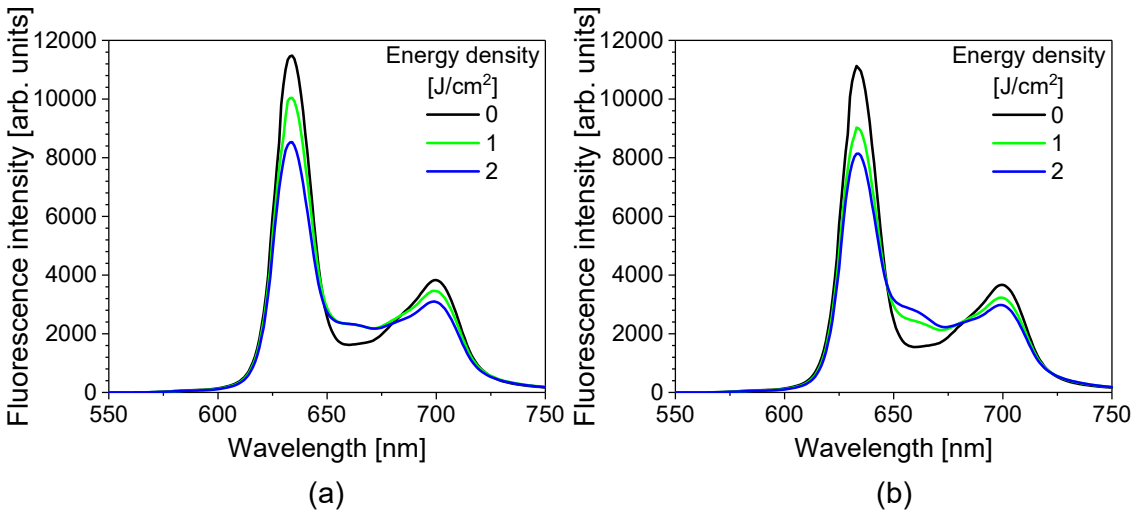

Figure 4.10: Fluorescence spectra of PpIX before and after irradiation with a 405 nm laser for 1 and 2 J/cm^2 for the fluence rates of (a) 10 and (b) 100 mW/cm^2.

MS analysis

The mass spectra of the blue-light irradiated PpIX are shown in Fig. 4.11. A noticeable difference in the photobleaching of the $[M+H]^+$ peak of PpIX between the two fluence rates is observed (Figs. 11(a) and 11(b)). The intensity at *m/z* 563.3 was reduced to 74% and 34% after 1 J/cm^2 irradiation for 10 and 100 mW/cm^2, respectively. No evident new peak, which may indicate the formation of a photoproduct, was detected in the mass spectra of PpIX after irradiation with the blue light.

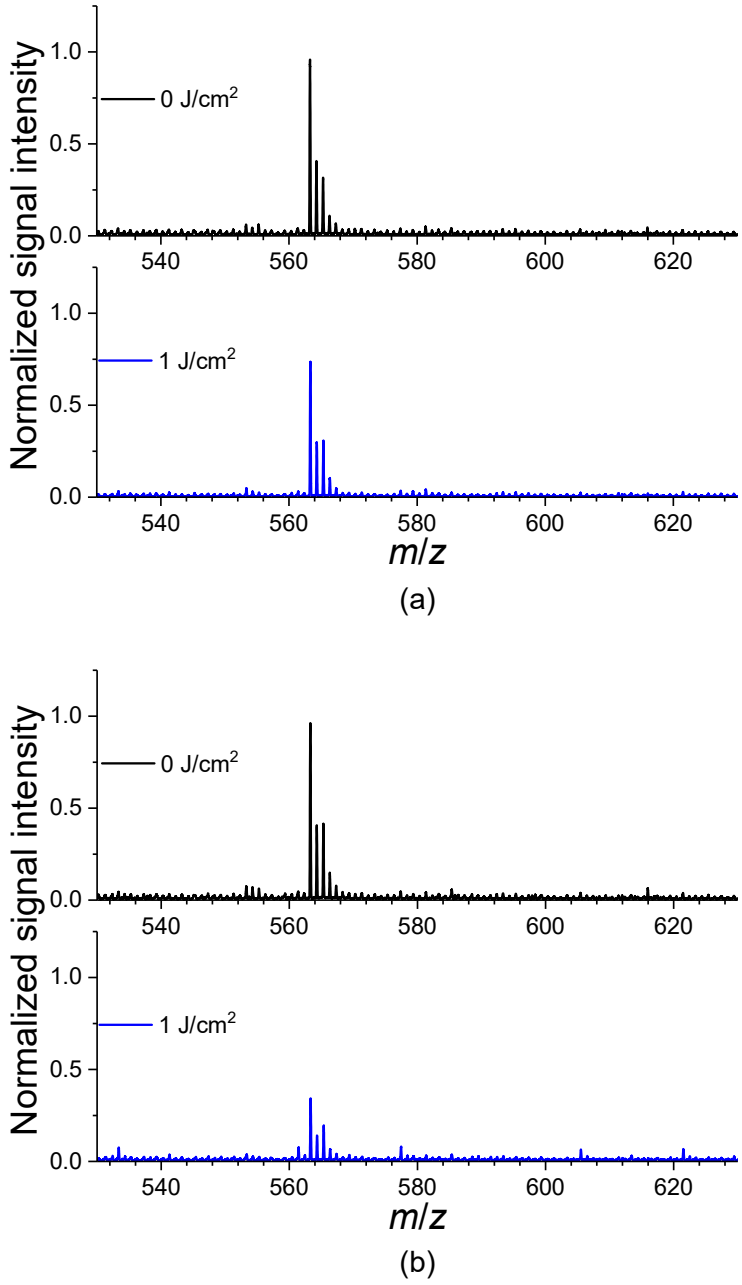

Figure 4.11: Mass spectra of PpIX before and after 405 nm irradiation with an energy density of 1 J/cm^2 at the irradiation power densities of (a) 10 mW/cm^2 (M_{B10}) and (b) 100 mW/cm^2 (M_{B100}).

Absorption analysis

In the absorption spectra of PpIX before and after irradiation with blue light (Fig. 4.12), a broad absorption peak emerges between 650 and 700 nm after irradiation. Additionally, the broadening of the peaks of PpIX occurs after irradiation. The difference spectra (Fig. 4.12(b)) display peak increases after PpIX irradiation. These intensities were higher in PpIX irradiation with a higher fluence rate (100 mW/cm^2).

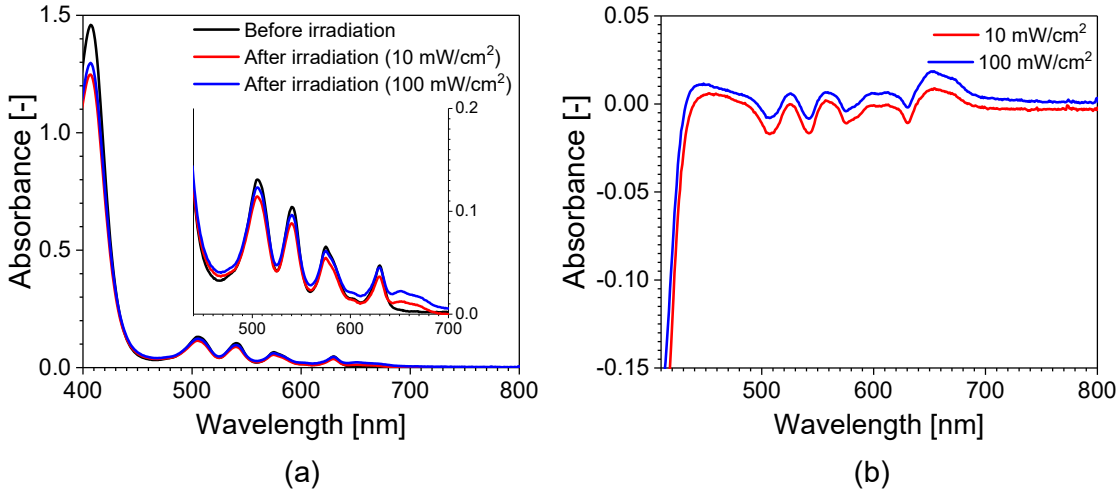

Figure 4.12: (a)Absorption spectra of PpIX before and after irradiation with 405 nm laser. PpIX was irradiated for 2 J/cm^2 at fluence rates of 10 and 100 mW/cm2. (b) Difference spectra of irradiated PpIX in (a). The spectrum of PpIX before irradiation was subtracted from the spectra after irradiation.

4.4. Discussion

Based on the emission wavelength, the peak at 673 nm observed after the red light irradiated PpIX in the fluorescence analysis (Fig. 4.2) is that of chlorin-type hydroxyaldehyde photoproduct, photoprotoporphyrin (Ppp) [1,8]. The absorption peak at 668 nm, which appeared after red-light irradiation of PpIX (Fig. 4.6), also belongs to Ppp [19–21]. A study has shown a high fluorescence intensity of Ppp at 675 nm when excited at 450 nm [8], indicating that Ppp has an absorption peak around 450 nm. Thus, the absorption peak at 450 nm observed in the difference spectra (Fig. 4.6(b)) may be that of Ppp. It is presumed that the new MS peak at *m*/*z* 595.3, which rose with increased red-light irradiation of PpIX, may also be attributed to the same photoproduct (Fig. 4.4). The

LC/MS/MS spectrum of this peak (Fig. 4.9) has a similar fragmentation pattern as that of PpIX [22]. Thus, the new peak should be a product of PpIX, having a chemical structure similar to that of PpIX. The findings by Cox et al. [16] claim that the hydroxyaldehyde photoproducts are formed by the cycloaddition of singlet oxygen to one of the two vinyl rings of PpIX. Accordingly, the protonated monoisotopic peak $[M+H]^+$ of Ppp should be detected around *m*/*z* 595.3. As an additional reference, a red-light irradiation of PpIX dimethyl ester under analysis conditions similar to that of PpIX was investigated. The result showed the formation of a new peak that can be explained by the photooxidation of PpIX dimethyl ester by singlet oxygen (data not shown). Inhoffen et al. [12] analysed irradiated PpIX dimethyl ester, which has been chromatographically separated and analysed using MS. Their result also corroborates the formation of Ppp by PpIX photooxidation. These further corroborate that the new MS peak at *m*/*z* 595.3 (Fig. 4.4) is attributed to Ppp.

Based on the extracted ion chromatogram at *m*/*z* 595.3 (Fig. 4.7), Ppp should have at least 3 isomers. As indicated by previous studies [12], two isomers are formed by the oxygenation of either of the diene ring substituted with the vinyl group (Fig. 4.13). An endoperoxide is formed after 1-4 cycloaddition of singlet oxygen to the diene (1→2), which then rearranges to form the hydroxyaldehyde photoproducts (2→3). If a higher concentration of Ppp is analysed, a further split of the chromatographic peak may occur, changing Peak C (Fig. 4.7) into a doublet. The oxygenation of the vinyl-substituted pyrrolidine ring in place of the diene ring could form a third and a fourth isomer.

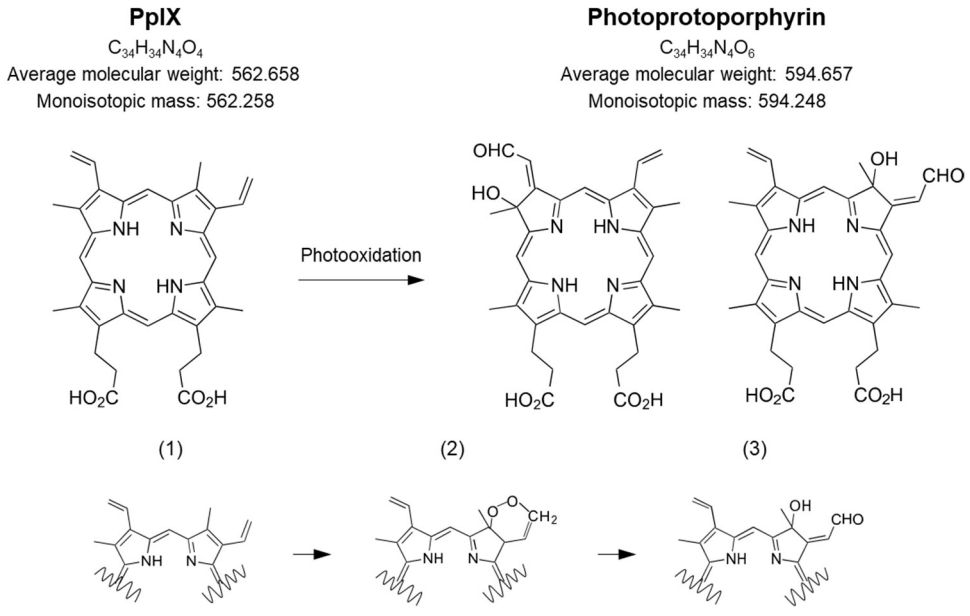

Figure 4.13: Structures of the hydroxyaldehyde photoproducts and their reaction scheme.

The fluorescence peak at 654 nm observed in the blue-light irradiation of PpIX (Fig. 4.10) is PpII, as reported by Dysart et al., and has been reported to be formed primarily from Ppp [7]. In line with that, Ppp should be present at the onset of the formation of Pp II. Unfortunately, in the fluorescence spectra where the peak of Pp II was observed, no fluorescence peak of Ppp was noted (Fig. 4.10). In the work by Dysart et al. [7], where both Ppp and Pp II fluorescence peaks were observed simultaneously, a detailed spectral decomposition was performed. Since both photoproducts' fluorescence peaks overlap with that of PpIX, a spectral decomposition may be needed for their detections in cases where their fluorescence intensities are small. Additionally, using a suitable wavelength to selectively excite each photoproduct may lead to their fluorescence detection from the same sample [8]. Based on some studies, selective irradiation of Ppp using 670 nm would yield peaks of Pp II around 650 nm, which can be detected by 450 or 543 nm excitations [8,19]. However, in such an analysis performed by Theodossiou et al. [19], after an 80 % reduction of Ppp, the fluorescence intensity of the photobleached Ppp had higher fluorescence intensity than that of Pp II. Thus, simultaneously observing the Ppp and Pp II fluorescence peaks with both emitting significant fluorescence intensities may be difficult. On the other hand, in the investigation performed by Cox et al., no new absorption band was noted in the visible region after the irradiation of Ppp formed from irradiated protoporphyrin IX dimethyl ester [6]. They hypothesised that if any photoproducts were formed from the irradiation of Ppp, they might be quickly degraded. From the fluorescence spectra of Fig. 4.10, the formation of Pp II in blue-light irradiation of PpIX was observed. Hence, if Pp II is a product of Ppp, it is expected that Ppp should be detected in the blue-light irradiated PpIX. As indicated earlier, the fluorescence peak of Ppp was not visible in the blue-light irradiated PpIX. The Ppp peak was also absent in the mass spectra of 405 nm irradiated PpIX for both fluence rates (Figs. 4.11). Thus, it may be speculated that Pp II is predominantly formed directly from PpIX, and they are the formyl porphyrin photoproducts. Formyl photoproducts have the main absorption band between 640 and 650 nm [23]. Our absorption analysis of blue-light irradiated PpIX indicated a dominant absorption at 650 nm occurring after PpIX irradiation. The formyl-type photoproducts are also formed by the reaction of PpIX with oxygen, with the oxygen binding to the vinyl ring (Fig. 4.14). The singlet oxygen is added directly to either or both of the vinyl-substituted diene or the pyrrolidine ring without affecting the double bond (1→2). This forms a dioxetane, which cleavages to form the formyl photoproduct [6,24].

The chemical structures of these formyl photoproducts indicate that the molecular weight is 564.63 g/mol for the two isomers having oxygenation of either of the vinyl rings and 566.60 g/mol for the oxygenation of both vinyl rings [6,24]. Hence, the protonated monoisotopic peak of these

photoproducts is expected at *m*/*z* 565.63 and 567.60, respectively. These peaks were not apparent in the mass spectra of irradiated PpIX (Figs. 4.4 and 4.11). Detecting these peaks may be challenging without a chromatographic separation, as they considerably overlap with the isotope peaks of PpIX. Additionally, the formation rate of the hydroxy aldehyde photoproducts is larger than that of the formyl-type photoproduct, with a ratio of 10:1 [15]. In the results of our fluorescence analyses (Figs. 4.2 and 4.10), the fluorescence intensity of Ppp is clearly higher than that of Pp II. Yet, the fluorescence intensity of Ppp is considerably low compared to the fluorescence intensity of the photobleached PpIX, with maximum Ppp intensity being half of the photobleached PpIX. Since the intensity of Ppp detected in the mass spectra (Fig 4.4) is low, detecting that of Pp II, which may have MS intensities $1/10^{th}$ less than that of Ppp, as well as overlapping *m*/*z* as that of PpIX, may hinder their detection. Investigations of higher blue-light irradiation of PpIX to increase Pp II formation may be helpful. Furthermore, changing the PpIX solvent may aid in the detection of Pp II, as the dominance of the formyl-type photoproducts over the hydroxyaldehyde photoproducts in micelles and liposomes has been reported [6].

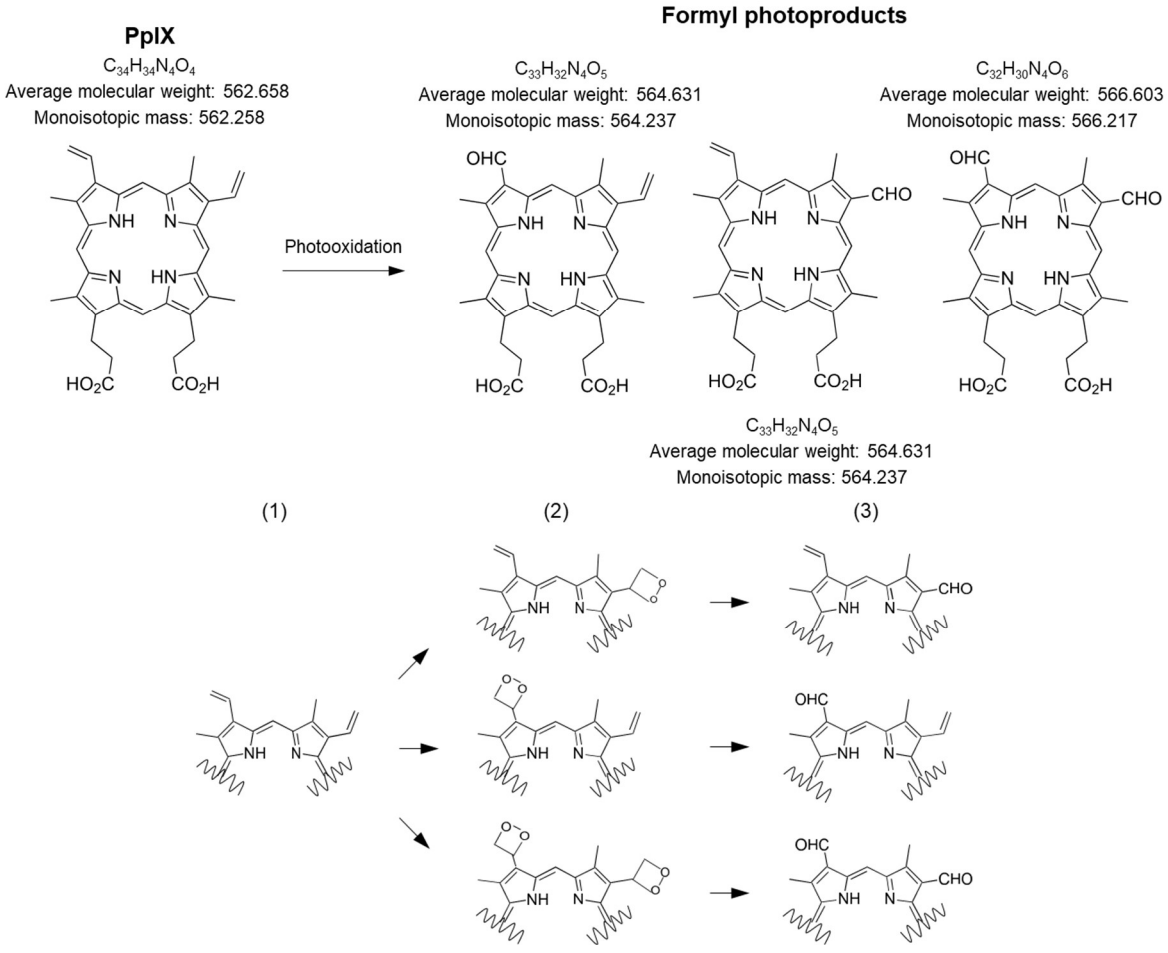

Figure 4.14: Structures of formyl-type photoproducts and their reaction scheme.

Photoproduct formation with irradiation wavelength and fluence rate

Results obtained in this chapter, as well as Chapter 3, indicate that the irradiation laser wavelength and the fluence rate influence both Ppp and Pp II formation. Based on the fluorescence results, Ppp is predominant in the red-light irradiated PpIX, while Pp II is the main photoproduct formed in the blue-light irradiation of PpIX. In fluorescence, absorption and MS analyses, a higher formation of Ppp was noted for lower fluence rate irradiation of PpIX (Figs. 4.3, 4.5 and 4.6). In contrast, Pp II formation was more favourable in PpIX irradiation at a higher fluence rate (Fig. 4.10 and 4.12. Additionally, Chapter 3, Fig. 3.2). Oxygen availability plays a role in the photoproducts formation, as the photoproducts result from the reaction of PpIX with singlet oxygen [7,10]. Since our analyses were performed in solution, we presume there was no shortage of oxygen to the PpIX. However, the singlet oxygen quantum yield can differ with the irradiation fluence rate. At high fluence rates, direct destruction of PpIX can occur, resulting in lower singlet oxygen production needed for photoproduct formation [25]. Furthermore, there may be a variation in the reaction rates of the PpIX and oxygen with the fluence rate.

Comparing the Ppp formation rate observed in the fluorescence and the MS analysis for lower fluence rate (Figs. 4.3 and 4.5), although the Ppp formation rates were slightly faster in the MS analysis, the intensity ratio of Ppp to PpIX after 100 J/cm^2, was comparable. For PpIX irradiation with a 635 nm laser set at 10 mW/cm^2, 1 J/cm^2 led to a 1.27 ± 0.30 and 1.14 ± 0.14 times rise in the fluorescence intensity and MS signal intensity of Ppp, respectively.

Application of PpIX photoproducts in PDD and PDT

Ppp may potentially be applied for PDD and PDT [1,13,14,26]. The results of this study show that a lower fluence rate favours the formation of Ppp. Lower fluence rates are preferable in PDT, as it offers higher tumour destruction due to incomplete vascular shutdown [27]. With higher Ppp formation at low fluence rates, Ppp may be potentially used as a photosensitizer in PDT. Ppp is less prone to photobleaching than PpIX in some conditions [16,28]. Hence, additional fluorescence diagnosis time during PDD could be achieved if Ppp formed during PDD is used in addition to PpIX.

In cases where higher fluence rates are desired [29–32], employing Pp II may be beneficial for fluorescence diagnosis involving fluorescence photoswitching. A similar diagnostics method using Ppp has been investigated [26]. Furthermore, the formyl photoproducts have a singlet oxygen quantum yield comparable to PpIX [6]. Thus, the formyl photoproducts could be instrumental to PDT if explored.

4.5. Chapter conclusion

In this chapter, we have employed fluorescence, absorption, mass spectrometry and HPLC-MS to analyse the PpIX photoproducts. The investigation showed that the predominant photoproduct changed with the wavelength of light (405 or 635 nm) used in the PpIX irradiation. The 635 nm irradiation of PpIX predominantly produced the hydroxyaldehyde photoproduct, photoprotoporphyrin, while the 405 nm irradiation of PpIX primarily had the product II, which is potentially the formyl photoproduct. We speculate that both of these photoproducts are directly formed from PpIX. In addition, the rates at which these photoproducts were formed were affected by the fluence rate.

The application of photoproducts for PDD and PDT has been previously explored. Similar to the photobleaching rate, it is speculated that the photoproduct formations may differ *in vivo*. If further utilisation is intended, a more detailed investigation of the photoproduct formation under various conditions needs to be studied. However, analysis of their formation in organic solvent, as was done in this study, would be instrumental in future analyses.

References

[1]. L. Ma, S. Bagdonas, and J. Moan, "The photosensitizing effect of the photoproduct of protoporphyrin IX," *Journal of Photochemistry and Photobiology B: Biology*, **60**(2–3), 108–113 (2001).

[2]. L. Brancaleon and H. Moseley, "Effects of photoproducts on the binding properties of protoporphyrin IX to proteins," *Biophysical Chemistry*, **96**(1), 77–87 (2002).

[3]. J. Moan, G. Streckyte, S. Bagdonas, Ø. Bech, and K. Berg, "Photobleaching of protoporphyrin IX in cells incubated with 5-aminolevulinic acid," *International Journal of Cancer*, **70**, 90–97 (1997).

[4]. R. L. Goyan and D. T. Cramb, "Near-Infrared Two-Photon Excitation of Protoporphyrin IX: Photodynamics and Photoproduct Generation," *Photochemistry and Photobiology*, **72**(6), 821–827 (2000).

[5]. D. J. Robinson, H. S. De Bruijn, N. Van Der Veen, M. R. Stringer, S. B. Brown, and W. M. Star, "Fluorescence Photobleaching of ALA-induced Protoporphyrin IX during Photodynamic Therapy of Normal Hairless Mouse Skin: The Effect of Light Dose and Irradiance and the Resulting Biological Effect," *Photochemistry and Photobiology*, **67**(1), 140–149 (1998).

[6]. G. S. Cox and D. G. Whitten, "Excited state interactions of protoporphyrin IX and related

porphyrins with molecular oxygen in solutions and in organized assemblies.," *Advances in experimental medicine and biology*, **160**, 279–292 (1983).

[7]. J. S. Dysart and M. S. Patterson, "Photobleaching kinetics, photoproduct formation, and dose estimation during ALA induced PpIX PDT of MLL cells under well oxygenated and hypoxic conditions," *Photochemical and Photobiological Sciences*, **5**(1), 73–81 (2006).

[8]. S. Bagdonas, L. W. Ma, V. Iani, R. Rotomskis, P. Juzenas, and J. Moan, "Phototransformations of 5-Aminolevulinic Acid–induced Protoporphyrin IX in vitro: A Spectroscopic Study," *Photochemistry and Photobiology*, **72**(2), 186–192 (2000).

[9]. C. Af Klinteberg, A. M. K. Enejder, I. Wang, S. Andersson-Engels, S. Svanberg, and K. Svanberg, "Kinetic fluorescence studies of 5-aminolaevulinic acid-induced protoporphyrin IX accumulation in basal cell carcinomas," *Journal of Photochemistry and Photobiology B: Biology*, **49**(2–3), 120–128 (1999).

[10]. J. C. Finlay, D. L. Conover, E. L. Hull, and T. H. Foster, "Porphyrin Bleaching and PDT-induced Spectral Changes are Irradiance Dependent in ALA-sensitized Normal Rat Skin In Vivo," *Photochemistry and Photobiology*, **73**(1), 54–63 (2001).

[11]. S. C. A. Yeh, M. S. Patterson, J. E. Hayward, and Q. Fang, "Time-resolved fluorescence in photodynamic therapy," *Photonics*, **1**(4), 530–564 (2014).

[12]. H. H. Inhoffen, H. B. Jr., and K. -M Bliesener, "Zur weiteren Kenntnis des Chlorophylls und des Hämins, XXX1) Photoprotoporphyrine und ihre Umwandlung in Spirographis- sowie Isospirographis-porphyrin2)," *Justus Liebigs Annalen der Chemie*, **730**(1), 173–185 (1969).

[13]. K. König, H. Schneckenburger, A. Rück, and R. Steiner, "In vivo photoproduct formation during PDT with ALA-induced endogenous porphyrins," *Journal of Photochemistry and Photobiology, B: Biology*, **18**(2–3), 287–290 (1993).

[14]. L. Giniūnas, R. Rotomskis, V. Smilgevičius, A. Piskarskas, J. Didžiapetrienė, L. Bloznelyte, and L. Griciute, "Activity of haematoporphyrin derivative photoproduct in photodynamic therapy in vivo," *Lasers in Medical Science*, **6**(4), 425–428 (1991).

[15]. R. Bonnett and G. Martínez, "Photobleaching of sensitisers used in photodynamic therapy," *Tetrahedron*, **57**(47), 9513–9547 (2001).

[16]. G. S. Cox and D. G. Whitten, "Mechanisms for the Photooxidation of Protoporphyrin IX in Solution," *Journal of the American Chemical Society*, **104**(2), 516–521 (1982).

[17]. K. Huang, L. Chen, S. Lv, and J. Xiong, "Protoporphyrin IX photobleaching of subcellular distributed sites of leukemic HL60 cells based on ALA-PDT in vitro," *Journal of*

Biomedical Science and Engineering, **05**(09), 548–555 (2012).

[18]. J. S. Dysart and M. S. Patterson, "Photobleaching kinetics, photoproduct formation, and dose estimation during ALA induced PpIX PDT of MLL cells under well oxygenated and hypoxic conditions," *Photochemical and Photobiological Sciences*, **5**(1), 73–81 (2006).

[19]. T. Theodossiou and A. J. MacRobert, "Comparison of the Photodynamic Effect of Exogenous Photoprotoporphyrin and Protoporphyrin IX on PAM 212 Murine Keratinocytes," *Photochemistry and Photobiology*, **76**(5), 530–537 (2002).

[20]. P. Charlesworth and T. G. Truscott, "The use of 5-aminolevulinic acid (ALA) in photodynamic therapy (PDT)," *Journal of Photochemistry and Photobiology, B: Biology*, **18**(1), 99–100 (1993).

[21]. E. T. Ponce Ayala, F. Alves Dias de Sousa, J. D. Vollet-Filho, M. Rodrigues Garcia, L. de Boni, V. Salvador Bagnato, and S. Pratavieira, "Photodynamic and Sonodynamic Therapy with Protoporphyrin IX: In Vitro and In Vivo Studies," *Ultrasound in Medicine & Biology*, **47**(4), 1032–1044 (2021).

[22]. A. Walke, E. S. Molina, W. Stummer, S. König, A. Walke, E. S. Molina, W. Stummer, and S. König, "Protoporphyrin IX Analysis from Blood and Serum in the Context of Neurosurgery of Glioblastoma," *Mass Spectrometry in Life Sciences and Clinical Laboratory*, (2020).

[23]. E. F. G. Dickson and R. H. Pottier, "On the role of protoporphyrin IX photoproducts in photodynamic therapy," *Journal of Photochemistry and Photobiology, B: Biology*, **29**(1), 91–93 (1995).

[24]. J. M. Wessels, R. Sroka, P. Heil, and H. K. Seidlitz, "Photodegradation of protoporphyrin-dimethylester in solution and in organized environments," *International journal of radiation biology*, **64**(5), 475–484 (1993).

[25]. C. R. Shea, Y. Hefetz, R. Gillies, J. Wimberly, G. Dalickas, and T. Hasan, "Mechanistic investigation of doxycycline photosensitization by picosecond-pulsed and continuous wave laser irradiation of cells in culture.," *Journal of Biological Chemistry*, **265**(11), 5977–5982 (1990).

[26]. S. J. Ogbonna, W. Y. York, T. Nishimura, H. Hazama, H. Fukuhara, K. Inoue, and K. Awazu, "Increased fluorescence observation intensity during the photodynamic diagnosis of deeply located tumors by fluorescence photoswitching of protoporphyrin IX," *https://doi.org/10.1117/1.JBO.28.5.055001*, **28**(5), 055001 (2023).

[27]. S. Iinuma, K. Schomacker, G. Wagnières, M. Rajadhyaksha, M. Bamberg, T. Momma, and

T. Hasan, "In vivo fluence rate and fractionation effects on tumor response and photobleaching: Photodynamic therapy with two photosensitizers in an orthotopic rat tumor model," *Cancer research*, **59**, 6164–6170 (2000).

[28]. W. Dietel and R. Wendenburg, "Phototransformation of ALA-induced protoporphyrin IX (PPIX) in carcinoma cells and of exogenous PPIX in cells and solutions," *https://doi.org/10.1117/12.203418*, **2371**, 567–571 (1995).

[29]. I. Buzalewicz, I. Hołowacz, A. Ulatowska-Jarża, and H. Podbielska, "Towards dosimetry for photodynamic diagnosis with the low-level dose of photosensitizer," *Journal of Photochemistry and Photobiology B: Biology*, **173**, 333–343 (2017).

[30]. T. Hirano, Y. Hagiya, H. Fukuhara, K. Inoue, T. Shuin, K. Matsumoto, K. Inoue, T. Tanaka, I. Okura, and S. I. Ogura, "Improvement of aminolevulinic acid (ALA)-mediated photodynamic diagnosis using n-propyl gallate," *Photodiagnosis and Photodynamic Therapy*, **10**(1), 28–32 (2013).

[31]. D. Kurakina, A. Khilov, M. Shakhova, N. Orlinskaya, E. Sergeeva, A. Meller, I. Turchin, and M. Kirillin, "Comparative analysis of single- and dual-wavelength photodynamic therapy regimes with chlorin-based photosensitizers: animal study," *Journal of Biomedical Optics*, **25**(06), 1 (2019).

[32]. T. Namikawa, T. Yatabe, K. Inoue, T. Shuin, and K. Hanazaki, "Clinical applications of 5-aminolevulinic acid-mediated fluorescence for gastric cancer," *World Journal of Gastroenterology*, **21**(29), 8817–8825 (2015).

Chapter 5
Photoproducts of PpIX for PDD of deeply located tumours

5.1. Introduction

Factors such as the photobleaching of the photosensitizer and the wavelength used in the photosensitizer excitation can affect the diagnostic efficacy of PDD. PpIX has multiple absorption bands [1,2], allowing for PpIX excitation at various wavelengths during fluorescence diagnosis. However, owing to light attenuation caused by absorption and scattering in tissue, the penetration depths of the excitation light within the tissue vary [1,3]. Thus, the diagnostic depth is affected by the excitation wavelength and the tissue's optical properties. Increased tissue penetration and reduced excitation light scattering can be achieved with longer wavelengths [1,2]. Increased penetration depth for PpIX excitation with red light during fluorescence detection has been ascertained [1,4]. Unfortunately, tumour detection with red light excitation might be challenging in clinical application, as PpIX emits reddish fluorescence, which overlaps with the red excitation wavelength. Studies by Ihara et al. [2] and Takishima et al. [5] investigated various wavelengths for PpIX excitation to obtain maximum fluorescence intensity at different depths of gastric and bladder tissue. Their results showed that using 505 nm light for excitation could extend the fluorescence diagnostics depth without overlaps with the PpIX fluorescence emission. However, these studies that aimed to improve the diagnostics depth did not consider the effect of photosensitizer photobleaching. The PpIX photobleaching that occurs during PDD limits the fluorescence observation time [6,7]. Again, the effect of the photobleaching may be notably large since the fluorescence emission from the photosensitizer is already low when used to detect deeply located tumours.

Concomitant with the PpIX photobleaching, its photoproducts are formed. One of the photoproducts formed from PpIX irradiation photoprotoporphyrin (Ppp) is a fluorophore [8]. Similar to PpIX, Ppp can be excited at various wavelengths. Additionally, Ppp can be less susceptible to photodegradation than PpIX [9–11]. Hence, there is a prospect of using fluorescence emitted from Ppp for fluorescence diagnosis of tumours. The study conducted in this chapter explores the use of fluorescence emission from both PpIX and Ppp to increase the fluorescence observation intensity and prolong the fluorescence observation time for deeply located tumours.

Changing the excitation light to an appropriate wavelength at an appropriate time would result in fluorescence photoswitching, with photoproducts yielding fluorescence intensity higher than that of PpIX at the time. It is intended that this would improve the diagnostic efficacy by increasing the fluorescence detection intensity and time.

In this chapter, first, the suitable wavelength for the excitation of Ppp was investigated. Then, the fluorescence photoswitching between PpIX and its photoproduct was investigated when irradiated and excited with green light and Ppp-excitation-suitable blue light at time intervals. The fluorescence intensity of PpIX and the photoproduct formed after PpIX photobleaching caused by green light excitation were studied in solution. *Ex vivo* analyses were carried out to determine the fluorescence detection of PpIX and its photoproduct within the gastric mucosa layer under similar excitations. Analyses were also performed *in vivo* to verify the results observed in solution and *ex vivo*.

5.5.1. Concept of fluorescence photoswitching

The concept of fluorescence photoswitching (Fig. 5.1) can be described in the following steps;

- **i.** PDD for deeply located tumours is performed by exciting the photosensitizer with green light.
- **ii.** The excitation of the photosensitizer for fluorescence detection leads to the photosensitizer photobleaching and the formation of the photosensitizer photoproducts.
- **iii.** With time, a notable amount of PpIX is photobleached, and there is an accumulation of the photoproducts formed.
- **iv.** At this time, the wavelength of the excitation light is changed to excite the accumulated photoproducts.
- **v.** The fluorescence emitted from the photoproducts would yield fluorescence intensity higher than that of the photobleached photosensitizer.

Thus, the tumour detection efficacy is improved with the increased fluorescence emission intensity, resulting in a longer detection time.

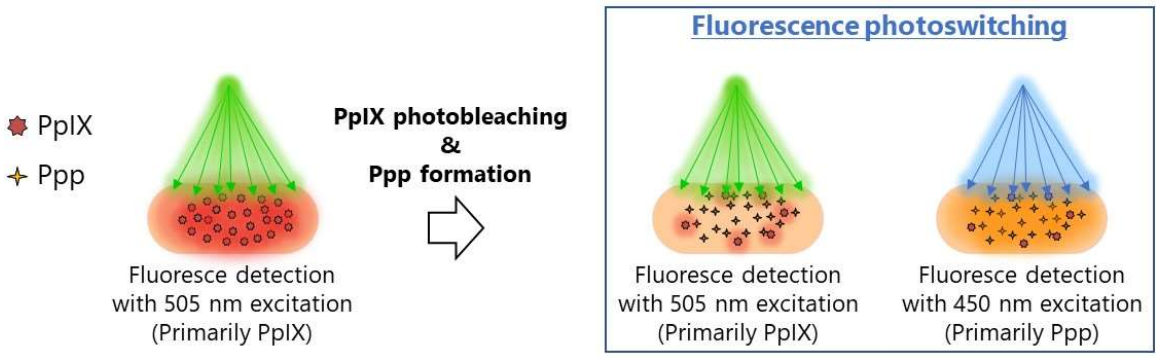

Figure 5.1: Concept of fluorescence photoswitching.

5.2. Materials and methods

5.2.1. Photoproducts detection with excitation wavelength

200 µL of 10 µM PpIX diluted with DMSO was irradiated with the setup described in Sec. 3.2.1. The sample was irradiated at 635 nm using the light source used in the PDT irradiation condition. The irradiation was performed at a fluence rate of 10 mW/cm^2 for 20 J/cm^2. Fluorescence emission from the sample was investigated as described in Sec. 3.2.2. It was reported that a high relative fluorescence intensity of Ppp was observed for excitation with 450 nm [9]. Thus, the fluorescence emission for the irradiated PpIX, excited at 450 nm, as well as that at 405, 514 and 532 nm, were also measured.

5.2.2. Solution analysis

60 µL of 10 µM PpIX diluted with DMSO was placed per well in a 96-well plate. The sample in each well was irradiated using the setup described in Sec. 3.2.1. The light source for the irradiation was changed to a green light-emitting diode (LED) with a nominal wavelength of 505 nm and a bandwidth (full width at half maximum (FWHM)) of 30 nm (M505L3, Thorlabs). The wells were irradiated with an increasing energy density between 0 and 50 J/cm^2 at fluence rates of 20 and 50 mW/cm^2. In addition to the variable neutral density filter (NDHN-50, Sigmakoki, Japan), the irradiation powers were set using a tuneable LED driver (LEDD1B, Thorlabs). The LED light was irradiated through a collimation adapter (COP1-A, Thorlabs). The fluorescence emissions from the irradiated PpIX solution were measured using the fluorescence microplate reader described in Sec. 2.2.1, with the excitation wavelengths at 450 and 505 nm.

5.2.3. *Fluorescence imaging setup*

The fluorescence emission images for the *ex vivo* and the *in vivo* analyses were carried out using the setup of Fig. 5.2.

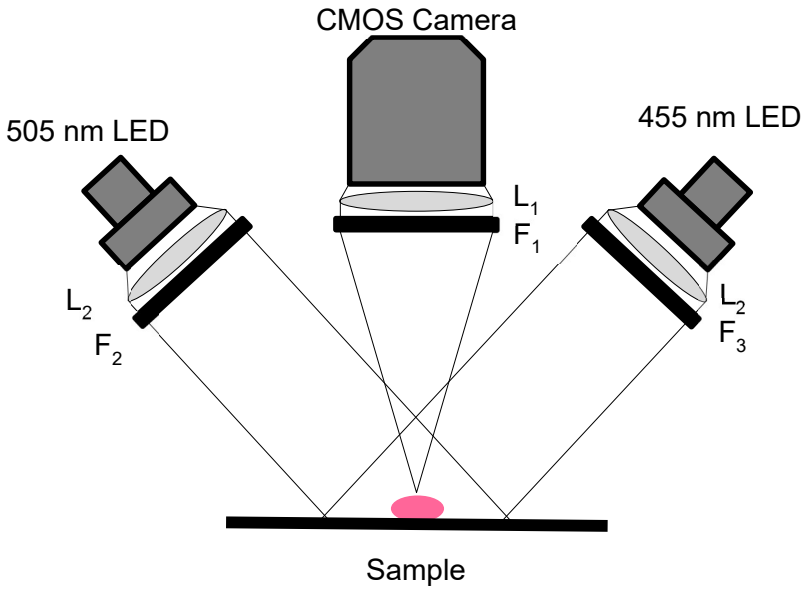

Figure 5.2: Optical setup for fluorescence imaging.

The fluorescence images were obtained by exciting the sample with 455 nm and 505 nm LEDs. The 505 nm LED was similar to that used in Sec. 5.2.2. The 455 nm LED has a nominal wavelength of 455 nm and bandwidth (FWHM) of 18 nm (M455L3, Thorlabs). The LEDs were irradiated through a lens, L_2 (ACL2520U-DG15-A, Thorlabs), and bandpass filters F_2 and F_3 with FWHM of 25 nm. F_2 (86-654, Edmund Optics) was placed in the 505 nm LED to give a centre wavelength of 500 nm, while F_3 (86-653, Edmund Optics) was used for the 455 nm LED to give a centre wavelength of 450 nm.

The fluorescence emission images from the samples were taken using a CMOS monochrome camera (Chameleon 3, CM3-U3-31S4M, FLIR; with a camera lens L_1 f = 16 mm, F/1.4, NMV-16M1, Navitar). The camera was fitted with a 600 nm long-pass filter, F_1 (FELH0600, Thorlabs), to cut off the excitation light. The surface for placing the sample was placed 26 mm from the long pass filter, F_1. The LEDs were angled 55° from the camera and placed approximately equal distances from the sample plate and the camera. The exposure time for obtaining the fluorescence images was

adjusted between 180 and 5000 μs to suit the *ex vivo* or the *in vivo* analysis.

5.2.4. Pellet preparation

PpIX was diluted to 1 mM with DMSO and further diluted to 10 μM with clear epoxy resin (87136, Tamiya, Japan). The solution was heated for about 1 minute in an 80 °C water bath to deaerate the mixture, poured into a Petri dish, and left to harden for more than 48 hours. PpIX pellets with a diameter of 3 mm and a thickness of 1 mm were cut out from the hardened epoxy resin sheet. A blank pellet was prepared with only DMSO, and were used as the background.

5.2.5. Ex vivo analysis

Porcine stomach obtained from IVTeC Co., Ltd., Tokyo, Japan, was rinsed in saline to remove mucus, wrapped in aluminium foil, sealed, and frozen at −25°C until use.

The porcine mucosa was sliced at an arbitrary depth using a cryotome (CM1850, Leica, Germany), and the PpIX pellet of Sec. 5.2.4 was placed between the sliced layer.

The fluorescence observation of the pellet within the mucosa was performed with the setup described in Sec 5.2.3 using the 505 nm LED at a power density of 2 mW/cm^2. Fluorescence images of the pellets were taken at intervals between 0 and 10 J/cm^2 of irradiation for excitations at 455 and 505 nm. Fluorescence images for both excitations were obtained using similar parameters.

The depth of mucosa at which the PpIX pellet was placed for the analysis was determined by sectioning the porcine mucosa used in the analysis to a thickness of 60 μm with the cryotome and analysing the section with a slide scanner (NanoZoomer 2.0 RS, Hamamatsu Photonics, Japan).

5.2.6. In vivo analysis

Seven-week-old female BALB/c nu/nu mouse was housed in plastic cages with stainless steel grid tops in an air-conditioned room with a 12 h light-dark cycle maintained at room temperature and provided with water and food in the institute for animal experiments of Kochi Medical School.

Human prostate cancer cell line (PC-3), obtained from Isaiah J. Fidler of the M. D. Anderson Cancer Center, Department of Cell Biology, University of Texas (Houston, TX, USA) were kept in Dulbecco's modified Eagle medium (D-MEM: 12100-046, GIBCO) containing 10 % fetal bovine serum (Hyclone, SH30910.03, Cytiva, Japan) and stored under 5 % CO_2 at 37 ℃.

The PC-3 cells (2×10^6) suspended in 100 μL of the D-MEM solution were subcutaneously injected into the mouse's dorsal region. After two weeks, a solution of aminolevulinic acid

hydrochloride (ALA HCl; Al-05-1, Neopharma, Japan) was intraperitoneally injected into the tumour-bearing mouse at a dose of 600 mg/kg. The PDD was performed 2 h after ALA HCl administration.

As was observed by other studies, high fluorescence emission from the skin of the mouse interfered with the fluorescence emission from the lesion [8,12]. For clear observation of the fluorescence emitted from the lesion, the skin of the mouse surrounding the lesion was cut open to expose the lesion, and 505 nm PDD was performed using the setup of Sec. 5.2.3. The fluorescence images of the lesion, excited at 455 and 505 nm were taken at intervals of 2.4 J/cm^2 for a total energy density of 9.6 J/cm^2 during the PDD. The mouse's skin was put back in place after 9.6 J/cm^2, and the fluorescence emission from the lesion was observed again for both excitations. The fluence rate of the LEDs used for the PDD and fluorescence imaging was approximately 4 mW/cm^2.

The position and size of the lesion were determined by analysing the section of the lesion by hematoxylin and eosin staining and measuring with a slide scanner.

All procedures were reviewed by the animal experiment and welfare committee of Kochi Medical School and were performed in compliance with the institutional guidelines and regulations.

5.3. Results

5.3.1. Photoproducts detection with excitation wavelength

Figure 5.3 shows the fluorescence spectra of PpIX after 635 nm irradiation obtained at various excitation wavelengths. The fluorescence intensities were normalised with the intensity of unirradiated PpIX at 633 nm for each excitation wavelength. Irradiation resulted in the formation of the Ppp peak at 673 nm. The intensities of the Ppp obtained at sample excitations of 405, 514, and 532 nm were comparable. Excitation at 450 nm yielded the highest Ppp intensity within the investigated excitation wavelengths. The Ppp intensity at 450 nm excitation was 4.45±0.26 times higher than the intensities obtained at 405, 514, and 532 nm excitations. Thus, to obtain a high fluorescence emission from Ppp, excitation with 450 nm is advantageous.

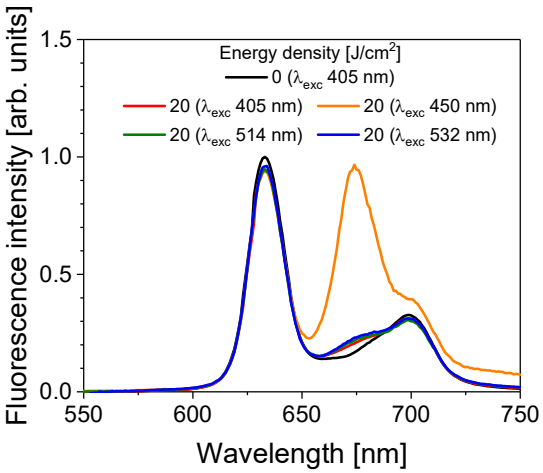

Figure 5.3: Fluorescence spectra of 635 nm irradiated PpIX at a fluence rate of 10 mW/cm^2 for 20 J/cm^2. The fluorescence spectra were obtained for excitations at 405, 450, 514, and 532 nm.

5.3.2. Fluorescence spectroscopic analysis

The fluorescence spectra of the PpIX solution of Sec. 5.2.2, before and after 50 J/cm^2 irradiation energy density, are shown in Fig. 5.4. Comparing the fluorescence intensity of the unirradiated PpIX, excitation with 505 nm yields higher fluorescence intensity than excitation with 450 nm. For the unirradiated PpIX (Fig. 5.4(a)), the highest fluorescence emission is noted at the 633 nm peak of the 505 nm excited PpIX. After irradiation, there was the photodegradation of the 633 nm peak and the appearance of a peak around 673 nm. The new peak indicates the formation of a photoproduct. After irradiation, the highest fluorescence intensity changes to the peak at 673 nm, excited at 450 nm (Fig. 5.4(b and c)). A more notable intensity at 673 nm is seen for irradiation performed at the fluence rate of 20 mW/cm^2 (Fig. 3(b)) than for irradiation performed at 50 mW/cm^2 (Fig. 3(c)).

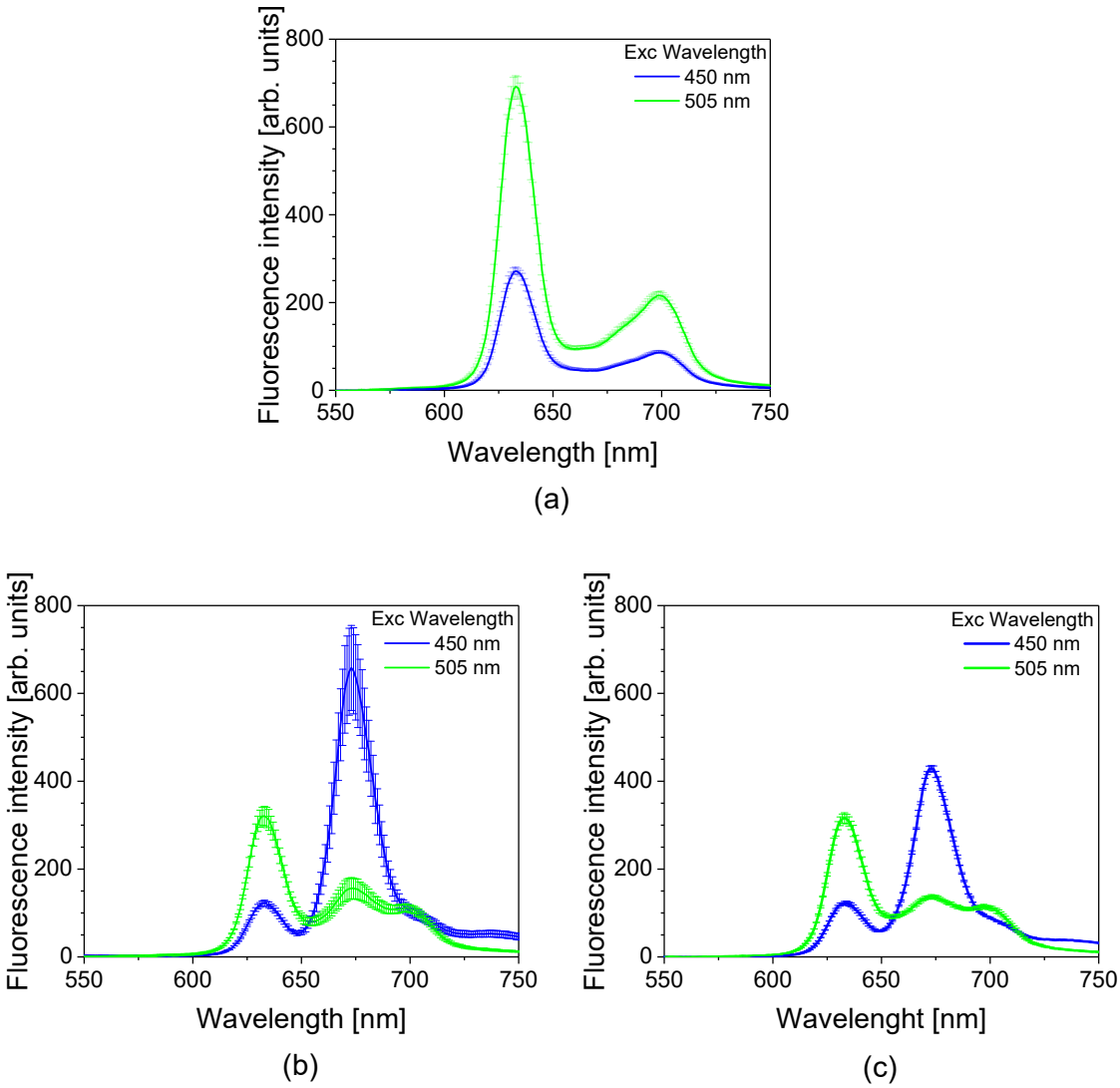

Figure 5.4: Fluorescence spectra of PpIX (a) before, and (b) after irradiation with a 505 nm light at fluence rate of 20 mW/cm^2, and (c) after irradiation with a 505 nm light at fluence rate of 50 mW/cm^2. The fluorescence spectra were obtained at excitation wavelengths of 450 nm and 505 nm. The error bars represent standard deviations for 3 independent experiments.

The fluorescence intensities at 633 nm (PpIX) and 673 nm (photoproduct) with increased irradiation were plotted in Fig. 5.5. The intensities at 633 nm were obtained at 505 nm excitation, and the intensities at 673 nm were obtained at 450 nm excitation. These intensities were termed I_G and I_B, respectively. For the two fluence rates investigated, the pattern of decay of the PpIX fluorescence intensity was similar. On the other hand, the rate of increase of the photoproduct was

faster for the 20 mW/cm^2 fluence rate. After the irradiation energy density of 28.5 and 37 J/cm^2 for 20 and 50 mW/cm^2, respectively, I_B became higher than that of I_G. This indicates the occurrence of fluorescence photoswitching. I_G continued to rise for the energy density investigated for both fluence rates.

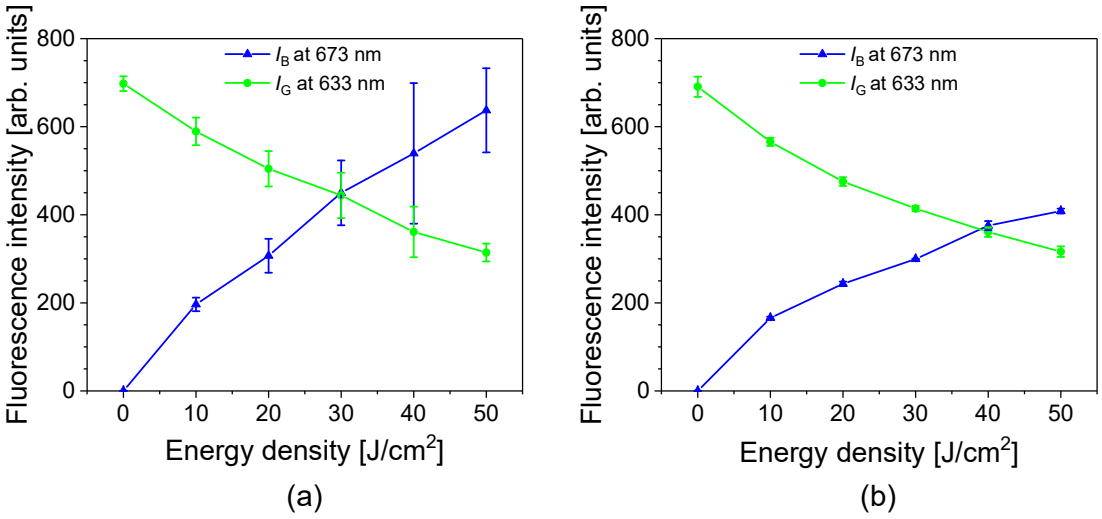

Figure 5.5: Fluorescence intensity of 505 nm irradiated PpIX, monitored at peak intensities of 633 and 673 nm for irradiation fluence rates of (a) 20, and (b) 50 mW/cm^2. PpIX was excited at 505 nm (I_G) and 450 nm (I_B). The error bars represent standard deviations from 3 independent experiments. The point at which I_B and I_G crosses indicates the point of fluorescence photoswitching.

5.3.3. Fluorescence imaging ex vivo

Figure 5.6 (a) displays the fluorescence images obtained from the *ex vivo* analysis of Sec. 5.2.5. Increase in the intensity of the pellets excited at 455 nm (I_B) after irradiation can be seen. For easier analysis of the fluorescence intensities of the pellets after each irradiation energy density, the fluorescence intensities of the pellets were plotted for each excitation (Fig. 5.6 (b)). For the plotted intensities, the tissue fluorescence at excitation of 455 or 505 nm was subtracted accordingly from that of the pellet as the background fluorescence.

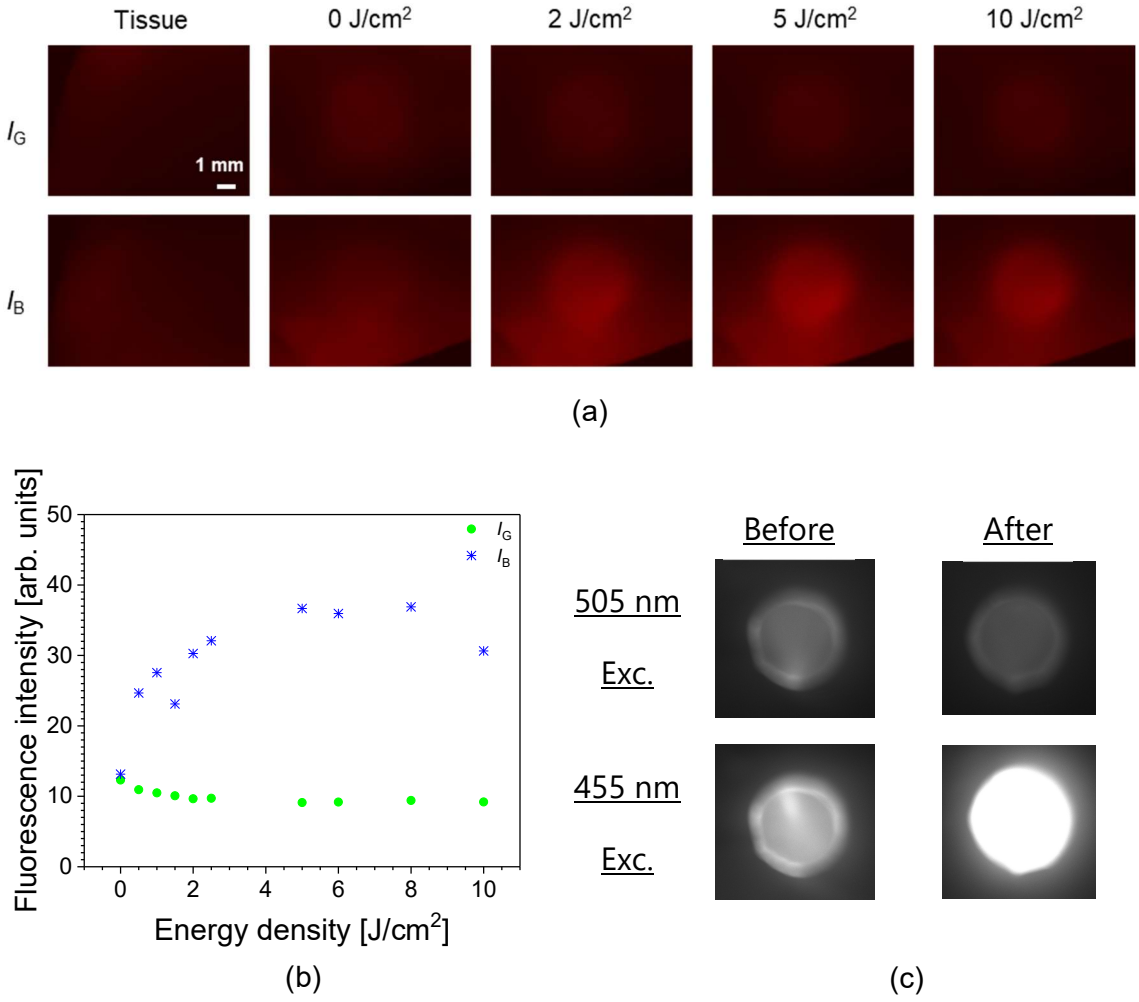

Figure 5.6: (a) Fluorescence images of the PpIX pellet within porcine mucosa with increasing irradiation. (b) A plot of fluorescence intensity of the PpIX pellet within the porcine mucosa vs irradiation energy density. (c) Fluorescence images of the pellet, outside the mucosa, before and after irradiation. The pellets were irradiated at 505 nm, while the fluorescence emissions were obtained at excitations of 455 and 505 nm.

The fluorescence emitted from the pellet at 0 J/cm^2 indicates that the intensity, I_B, was higher than I_G by 1.07 after the background fluorescence was subtracted. Based on the plot of Fig. 5.6 (b), an increase in I_B and a decrease in I_G was seen after 0.5 J/cm^2 of irradiation. I_B increased to a maximum of 2.8 times its initial fluorescence intensity (after 8 J/cm^2), while I_G photobleached to 0.74 times its initial fluorescence intensity. A spectroscopic analysis of the pellets before and after irradiation was performed using the fluorescence microplate reader of Sec. 2.2.1. The spectra indicate the appearance of 673 nm. Therefore, it can be presumed that the increase in the

fluorescence intensity with pellet irradiation is caused by the photoproduct, Ppp. Figure 5.6 (c) shows the fluorescence images of the pellets outside of the mucosa, taken before (0 J/cm^2) and after (10 J/cm^2) irradiation with 505 nm LED. Just as observed in the fluorescence images of the tissue within the mucosa, the fluorescence emission from the 455 nm excited pellet prior to irradiation (0 J/cm^2) is higher than that of 505 nm. A decrease in the fluorescence intensity of the PpIX pellet after irradiation is seen when the pellet is excited at 505 nm. On the contrary, we observed an evident increase in the intensity of the irradiated pellet when excited with 455 nm, with an increase leading to a saturated fluorescence image.

Figure 5.7 displays one of the section views of the mucosa used in the *ex vivo* analysis. The depth at which the mucosa was placed was determined by averaging the measured depths at 20 different points. The mucosa depth at which the fluorophore was placed for this analysis was calculated to be 1.28 ± 0.27 mm from the surface.

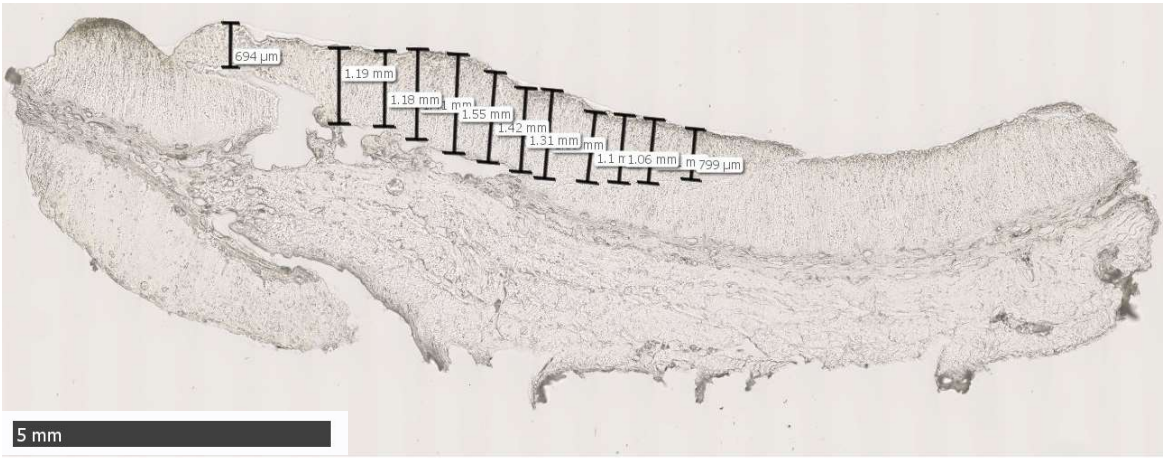

Figure 5.7: A section view of the mucosa which was used in the *ex vivo* analysis. The depth at which the mucosa was placed was calculated by averaging the measured depths.

5.3.4. Fluorescence imaging in vivo

The fluorescence emission images of the ALA-administered lesion of Sec. 5.2.6 are shown in Fig. 5.8. The fluorescence emission from the normal tissue surrounding the lesion was subtracted from that of the lesion, and the intensities were normalized using the fluorescence emission before irradiation (0 J/cm^2) for each excitation wavelength. The images have been displayed in a colour map for easier visualisation of the changes in the fluorescence intensity.

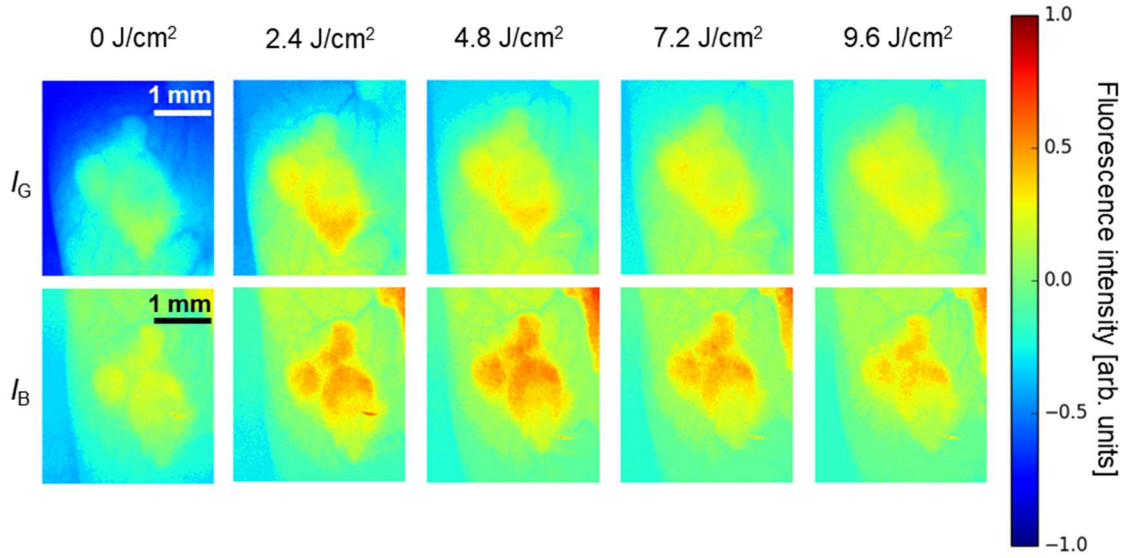

Figure 5.8: Fluorescence emission images of ALA-HCl-administered PC-3 tumour-bearing mouse with increasing irradiation. Irradiation was performed with a 505 nm LED. The fluorescence images were obtained at intervals for excitation wavelength of 505 nm (I_G) and 455 nm (I_B).

The fluorescence emission from the lesion for 455 nm excitation (I_B) before irradiation (0 J/cm^2) was slightly higher than in 505 nm excitation (I_G). In both the fluorescence image of the lesion, I_B and I_G, an increase in the fluorescence intensity of the lesion with increased irradiation energy density is observed. The intensities continue to rise until 4.8 J/cm^2, after which the fluorescence intensity decreases. The continual production of PpIX from the administered ALA-HCL [13] can possibly contribute to the increase in the fluorescence intensity seen in the lesion. Nonetheless, the increase in the fluorescence intensity of the lesion observed is likely caused by the photoproduct formations, as the fluorescence increase should be observed in the same region of the lesion for both blue-light (I_B) and green-light (I_G) excitations if the increased fluorescence intensity was due to continual formation of PpIX.

The white light image and unprocessed fluorescence images of the lesion before and after irradiation are shown in Fig. 5.9. The images were obtained at excitations of 505 nm (I_G) and 455 nm (I_B). The images after irradiation (9.6 J/cm^2) were taken after the mouse skin was sewn back into place. No notable rise in the I_B fluorescence image was detected in Fig. 5.9 due to the photobleaching of both PpIX and Ppp. The colour map images of Fig. 5.8 indicate that at final irradiation (9.6 J/cm^2), the photobleaching of both PpIX and Ppp had already commenced.

Nonetheless, we can see that the fluorescence intensity of I_G reduced after irradiation, while that of I_B was almost comparable.

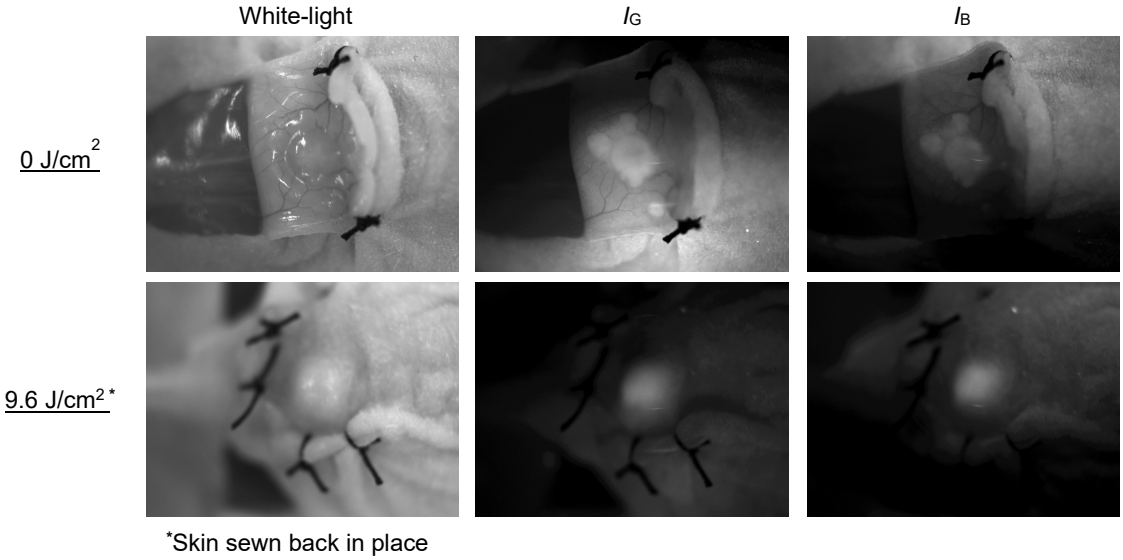

Figure 5.9: Images of the ALA-HCl administered lesion before and after irradiation with a 505 nm LED for 9.6 J/cm^2. The images were obtained with white light, 505 nm, and 455 nm excitation wavelengths. The skin of the mouse was sewn back in place before acquiring the images after irradiation.

Figure 5.10 shows the section view of the lesion used in the *in vivo* analysis. The lesion has been H and E stained. The dimensions of the lesion are shown in the figure. The lesion is located 167.6 µM from the surface.

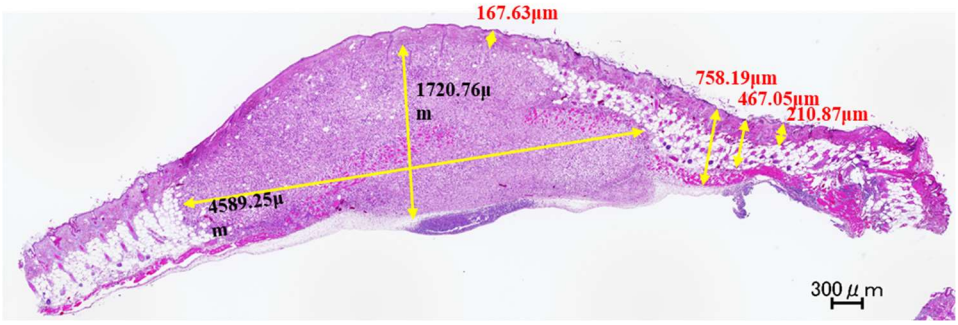

Figure 5.10: A section view of the lesion used in the *in vivo* analysis. The lesion has been H&E stained for easier observation of the tumour size.

5.4. Discussion

The observation of Fig. 5.3 indicates that photoproducts can be excited at multiple wavelengths. Similar to the previous study, a considerable Ppp emission intensity relative to PpIX was observed for excitation at 450 nm [9]. Excitation at this wavelength is advantageous, as excitation with 450 nm offers less tissue scattering and deeper penetration than 405 nm. The absorption peak of PpIX at 505 nm is higher than that at 450 nm, as indicated in Sec. 2.3.2 and other studies [2]. Thus, it is expected that the intensity of unirradiated PpIX excited at 505 nm would be higher than that obtained with excitation at 450 nm (Fig. 5.4 (a)). Photobleaching was observed in all forms of PpIX used for the investigation in this study. It is difficult to compare the photobleaching across the different forms of PpIX due to the environmental effect on the photophysical property of PpIX [14]. There was no variation in the photobleaching between the fluence rates of 20 and 50 mW/cm^2 for both excitation wavelengths. This is consistent with other studies [15,16]. A detailed analysis of PpIX photobleaching in solution has been performed in Chapter 3.

The fluorescence emission obtained using the optical setup of Fig. 5.2 involves the simultaneous excitation of the PpIX and the photoproduct. Both PpIX and Ppp have nonnegligible absorption at both 450 and 505 nm. Thus, accurate analysis of the PpIX photobleaching cannot be performed using the fluorescence images (Figs. 5.6 and 5.8). Additionally, the 455 and 505 nm excitation light sources of the optical setup (Fig. 5.2) have a 25 nm excitation bandwidth (FWHM). This resulted in the extended excitation of PpIX by ±25 nm, causing the slightly higher fluorescence intensity of I_B than I_G before irradiation in the *ex vivo* and *in vivo* analyses (Figs. 5.6 and 5.8). Since the fluorescence comparison is relative to the initial fluorescence intensity of PpIX (before irradiation) for each excitation, the extended excitation of PpIX in both I_G and I_B should be no issue in the result interpretation.

The photoproduct peak at 673 nm indicates that the photoproduct obtained here is Ppp [9,10]. The Ppp peak is detected for both 450 and 505 nm excitation wavelengths. Similar to the analysis performed with 635 nm irradiation of PpIX in the previous chapter (Fig. 4.2), a higher formation rate of Ppp with a lower fluence rate is seen for 505 nm irradiation of PpIX (Fig. 5.4 (b) and (c)). A more intense photoproduct absorption from irradiated haematoporphyrin at low irradiation has been reported by others [17]. The reduced formation of Ppp at a high fluence rate may be explained by the difference in the singlet oxygen quantum yield with the irradiation fluence rate [18] and possibly the variation in the reaction rates between PpIX and oxygen at various fluence rates.

The results of the photobleaching and photoproducts are in line with previous studies. This highlights that the methods of analysis applied in this study can be verified.

Based on our experimental results, the extension of fluorescence observation time for deeply located tumours may be possible by using fluorescence emission from PpIX followed by Ppp. Increased fluorescence emission intensity, nearing that of PpIX, may be achieved with fluorescence photoswitching. Table 5.1 summarises the photoswitching time, the maximum fluorescence emission obtained after photoswitching, and the time taken to attain it, as well as the relative fluorescence intensity of PpIX obtained with excitation using blue light (I_B) to that with green light excitation (I_G). In the present analysis, fluorescence intensities were obtained after discrete irradiation time. Aside from the solution analysis, the fluorescence photoswitching occurred at the first analysis point. Thus, the fluorescence photoswitching time could be less in the *ex vivo* and *in vivo* analyses.

Table 5.1 Summary of the results of the fluorescence photoswitching analysis. I_B and I_G indicate fluorescence intensity obtained at blue-light (450 or 455 nm) and green-light (505 nm) excitation, respectively.

	In solution (20 mW/cm^2)	*Ex vivo*	*In vivo*
Fluorescence photoswitching time [s]	1500	500	600
I_B/I_G at fluorescence photoswitching [-]	1.08	2.25	1.47
$I_{B\,Max}$ time [s]	2500	8000	1200
I_B/I_G at maximum [-]	2.1	3.92	1.65
$I_{B\,Max}/I_{G\,initial}$ [-]	0.94	3.00	0.89

The observed time for the photoswitching of PpIX in solution is much longer than the *ex vivo* and the *in vivo* photoswitching time. The variation in the photoswitching time may be explained by the initial amount of PpIX. The quantity of PpIX used in the solution analysis is at least twice that used in the *ex vivo* analysis. Quantifying the amount of PpIX used in the *in vivo* experiment is difficult, as the conversion rate of ALA to PpIX varies. In the solution analysis, no photobleaching of I_B was noted within the investigated irradiation time (Fig 5.5). Thus, an additional increase in I_B with further irradiation may occur, leading to longer fluorescence observation time with blue-light excitation.

In the solution and the *ex vivo* analysis, the fluence rate is the main factor affecting the fluorescence photoswitching. However, in the *In vivo* analysis, other factors, such as the concentration of ALA converted to PpIX, the distribution of PpIX within the tumour, and oxygen availability at the lesion, affect the fluorescence photoswitching. Thus, considerable differences in the fluorescence photoswitching time and the intensity of I_B are expected with *in vivo* analysis. Thus, optimisation of the irradiation condition and the switching of the excitation light is necessary during actual PDD.

For ALA-PDD of deeply located tumours, the 505 nm excitation is preferred over red light excitation [2]. Using 505 nm could extend the diagnostics depth for lesions in the mucosa to a depth of 1.1 mm or more. Although 505 nm is suitable for detecting deep intramucosal tumours at the initial state, a reduction in the fluorescence emission from PpIX during fluorescence detection caused by PpIX photobleaching is expected. The *ex vivo* analysis was performed at a depth of about 1.28 mm, which is in the range of depth suitable for the green light PDD. The *ex vivo* investigation in this study was performed using a porcine gastric mucosa similar to that used by Ihara et al. [2]. The light penetration depth of the human gastric mucosa is similar to that of porcine gastric mucosa [2,19]. Thus, we can presume that the clinical applications of PDD of deeply located tumours discussed by Ihara et al. apply to this study.

The results of the present study show that the use of 505 nm followed by 450 nm excitation has merits for the ALA-PDD of deeply located lesions. The technique can be employed in detecting undifferentiated adenocarcinoma in mucosal tissues with absorption and scattering coefficients similar to the gastric mucosa. Again, fluorescence photoswitching may be employed using other photosensitizers that produce fluorescent photoproducts to improve PDD diagnostics efficacy. The formation of photoproducts from other porphyrin photosensitizers has been observed [17,20,21] and may be worth exploring.

The Ppp formation is dependent on the concentration of PpIX and oxygen [9,14,22], as well as the fluence rate of the irradiation light. Additionally, the excitation wavelength affects the fluorescence emission intensity of Ppp [9,23]. Unfortunately, it is difficult to control the photosensitizer and the oxygen concentrations *in vivo*. Based on the location of the tumour, the oxygen supply may be limited, PpIX generation from ALA is not fixed, ALA continually forms PpIX, and PpIX can relocalize during PDD [13]. Based on the above, optimisation of the irradiation conditions for the fluorescence photoswitching is primarily based on the light source. We have noted that in solution, Ppp formation is higher for lower fluence rates. This may not be the case in *in vivo* analysis. Thus, investigation towards that is necessary. It is also crucial to note that Ppp

photobleaches and their photobleaching rate may depend on the fluence rate.

We speculate that the increase in the fluorescence intensity with irradiation of PpIX *in vivo* is caused by the formation of Ppp. The result indicated the potential of fluorescence photoswitching. However, the lesion was approximately 167.6 μm from the surface and was exposed to the irradiation light directly during the fluorescence observation. Thus, to verify fluorescence photoswitching in a deeply located tumour, it is necessary to perform analysis for lesions located deeper.

5.5. Chapter conclusion

This chapter studied the concept of fluorescence photoswitching of PpIX in an organic solvent, *ex vivo* and *in vivo*. Fluorescence photoswitching was observed in all of the investigations. By simultaneously exciting PpIX and Ppp, we attained a fluorescence intensity increase ranging between 1.6 and 3.9 times that of exciting PpIX alone. Owing to the variation in the formation of photoproducts with the fluence rate and other factors, the photoswitching time differed with the investigation. Nonetheless, the result of this study suggests that with appropriate irradiation conditions, fluorescence photoswitching could be potentially used to prolong the fluorescence observation time of deeply located tumours. It is presumed that photosensitizers other than PpIX may be used in fluorescence photoswitching, provided they generate photoproducts that emit fluorescence.

References

[1]. N. A. Markwardt, N. Haj-Hosseini, B. Hollnburger, H. Stepp, P. Zelenkov, and A. Rühm, "405 nm versus 633 nm for protoporphyrin IX excitation in fluorescence-guided stereotactic biopsy of brain tumors," *Journal of biophotonics*, **9**(9), 901–912 (2016).

[2]. D. Ihara, H. Hazama, T. Nishimura, Y. Morita, and K. Awazu, "Fluorescence detection of deep intramucosal cancer excited by green light for photodynamic diagnosis using protoporphyrin IX induced by 5-aminolevulinic acid: an ex vivo study," *Journal of Biomedical Optics*, **25**(06), 1 (2020).

[3]. F. van Beurden, D. M. van Willigen, B. Vojnovic, M. N. van Oosterom, O. R. Brouwer, H. G. van der Poel, H. Kobayashi, F. W. B. van Leeuwen, and T. Buckle, "Multi-Wavelength Fluorescence in Image-Guided Surgery, Clinical Feasibility and Future Perspectives," *Molecular Imaging*, **19**, (2020).

[4]. D. W. Roberts, J. D. Olson, L. T. Evans, K. K. Kolste, S. C. Kanick, X. Fan, J. J. Bravo, B.

C. Wilson, F. Leblond, M. Marois, and K. D. Paulsen, "Red-light excitation of protoporphyrin IX fluorescence for subsurface tumor detection," *Journal of Neurosurgery*, **128**(6), 1690–1697 (2018).

[5]. H. Takishima, D. Ihara, T. Nishimura, H. Hazama, and K. Awazu, "Investigation of the Excitation Wavelength for Extension of Diagnostic Depth in 5-aminolevulinic Acid-based Photodynamic Diagnosis of Bladder Cancer," *Nippon Laser Igakkaishi*, **41**(4), 297–306 (2021).

[6]. T. Yamashita, H. Kinoshita, T. Sakaguchi, and H. Isomoto, "Objective tumor distinction in 5-aminolevulinic acid-based endoscopic photodynamic diagnosis, using a spectrometer with a liquid crystal tunable filter," *Annals of Translational Medicine*, **8**(5), 178–178 (2020).

[7]. T. Hirano, Y. Hagiya, H. Fukuhara, K. Inoue, T. Shuin, K. Matsumoto, K. Inoue, T. Tanaka, I. Okura, and S. I. Ogura, "Improvement of aminolevulinic acid (ALA)-mediated photodynamic diagnosis using n-propyl gallate," *Photodiagnosis and Photodynamic Therapy*, **10**(1), 28–32 (2013).

[8]. K. König, H. Schneckenburger, A. Rück, and R. Steiner, "In vivo photoproduct formation during PDT with ALA-induced endogenous porphyrins," *Journal of Photochemistry and Photobiology, B: Biology*, **18**(2–3), 287–290 (1993).

[9]. S. Bagdonas, L. W. Ma, V. Iani, R. Rotomskis, P. Juzenas, and J. Moan, "Phototransformations of 5-Aminolevulinic Acid–induced Protoporphyrin IX in vitro: A Spectroscopic Study," *Photochemistry and Photobiology*, **72**(2), 186–192 (2000).

[10]. L. Ma, S. Bagdonas, and J. Moan, "The photosensitizing effect of the photoproduct of protoporphyrin IX," *Journal of Photochemistry and Photobiology B: Biology*, **60**(2–3), 108–113 (2001).

[11]. W. Dietel and R. Wendenburg, "Phototransformation of ALA-induced protoporphyrin IX (PPIX) in carcinoma cells and of exogenous PPIX in cells and solutions," *https://doi.org/10.1117/12.203418*, **2371**, 567–571 (1995).

[12]. I. Kirino, K. Fujita, K. Sakanoue, R. Sugita, K. Yamagishi, S. Takeoka, T. Fujie, S. Uemoto, and Y. Morimoto, "Metronomic photodynamic therapy using an implantable LED device and orally administered 5-aminolevulinic acid," *Scientific Reports*, **10**(1), (2020).

[13]. D. Kessel, "Relocalization of cationic porphyrins during photodynamic therapy," *Photochemical and Photobiological Sciences*, **1**(11), 837–840 (2002).

[14]. J. S. Dysart and M. S. Patterson, "Photobleaching kinetics, photoproduct formation, and dose estimation during ALA induced PpIX PDT of MLL cells under well oxygenated and

hypoxic conditions," *Photochemical and Photobiological Sciences*, **5**(1), 73–81 (2006).

[15]. S. Iinuma, K. Schomacker, G. Wagnières, M. Rajadhyaksha, M. Bamberg, T. Momma, and T. Hasan, "In vivo fluence rate and fractionation effects on tumor response and photobleaching: Photodynamic therapy with two photosensitizers in an orthotopic rat tumor model," *Cancer research*, **59**, 6164–6170 (2000).

[16]. R. Sørensen, V. Iani, and J. Moan, "Kinetics of Photobleaching of Protoporphyrin IX in the Skin of Nude Mice Exposed to Different Fluence Rates of Red Light," *Photochemistry and Photobiology*, **68**(6), 835–840 (1998).

[17]. J. C. Finlay, D. L. Conover, E. L. Hull, and T. H. Foster, "Porphyrin Bleaching and PDT-induced Spectral Changes are Irradiance Dependent in ALA-sensitized Normal Rat Skin In Vivo," *Photochemistry and Photobiology*, **73**(1), 54–63 (2001).

[18]. C. R. Shea, Y. Hefetz, R. Gillies, J. Wimberly, G. Dalickas, and T. Hasan, "Mechanistic investigation of doxycycline photosensitization by picosecond-pulsed and continuous wave laser irradiation of cells in culture.," *Journal of Biological Chemistry*, **265**(11), 5977–5982 (1990).

[19]. A. N. Bashkatov, E. A. Genina, V. I. Kochubey, A. A. Gavrilova, S. V. Kapralov, V. A. Grishaev, and V. V. Tuchin, "Optical properties of human stomach mucosa in the spectral range from 400 to 2000 nm," 653513-653513–11 (2007).

[20]. E. F. G. Dickson and R. H. Pottier, "On the role of protoporphyrin IX photoproducts in photodynamic therapy," *Journal of Photochemistry and Photobiology, B: Biology*, **29**(1), 91–93 (1995).

[21]. P. F. Menezes, H. Imasato, J. R. Perussi, C. A. S. Melo, and V. S. Bagnato, "Cytotoxicity of the photoproducts of Photogem after photobleaching induced by intense illumination," 51–55 (2004).

[22]. K. Huang, L. Chen, S. Lv, and J. Xiong, "Protoporphyrin IX photobleaching of subcellular distributed sites of leukemic HL60 cells based on ALA-PDT in vitro," *Journal of Biomedical Science and Engineering*, **05**(09), 548–555 (2012).

[23]. R. L. Goyan and D. T. Cramb, "Near-Infrared Two-Photon Excitation of Protoporphyrin IX: Photodynamics and Photoproduct Generation," *Photochemistry and Photobiology*, **72**(6), 821–827 (2000).

Conclusion

This study aimed to improve the diagnostics and treatment efficacies of PDD and PDT by studying photosensitizer photobleaching and photoproduct formation, two important phenomena that are used for PDD and PDT dosimetry estimation. These were analysed for the photosensitizer, PpIX, using fluorescence spectroscopy and mass spectrometry. The potential use of the PpIX photoproducts to complement PpIX for PDD of deeply located tumours has also been investigated.

In the introduction, the importance of studying photosensitizer photobleaching and its photoproduct for improved PDD and PDT was highlighted. The results of Chapter 2 showed that a linear relationship exists between PpIX concentration and MS signal intensity, while that is not the case between the fluorescence intensity and PpIX concentration. At high concentrations, there is the aggregation of PpIX, which affects its fluorescence emission intensity. The result indicates the preference of MS over fluorescence for the analysis of photobleaching and photoproducts.

Chapters 3 and 4 analysed and compared the photobleaching and the photoproduct formation rates using MS and fluorescence. Differences in the photobleaching rates obtained using the two analysis methods were found. There was a dependency of the MS-based photobleaching rate on the fluence rate, while the fluorescence-based photobleaching rate did not show this dependency. The effect of wavelength and fluence rates on the type and amount of photoproduct was also noted. Irradiation of PpIX with 635 nm light typically used in PDT favoured the formation of Ppp, especially at lower fluence rates. In 405 nm irradiation of PpIX, we saw the higher formation of PpII at higher fluence rates. These photoproducts are speculated to be formed directly from PpIX reacting with oxygen.

Investigation of fluorescence photoswitching for the fluorescence diagnosis of deeply located tumours, performed in solution, *ex vivo* and *in vivo*, was performed in Chapter 5. With the excitation of PpIX and Ppp at the same time, after notable PpIX photobleaching and photoproduct formation during the initial PDD, a fluorescence intensity increase between 1.6 and 3.9 times that of exciting PpIX alone was achieved. A maximum fluorescence emission of 94 % initial PpIX intensity was obtained with the excitation of the photoproduct. Thus, with optimised conditions, fluorescence photoswitching may prolong the fluorescence observation time and increase the fluorescence intensity during fluorescence detection of deeply located tumours. Additionally, this technique is not limited to PpIX and its photoproducts. The utilisation of other photosensitizers may be explored, provided they form photoproducts that emit fluorescence upon irradiation.

The overall results of this study have a potentially considerable effect on the diagnostics and treatment efficacies of PDD and PDT and can be exploited for improved PDD and PDT. Additionally, this work sets an antecedent for exploring the use of photoproducts for the dosimetry estimation as well as diagnosis and treatment.

Acknowledgements

This research was conducted in the Medical Beam Physics Laboratory of Quantum Energy Engineering course, Division of Sustainable Energy and Environmental Engineering, Graduate School of Engineering, Osaka University.

I would like to start by expressing my extreme gratitude to the late Prof. Kunio Awazu, who was willing to accept me into his laboratory and for his constant words of encouragement. I am grateful to Assoc. Prof. Hisanao Hazama, who supervised me during the duration of this course and made this work possible. I sincerely thank the dissertation committee, Prof. Isao Murata of the Quantum Reaction Engineering Laboratory, and Prof. Fuminobu Sato of the Quantum Beam and Biomaterials Engineering Laboratory for their invaluable insight and assistance in the review of the dissertation. A heartfelt acknowledgement to Asst. Prof. Takahiro Nishimura, who always gave his time for discussions.

I would like to extend my appreciation to Prof. Katsuyoshi Masuda of the Graduate School of Medicine, Kyoto University, for his expertise, and was instrumental in the mass spectrometry-related analyses, and to Prof. Hideo Fukuhara and Prof. Keiji Inoue of the Department of Urology, Kochi Medical School for their contribution during the *in vivo* analyses. I also thank Mr. Yasuhiro Takegawa of Thermo Fisher Scientific Co., Ltd., who helped with part of the analyses used in this study.

Many thanks to my past and present labmates for their cooperation. Lastly, I cannot begin to express my thanks to my family for their love, understanding, and generous support.

Research Achievements

Peer-Reviewed Papers

1. Sochi Judith Ogbonna, Hisanao Hazama, Kunio Awazu: "Mass Spectrometric Analysis of the Photobleaching of Protoporphyrin IX Used in Photodynamic Diagnosis and Therapy of Cancer," *Photochemistry and Photobiology* 97(5):1089-1096 (2021).

2. Sochi Ogbonna, William Y. York, Takahiro Nishimura, Hisanao Hazama, Hideo Fukuhara, Keiji Inoue, and Kunio Awazu: "Increased fluorescence observation intensity during the photodynamic diagnosis of deeply located tumors by fluorescence photoswitching of protoporphyrin IX," *Journal of Biomedical Optics* 28(5):055001 (2023).

3. Sochi J Ogbonna, Katsuyoshi Masuda, Hisanao Hazama: "The effect of fluence rate and wavelength on the formation of protoporphyrin IX photoproducts," *Photochemical and Photobiological Sciences* (under review).

International conference proceeding

1. Sochi Ogbonna, William York, Takahiro Nishimura, Hisanao Hazama, and Kunio Awazu: "Analyses of protoporphyrin IX fluorescence photoswitching for prolonging the photodynamic diagnosis time of deeply located tumours" *Proc. SPIE* 12627, Translational Biophotonics: Diagnostics and Therapeutics III, 1262716 (August 11, 2023).

Domestic conference proceeding

1. Sochi Ogbonna, Hisanao Hazama, Kunio Awazu: "Mass Spectrometric Analysis of the Photobleaching coefficient of Protoporphyrin IX used in Photodynamic Diagnosis and Therapy of Cancer," 電気学会研究会資料 OQD-20-009-016: 15-18 (2020).

International Conferences

[Oral presentation]

1. Sochi Ogbonna, William York, Takahiro Nishimura, Hisanao Hazama, and Kunio Awazu: "Analyses of protoporphyrin IX fluorescence photoswitching for prolonging the photodynamic diagnosis time of deeply located tumours" 2023 European Conferences on Biomedical Optics

(Munich, Germany, June 27, 2023).

[Poster presentation]

1. Sochi Ogbonna, Hisanao Hazama, Katsuyoshi Masuda, and Kunio Awazu: “Photobleaching and photoproducts analyses of the photosensitizers, protoporphyrin IX and protoporphyrin IX dimethyl ester, for photodynamic diagnosis/therapy of cancers “71st ASMS Conference on Mass Spectrometry and Allied Topics, MP 083 (Houston, USA, June 5, 2023).

Domestic Conferences

1. Sochi Ogbonna, Hayato Kawai, Hisanao Hazama, Kunio Awazu: “Atmospheric Pressure Laser Ionization Imaging Mass Spectrometry at Intracellular Scale using Transmission Geometry Optical System,” The 67th Annual Conference on Mass Spectrometry (Tsukuba, May 16, 2019).

2. Sochi Ogbonna, Hisanao Hazama, Kunio Awazu: “Mass Spectrometry Based Investigation of Photobleaching Coefficient of Protoporphyrin IX Used in Photodynamic Diagnosis and Therapy of Cancer,” The 68th Annual Conference on Mass Spectrometry (May 2020).

3. Sochi Ogbonna, Hazama Hisanao, Awazu Kunio: “Mass Spectrometry-based Evaluation of the Photobleaching Rate of Protoporphyrin IX used in the Photodynamic Diagnosis and Therapy of Cancer,” The 69th Annual Conference on Mass Spectrometry (Online, May 21, 2021).

4. Sochi Ogbonna, Hisanao Hazama, Katsuyoshi Masuda, and Kunio Awazu: “Analysis of the Photoproducts of the Photosensitizer, Protoporphyrin IX, used in Photodynamic Therapy of Cancers” The 71st Annual Conference on Mass Spectrometry (Osaka, May 17, 2023).

Award

1. Osaka University Female Graduate Student Excellence Research Award.